8-2019

Energy Harvesting Techniques to Power Onboard Railway Bearing Condition Monitoring Systems

Jacob Nathaniel Bensen
The University of Texas Rio Grande Valley

ENERGY HARVESTING TECHNIQUES TO POWER ONBOARD RAILWAY BEARING CONDITION MONITORING SYSTEMS

A Thesis

by

JACOB NATHANIEL BENSEN

Submitted to the Graduate College of
The University of Texas Rio Grande Valley
In partial fulfillment of the requirements for the degree of

MASTER OF SCIENCE IN ENGINEERING

August 2019

Major Subject: Mechanical Engineering

ENERGY HARVESTING TECHNIQUES TO POWER ONBOARD RAILWAY BEARING CONDITION MONITORING SYSTEMS

A Thesis
by
JACOB NATHANIEL BENSEN

COMMITTEE MEMBERS

Dr. Constantine Tarawneh
Chair of Committee

Dr. Heinrich Foltz
Committee Member

Dr. Stephen Crown
Committee Member

Jazmin Ley
Committee Member

August 2019

ABSTRACT

Bensen, Jacob N., Energy Harvesting Techniques to Power Onboard Railway Bearing Condition Monitoring Systems. Master of Science in Engineering (MSE), August 2019, 96 pp., 7 tables, 43 figures, 23 references.

Limitations of the standard wayside hotbox detection system as a method to identify failing railway bearings severely inhibit the reliability and safety of rail transport. An onboard bearing condition monitoring system would address and ameliorate the issues present in the current detection system. The onboard system would provide more frequent and reliable information regarding bearing condition. For the system to succeed in reducing maintenance time and preventing bearing failure, a method of providing the system with sufficient energy to power its instrumentation is necessary. The instrumentation location environment poses a significant challenge. The device must be placed on the steel adapter adjacent to the bearing, where it will experience high temperatures, corrosion and significant loading conditions. The goal of this thesis is to investigate an energy harvesting medium in such an environment. An investigation of vibration of the bearing adapter during typical railway use is coupled with magnetostrictive elements and the Villari effect to develop a set of simulations to determine the energy harvesting capabilities of a vibrational-based energy harvesting system located on the bearing adapter. The work in this thesis summarizes the potential energy harvesting capability of a giant magnetostrictive material-based vibrational energy harvester for railway use.

DEDICATION

I would like to dedicate this thesis to my family. To my wife, Shyala, thank you for believing in me. I could not have accomplished this without your constant love and support. You inspire me to be the best version of me that I can. Thank you for being there and for keeping me sane, happy and focused. I love you. To my children, Jaxon, Maya, and now Wyatt, I did it! You can do anything if you are willing to work hard. Thank you for pushing me to be a better role model and for helping keep me grounded when I needed to relax and refocus. To my father, Ted, for inspiration and support. To my mother, Gloria, for your love and support. To Jesse, Michel and Joseph, for believing in me.

ACKNOWLEDGEMENTS

I would like to graciously thank Dr. Constantine Tarawneh. The opportunity to work with you and the UTCRS research team has been immensely challenging and rewarding. You pushed me to be better, motivated me, and were always willing to take time to help me. You believed in my capabilities and inspired me to work harder. You helped me to learn, grow and become a better engineer. You represent so many things that an exceptional engineer and mentor should be. I am grateful for this opportunity to work with you.

Dr. Heinrich Foltz, thank you for your time and expertise. You were always available to help, and your input was instrumental to the completion of this thesis.

To the mechanical engineering faculty at UTRGV, I humbly thank you for your willingness to invest in the students here. Having been at a larger university, the extra time and effort you give to students every day has not been wasted. I count myself blessed to have had the opportunity to learn from extraordinary teachers who truly care.

To everyone at the University Transportation Center for Railway Safety, this team is incredible. I was happy to meet each of you, learn with you, work with you and goof off with you. I appreciate you all immensely. Marco Barrera, thanks for helping me knock this out. A cuanto la bolsa?

Lastly, this study has been made possible by funding provided by The University Transportation Center for Railway Safety (UTCRS) through a USDOT Grant No. #DTRT 13-G-UTC59.

DISCLAIMER

The contents of this thesis reflect the views of the authors, who are responsible for the facts and the accuracy of the information presented herein. This document is disseminated under the sponsorship of the U.S. Department of Transportation's University Transportation Centers Program, in the interest of information exchange. The U.S. Government assumes no liability for the contents or use thereof.

TABLE OF CONTENTS

Page

LIST OF TABLES

Page

LIST OF FIGURES

Page

CHAPTER I

INTRODUCTION AND MOTIVATION

1.1 Introduction

Improvements to motor vehicle and aerospace transportation has led to an overall decline in train usage as passenger vehicles. The railway system is still heavily used for freight transport. About 40% of freight transported in the US is shipped via rail [1]. This reliance on rail for freight transportation is expected to continue. New intermodal transportation containers offer a versatile and sustainable alternative to other shipping methods, rising in popularity dramatically in the United States from 5.6 million containers in 1990 to 14.5 million units in 2018 [2]. Despite the continued prevalence of rail transportation, the primary systems monitoring the health of bearings are two varieties of wayside units. All wayside units are systems attached to certain locations along the rail to perform measurements to determine the condition of train equipment as the locomotive passes by them. Hot-box detection systems use infrared sensors to determine the temperature of bearings and other train components. Nationally, hot-box detection units are operational at over 6,000 locations [3]. A newer wayside detection technology, Trackside Acoustic Detection System (TADS), is available which utilizes microphones to record and analyze audio produced by a passing train to identify bearing defects. Although TADS present an improvement over the hot-box detector units, there are currently only 30 TADS in the US and Canada, and 70 systems in service worldwide [4, 5]. Wayside systems have been very useful at removing some faulty equipment from service, but they also have

presented some problems which need to be addressed. By as much as forty percent, wayside detection units have been found to overreport bearings, which upon further inspection were not faulty [6]. Additionally, from 2010 to 2016, there were 119 reported cases in the United States and Canada of bearings that passed a wayside detection location undetected only to fail shortly thereafter, causing the train to derail [7]. Each individual derailment can cost millions of dollars in damages to the train, track, cargo and the environment.

The primary limitations of the hotbox detection system lie in the reliability of its measurements to determine if a bearing is indeed faulty. The forty percent of bearings that are marked for removal, but upon inspection are found to be in good condition are termed "non-verified". More notably, despite the use of the wayside detection systems, there have been derailments due to bearing failure. Research conducted at the University Transportation Center for Railway Safety (UTCRS) at the University of Texas Rio Grande Valley (UTRGV) in Edinburg, Texas in 2018 investigated the use of hot-box detectors as a primary means of bearing health monitoring. The study noted the failure in these systems to detect a damaged bearing can be attributed to the reactive nature of the detection method and emphasized the importance of properly calibrating the infrared sensors to the scanning location to obtain an accurate bearing temperature measurement [6]. Additionally, a damaged bearing can progress to failure rapidly. There are wayside detection systems approximately every fifteen to thirty miles of rail [8]. The physical separation between successive wayside detection locations cannot guarantee that measurements produced from a bearing will be significant enough to indicate an abnormal reading before it fails. In fact, a bearing was documented to progress from a healthy scan at a wayside detection location to catastrophic failure only 96 seconds after the checkpoint [9].

Expanding the current wayside system to cover every stretch of track more frequently might improve the situation, but to expand a system with known accuracy issues would be illogical.

1.2 Motivation

If the improvement of a bearing condition detection system can lead to more positively identified faulty bearings, the incidence of train derailments will be decreased. If the system can also decrease the false reporting of suitable bearings as defective, the railway industry can operate on schedule and plan maintenance appropriately. The UTCRS is investigating an onboard bearing condition monitoring system. The onboard monitoring system shows great promise as a method of accurately detecting bearing defect size and location, even for spalls smaller than 1 in^2 [10]. This type of system can provide accurate condition information that can characterize and monitor damage. With sufficient energy input, the system could feasibly provide continuous system monitoring. The motivation to utilize an onboard system has marked benefits to improve the safety and efficiency of the railway transportation system.

The implementation of such a system would be costly, as every bearing adapter would need to be instrumented. The return would include the decreased incidence of non-verified bearings, appropriately planned maintenance for at-risk bearings, and decreased progression to catastrophic failure or derailment.

For new technology to improve upon the faults of the wayside system, it must be able to match or increase the frequency of data collection. Each onboard monitoring system is minimally comprised of one accelerometer, two temperature sensors, and a low-power Bluetooth device. To provide power to this system while satisfying the goal of reducing maintenance, the ideal solution would incorporate an energy harvesting mechanism that would perpetually power all devices. Primary, or non-rechargeable, batteries would require maintenance to replace, and

the system would be non-functional and dangerous should the charge deplete. In contrast, an energy harvesting system that uses the train's environment to gather enough energy to support the monitoring system would not demand significant down time for maintenance.

CHAPTER II

BACKGROUND AND LITERATURE REVIEW

2.1 Energy Harvesting in Rail Applications

The successful implementation of an energy harvesting system is necessary to support the bearing monitoring equipment. A literature review shows development of different energy harvesting technologies with the desire to see effective use of the energy available in a railway setting.

A possible green energy source is solar power. Improvements to photovoltaic systems are significant over the past decade, although some limitations to the successful implementation in a freight railway setting have yet to be resolved. Photovoltaic cells were found to be inefficient in a setting that could not consistently control the incident angle of rays reaching the panel. Recently, solar panels have been attached to passenger trains successfully and are used to power lights, air conditioning system and other electronics [11]. The uniformity and consistency of passenger locomotives make solar panels a reasonable solution for this particular application. Freight transportation involves the use of a wide variety of car types, and the industry is increasingly using stackable intermodal containers. The inability to develop a singular solution for all freight car types is an imposing obstacle to the feasibility of utilizing solar energy for freight.

An alternative energy source that has been investigated is wind energy. Simply put, the implementation of wind energy requires the advantageous generation of energy compared to the

additional effort required to overcome the extra air drag added by the wind turbines. A feasibility study was performed by Nurmanova et al [12] which confirmed the potential for a successful implementation of wind turbines aboard moving trains. The output power of the wind turbines is significantly more efficient than the solar panels. It is notable, however, in both cases that the effectiveness of either method relies heavily on the surrounding environmental conditions. Additionally, while this may have usefulness to the constant design of passenger locomotive cars, the placement of such structures on a series of inconsistent freight containers is problematic.

Pyroelectric materials produce power from the change in temperature over time [13]. As such, steady-state conditions would not produce power in a pyroelectric energy harvester. Railcars typically do not experience frequent transient speeds that can produce a significant temperature change near the bearing adapter. Most often, drastic temperature changes are an indication of poor bearing health, making pyroelectric materials impractical for a railcar application. Thermoelectric materials, however, operate on the constant temperature gradient exhibited between the material's two ends [13]. Elefsiniotis et al [14] investigated the implementation of a thermoelectric phase change material intended for use in aircraft. The study concluded that, although their worst-case scenario produced enough energy to power a wireless sensor node, great importance lies in the temperature gradient; as the phase change material approaches the ambient temperature, the power produced decreases to zero. Although the steady-state case may have a constant temperature gradient initially, the phase change material physically must approach the ambient temperature of its contact to generate power. Although it is not the focus of this thesis, research shows that thermoelectric materials advances present a reasonable opportunity in railcar applications.

Vibration-based energy harvesters have been developed in many forms and for different purposes. Traditionally, there are two primary types: piezoelectric materials and electromagnetic vibrational energy harvesters. Wang et al [15] studied piezoelectric transducers instrumented along the track to harvest vibrations present in the rail. As of the present time, the author is unable to find research regarding piezoelectric materials used for onboard energy harvesting. Piezoelectric materials are typically able to function under low loads and, when subjected to high strain conditions are prone to failure. Woo et al [16] studied the relationship between strain, frequency and output power of a piezoelectric module and found the material, when submitted beyond a strain threshold, would fracture.

Electromagnetic vibration-based energy harvesters are being studied in a variety of configurations. Deng and Dapino [17] produced a recent review of magnetostrictive vibration energy harvesters. De Pasquale et al [18] developed an energy harvester with magnetic suspensions for train vibrations with positive results. The harvester developed was tuned to specific resonance frequencies and the results corroborated that fact. The size and location of this energy harvester is inconsistent with the specifications required of the current on-board monitoring unit. Mori et al [19] studied the utilization of a giant magnetostrictive cantilever with a focus on the feasibility of designing a self-tuning vibration-based energy harvester. Dai [20] experimented with creating a vibration-based energy harvester based on rotary pendulums that would have broadband characteristics. The versatility, strength and potential of electromagnetic vibration-based energy harvesters is being investigated for many specific applications with some success.

2.2 Selection of Energy Harvesting Technique

Freight trains are not universally capable of accepting such a large adaptation as a solar panel or wind turbine on every roof. There are many railcar styles. Some cars have no roof. Intermodal containers are stackable, and can even be ejected completely to a transport truck. Use of a remote energy harvesting source, regardless of energy output, would require additional installation, instrumentation and maintenance resources. The intention is to develop one comprehensive solution with minimum maintenance.

Although the power needs of an onboard system could potentially be satisfied by many of these systems, there remain specific obstacles to the feasibility of an energy harvesting system applied to onboard freight rail use. Principally, the energy harvesting method must be compatible with the needs of the system it intends to power. This thesis focuses on developing an energy harvesting system that would be able to cooperate with the specific problems faced by the onboard monitoring system (OMS) in development at UTRGV.

The OMS is composed primarily of one accelerometer, two low-power temperature sensors, and one low-power Bluetooth device. The system requires roughly 33 mW for measurements sent wirelessly every 120 seconds [21]. With the improved performance of the OMS over wayside detection, 120 seconds will be sufficient to monitor and track developing spalls before they become problematic. The development and functioning of the OMS are not of concern, only the power requirements to operate it and the physical and environmental constraints imposed. The location of a harvester for the OMS must be instrumented onto the bearing adapter. This simplifies the design to a singular product that can be instituted universally across each freight train bearing and not require additional wiring or power to be functional.

2.3 Giant Magnetostrictive Materials in Energy Harvesting

Terfenol-D has recently had a resurgence in popularity as a component of energy harvesters. The advantage Terfenol-D presents over alternative materials is its giant magnetostrictive properties. Magnetostriction is a property of ferromagnetic alloys in which the material exhibits a strain when subjected to a magnetic field. The Villari effect is the opposite of this phenomenon; a magnetostrictive material, when caused to strain, will produce a magnetic field. Specifically, giant magnetostrictive materials are those that have a large strain-magnetic field coupling. When exposed to the same magnetic field, Terfenol-D will exhibit a strain response one hundred times greater than most ferromagnetic materials [22]. Developed by the Naval Ordnance Laboratory, Terfenol-D has historically been utilized as a sensor or transducer. The brittle nature of Terfenol-D has prevented its use in high strain applications. Nevertheless, Terfenol-D does have the largest magnetostriction of any material currently known. This potential for energy harvesting has not gone unnoticed, as it has been the material of choice in much of current magnetostrictive vibration-based energy harvester literature. Additionally, prior research conducted at UTCRS has concluded that this material may be effective in producing the desired results and is worth further investigation [20].

CHAPTER III

TEST SYSTEM DEVELOPMENT

3.1 Historical Overview

Prior work at the UTCRS has shown the utility of Terfenol-D as a load sensor and demonstrated the additional potential for harvesting energy as well [20]. The initial device developed by Estrada had the potential to harvest over 80 mW with simple harmonic conditions. However, that device was not developed with a goal for a specific energy harvesting implementation. The former project focused on the load sensing capabilities of Terfenol-D. The material was able to function well as a sensor but was unable to perform both load sensing and energy harvesting simultaneously. Optimizing the device to one task limits the functionality of the other. As such, this thesis focuses on investigating the device configuration and engineering specifications to simulate the energy harvesting potential of a feasibly sized instrumented product subjected to railway car operations typical use.

The device from Estrada's [20] work is presented in Figure 1 as a CAD drawing with an exploded view of the fixture's components. An aluminum spool (Item 4) is wound with 200 turns of 26 AWG magnet wire (Item 5), and the Terfenol-D rod (Item 3) was placed in the center as a core. A 1018 steel notched ring (Item 2) surrounds these components radially to protect and contain them; the notch serves to allow a port for the leads of the coil to emerge from the fixture safely. A 1018 steel base (Item 7) is used to protect and contain the components of the entire assembly, while a 1018 steel rod (Item 1) is used to direct the force through the Terfenol-D. An

aluminum washer (Item 6) was a necessary addition to orient the coil more efficiently around the Terfenol-D allowing the assembly to produce more energy.

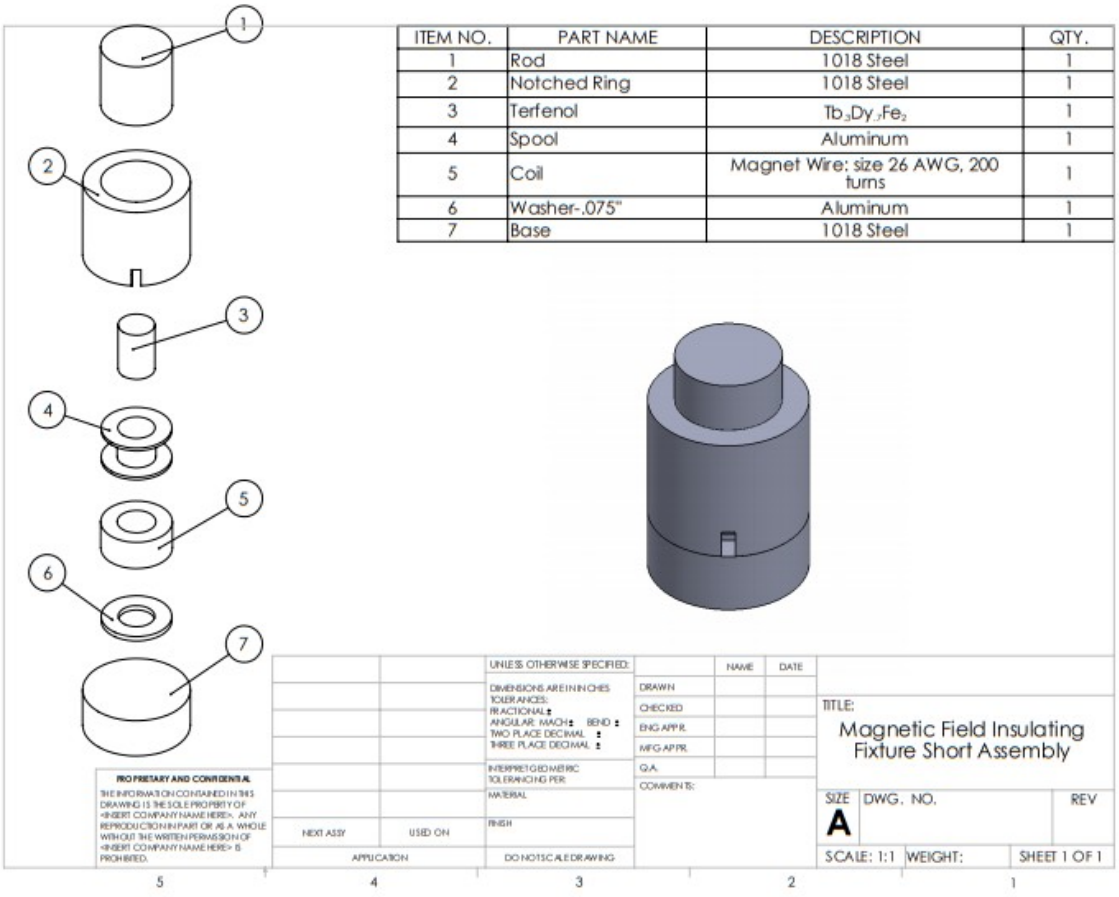

Figure 1. Assembly of Terfenol-D test fixture from prior work [20].

3.2 Test Modifications and Initial Tests

The experiments are intended to relate the force and frequency of vibrations present in a typical freight car to the energy harvesting potential of a Terfenol-D based energy harvester. To complete such an experiment, control of a compressive force was required. A Material Test System (MTS) was chosen to perform the compressive duties required within the design of these experiments. The original design was tested in different scenarios to determine modifications that would improve the performance of the energy harvester and improve the quality of the data

produced. Figure 2 shows the MTS instrumented for the final iteration of tests. The MTS system controls the bottom crosshead to perform tension or compression forces at programmed cycles. The system is limited to a maximum compressive force of 20 kips. The leveling plate is used to ensure axial force through the Terfenol-D fixture. The power supply powered the signal amplification board attached to the strain gauge on the Terfenol-D. A data acquisition (DAQ) device was used to collect signals from the MTS as readouts of displacement and force, voltage measured across the leads of the coil, and amplified strain measured by the strain gauge.

Figure 2. Material Test System (MTS) with instrumentation.

The test fixture underwent modifications to account for improvements to the trial methods. A larger Terfenol-D piece was used to perform trial experiments and a similar size

increment was necessary for associated fixture components. Magnets were implemented to improve the energy output. A Delrin spool replaced the aluminum spool to decrease electromagnetic interference. Original tests used the data acquisition capabilities of the MTS, whereas, the desire to include external signals required an external DAQ device that could read signals from the MTS and the fixture's instrumentation.

3.2.1 Energy Harvesting Test

The energy harvesting tests were performed using the initial apparatus and a Terfenol-D rod measuring 19 mm in length and 13 mm in diameter, as pictured in Figure 3. It was determined that the use of magnets appropriately could tune the performance of the Terfenol-D, resulting in improved energy harvesting capability. The test protocol for the initial energy harvesting experiments is presented in Figure 4. With a compressive force ranging from 50 to 1,950 lb, the sine-shaped cyclic test doubles frequency from ½ Hz through 32 Hz frequencies. This experiment was the first to implement the output capabilities of the MTS system and the DAQ equipment. Figure 4 relates the force driving the test to the measured responses of displacement, representative of the movement of the lower crosshead, and voltage measured from the coil surrounding the Terfenol-D. With a nearly constant force amplitude, the voltage, and thus power generated from the system, increases with frequency.

Subsequent testing utilized either a force amplitude of 100 or 900 lb and the frequencies varied from 8 to 32 Hz. The experiments included a 20-Ohm resistive load, correlated to the maximum power transfer theorem, and capacitors of varying value were used to test their influence on the power output. Power was calculated simply as an average of voltage squared divided by the resistive load. As such, it is more accurately thought of as a calculation of a multi-cycle average power. The results of this testing are shown in Table 1. The power garnered

from these experiments are positively correlated with force amplitude and frequency. Measurements without a resistive load did not provide an associated power.

Figure 3. Terfenol-D rod with 3300 Gauss neodymium magnets.

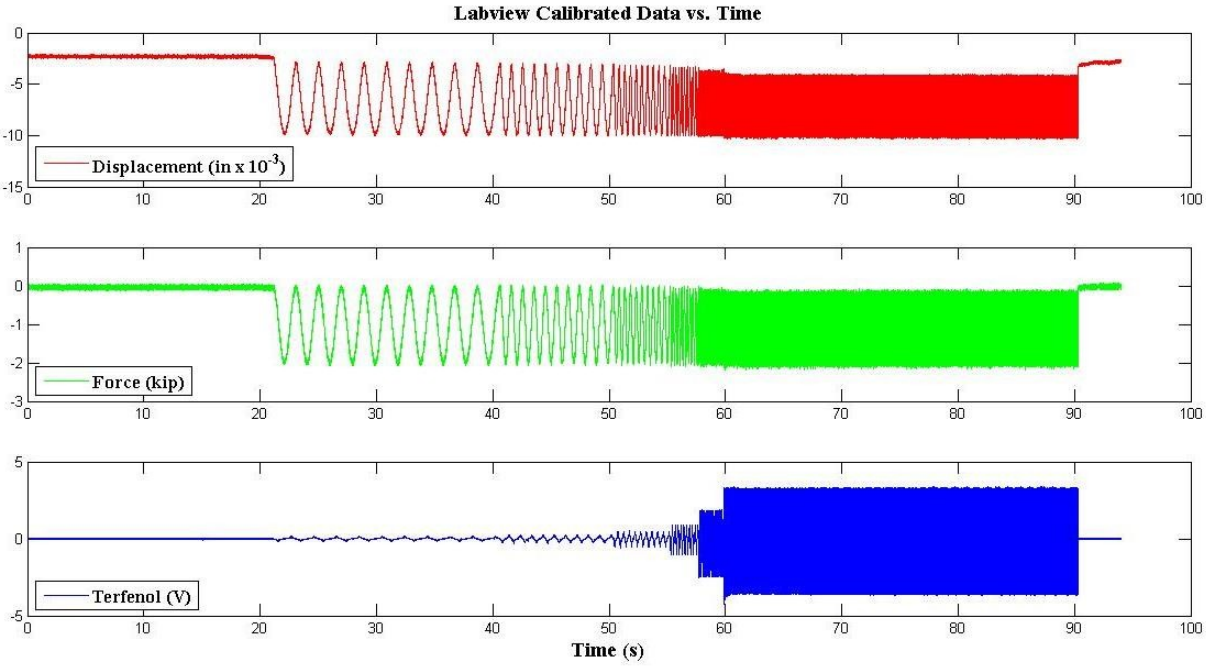

Figure 4. MTS cyclic test trial one.

Table 1. Power generated due to force and frequency variation.

Test	Force (lb)	Frequency (Hz)	Resistance (ohm)	Capacitance (uF)	Power (mW)
1	100	8	0	0	N/A
2	100	8	20	0	0.063
3	100	8	20	47	0.064
4	100	8	20	100	0.061
5	100	8	20	220	0.058
6	100	16	0	0	N/A
7	100	16	20	0	0.278
8	100	16	20	47	0.272
9	100	16	20	100	0.268
10	100	16	20	220	0.256
11	100	32	0	0	N/A
12	100	32	20	0	1.675
13	100	32	20	47	1.253
14	100	32	20	100	1.179
15	100	32	20	220	1.144
16	900	8	0	0	N/A
17	900	8	20	0	7.43
18	900	8	20	47	7.37
19	900	8	20	100	7.311
20	900	8	20	220	7.181
21	900	16	0	0	N/A
22	900	16	20	0	25.057
23	900	16	20	47	25.011
24	900	16	20	100	24.785
25	900	16	20	220	23.977
26	900	32	0	0	N/A
27	900	32	20	0	132.86
28	900	32	20	47	133.076
29	900	32	20	100	129.294
30	900	32	20	220	114.477

3.2.2 Strain Gauge Test

In analyzing the information from the MTS, the displacement readout is a property of the LVDT of the MTS crossheads. The displacement value from the DAQ readout is not a function of the Terfenol-D alone, but of the crossheads, compression platens, and supporting rods of the MTS machine itself. The displacement of the Terfenol-D rod was therefore not known; however, because the force was driven solely through the Terfenol-D by the assembly, the data is assumed to be a value similar in shape but lower in amplitude to the value collected. From the initial MTS displacement collected by the DAQ, Terfenol-D strain calculations were conducted. A strain gauge, shown in Figure 5, was added to compare the calculated data to the actual strain seen by the material.

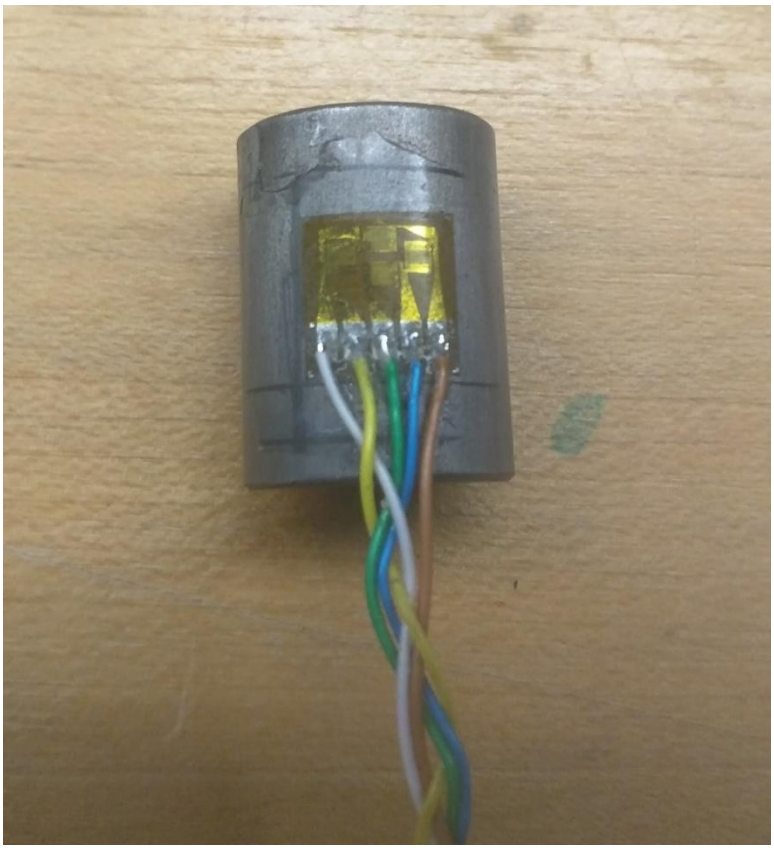

Figure 5. Strain gauge applied for Terfenol-D strain analysis.

Initial trials of the strain gauge showed a discrepancy in the behavior of the displacement read by the strain gauge and the MTS. To judge congruency between LVDT and strain gauge data, the Terfenol-D assembly was subjected to stepwise increases and decreases in compressive forces by the MTS. The results are given in Figure 6. The starting and ending points do not coincide. A subsequent test, shown in Figure 7, implemented a pre-stress of fifteen minutes, followed by three consecutive 100-cycle commands that were designed to determine if there had been a sufficient pre-stress applied to the assembly. The third cyclic procedure resulted in coincident starting and ending points, indicating appropriate pre-stress, as evidenced in Figure 8, which shows results of the third 100-cycle command.

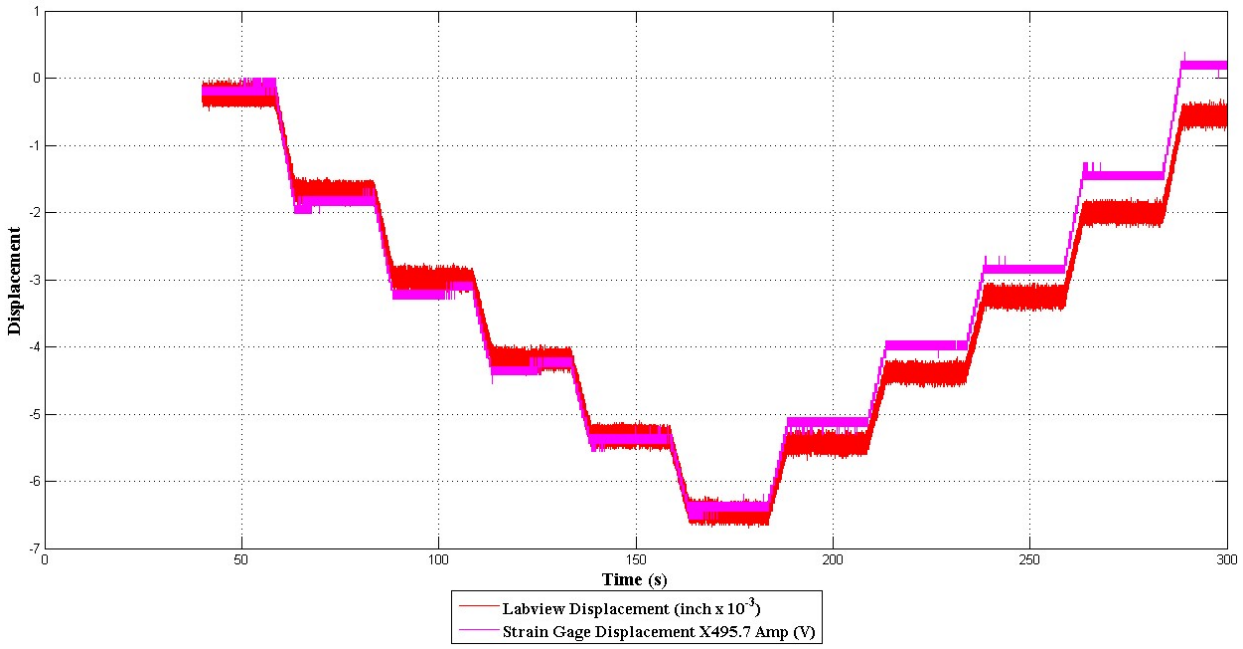

Figure 6. Strain gauge congruency test.

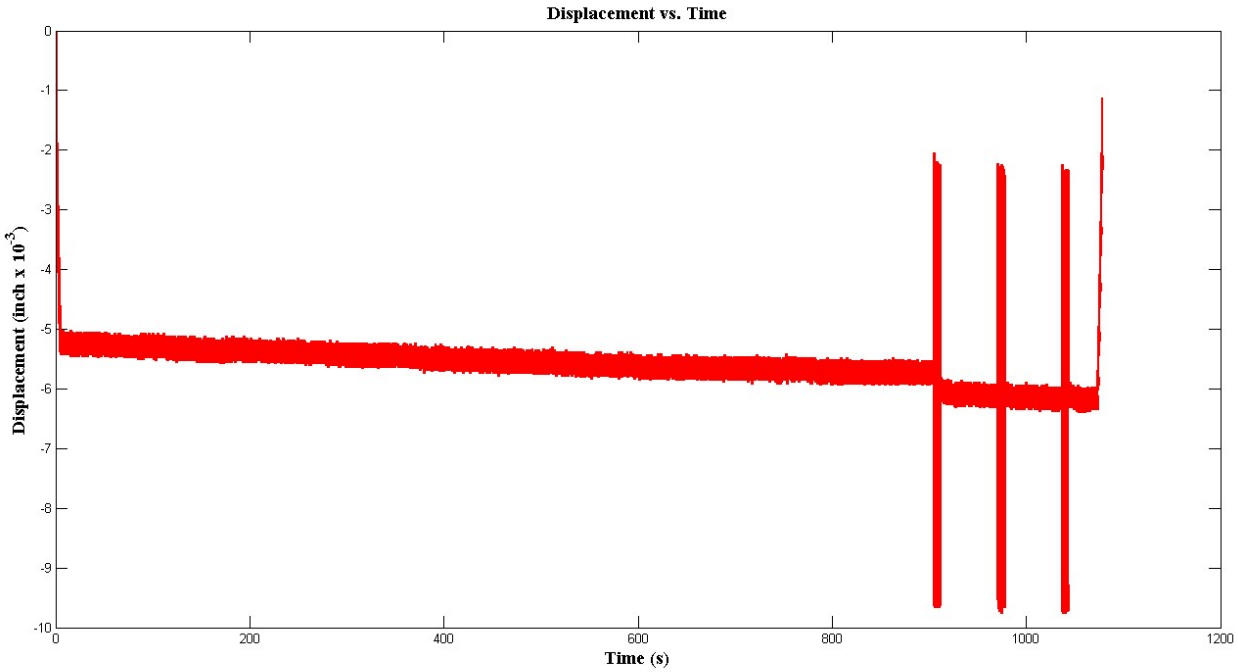

Figure 7. Pre-stress testing.

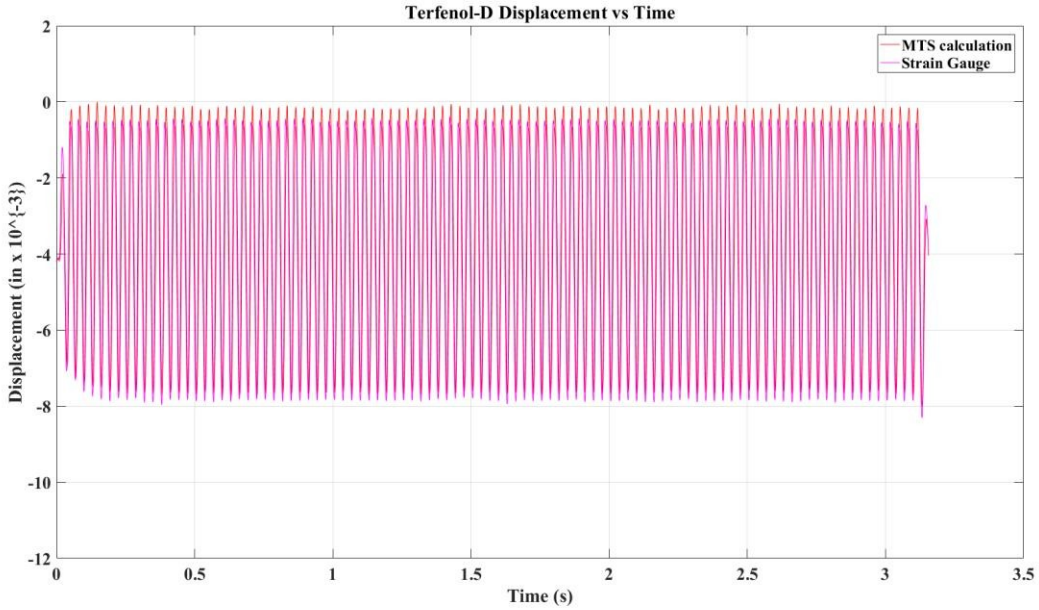

Figure 8. Terfenol-D pre-stress comparison.

3.2.3 Permalloy Test

As suggested by the work of Colussi et al [23], the fracture incidence of Terfenol-D is dependent on the load rate. Terfenol-D is known to be a brittle material. Many of the tests performed during the initial testing phase of this thesis ended prematurely because a rod of Terfenol-D cracked or fractured. Although the loading was intended to be entirely axial, due to the fracture pattern initiating along the radial extremities, it was surmised that barreling could be contributing to the brittle fracture of the Terfenol-D pieces. To combat this, Permalloy film was applied to the ends of the Terfenol-D sample, as shown in Figure 9. Figure 9a shows the Permalloy before trim and application, and Figure 9b shows the Permalloy above and below the Terfenol-D piece post-test. The curl at the edges occurs when the piece is removed from the fixture.

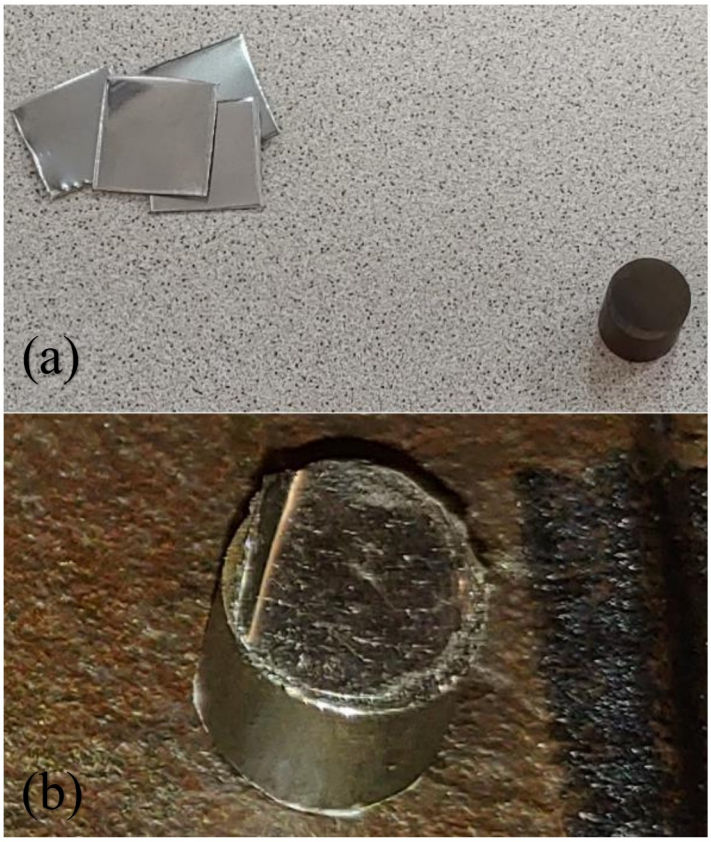

Figure 9. (a) Thin film Permalloy application, and (b) Permalloy film close-up post-test.

Permalloy 80 is an alloy composed of about 80% nickel, 15% iron, and 5% molybdenum. Theoretically, the soft metal would function as a lubricant, preventing barreling and allowing fully axial force transmission. Although this thesis does not attempt to investigate or quantify the phenomenon of increasing the fracture toughness of the specimen by addition of the alloy, but rather focuses on attaining a reliable energy source from the Terfenol-D assembly. If the energy harvester cannot be relied upon to withstand the forces of the environment, it is a liability. The primary benefit of adding Permalloy to the ends of the Terfenol-D sample are that the sample will be protected. Secondly, it was important to make sure the energy harvested from the system would not be greatly reduced. To verify the Permalloy effects on the assembly, one Terfenol-D sample was tested with and without Permalloy applied to the ends. The Permalloy had a thickness of 0.003 inch and was cut-to-size with shears using the magnets as a guide. The results of this test, shown in Table 2, suggest that the efficiency of the energy harvester is reduced by roughly twenty-five percent.

Table 2. Permalloy power loss comparison.

Direct comparisons							
Repeated tests with Permalloy applied							
Test	Force (lb)	Frequency (Hz)	Resistance (ohm)	Permalloy	Power (mW)	FFT Frequency (Hz)	Power %
1A	900	32	20	No	132.860	32.0435	100
1B	900	32	20	Yes	103.225	32.0435	77.7
2A	900	32	20	No	133.076	32.0435	100
2B	900	32	20	Yes	103.295	32.0435	77.6
3A	900	32	20	No	129.294	32.0435	100
3B	900	32	20	Yes	98.838	32.0435	76.4
4A	900	32	20	No	114.477	32.0435	100
4B	900	32	20	Yes	87.669	32.0435	76.6
5A	900	32	200	No	40.495	32.0435	100
5B	900	32	200	Yes	30.396	32.0435	75.1

Though there was a drop in the energy harvesting efficiency, the material was kept safe by the addition of the Permalloy. The reduction in efficiency was not further investigated and can be left for future work. The samples tested since the introduction of Permalloy to the fixture have not fractured.

3.2.4 Energy Harvesting Setup

The aforementioned improvements have been implemented with the goal of providing a set of conditions that would produce the best results within the smaller confined environment available. The energy harvester is intended as an addition to the steel bearing adapter, pictured in Figure 10. Today, most railroad bearing adapters consist of a metal and elastomer component, as opposed to those made entirely of metal.

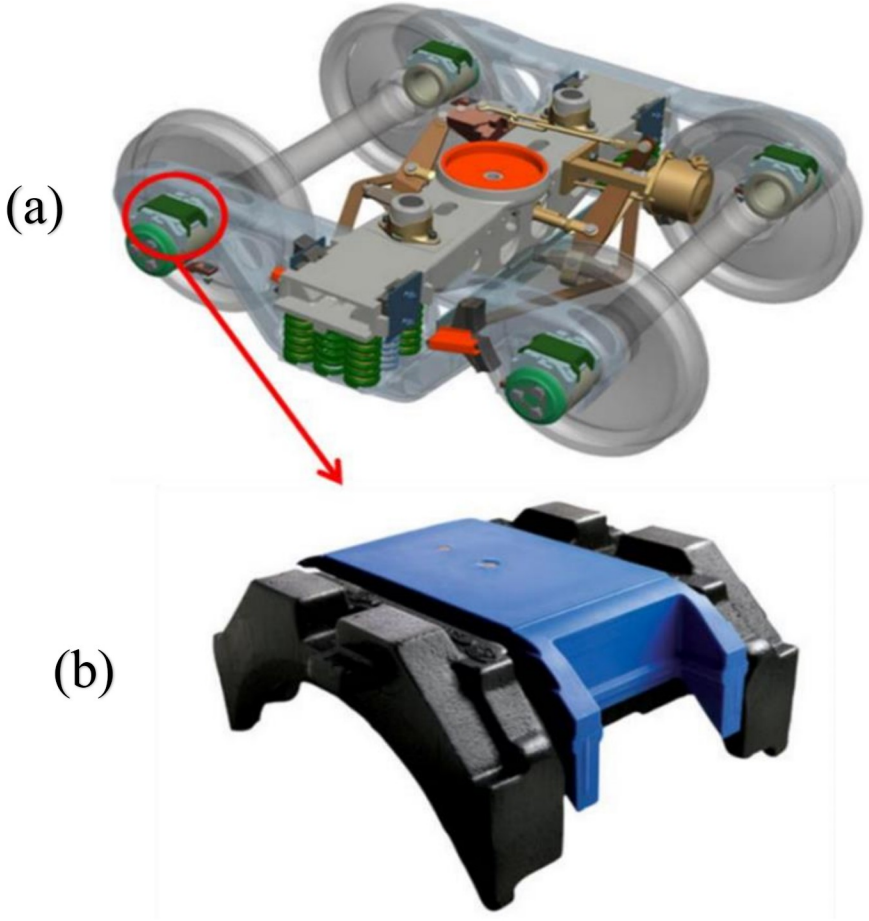

Figure 10. (a) Railroad bogey, and (b) Railroad bearing adapter.

The Terfenol-D energy harvesting fixtures initially allowed improvement to the energy harvester before proceeding with the manufacture of a prototype instrumented bearing adapter. To that end, it is imperative that an appropriate location for the inclusion of an energy harvester is attained.

3.3 Pressure Film Test

To determine where a magnetostrictive energy harvester might be instrumented into the bearing adapter, a pressure test was applied to a dynamic test on the single-bearing test rig. The goal is to determine where the highest pressure is located, coinciding with the greatest potential for energy harvesting. Additionally, it is important to ensure the location remains in contact throughout a service cycle. The energy harvester must be able to withstand the worst conditions present on a full-speed train, in addition to traversing grades, speed changes and impacts. A pressure film is a set of miniature opaque color-filled spheres interspersed between two sheets. As a pressure is applied, some spheres will burst, causing color to appear on the sheet. Greater pressures will produce areas of higher-intensity color on the sheet. Calibration allows the pressures, within the specified usage range, to be determined by the corresponding charts provided by the film's manufacturer.

A pressure film was applied between the bearing adapter and the elastomer pad-liner. In normal service, a bearing with a fully-loaded freight car atop will experience 34,400 pounds of force, or 100% load. An unloaded car will still provide 17% of that load or 5,850 pounds of force to each bearing. For simplicity, the loads referenced will be in reference to those carried by a single bearing installed on a train equipped with four axles and eight bearings per freight car. The dynamic test was run at 120% load (41.28 kips of force) to account for a worst-case loading condition of a Terfenol-D rod. The resulting film, along with calibration swatch is

shown in Figure 11. Note the magnitude of pressure on the left-hand side is greater than the pressure on the right-hand side. This phenomenon is due to the direction of axle rotation.

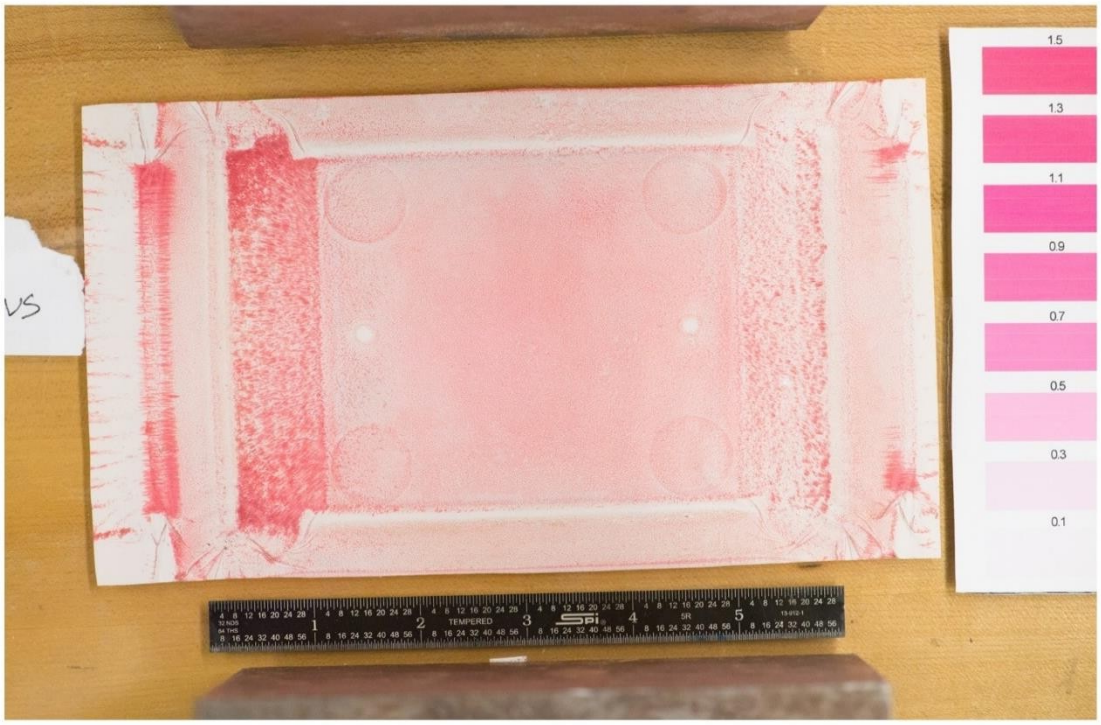

Figure 11. Fujifilm pressure film, 120% dynamic load applied (41.28 kips).

It can be inferred that the energy harvesting potential will be dependent on the direction of travel of the train. The highest pressure is found along the channel on the left-hand side known as the interlock of the bearing adapter. Using image processing software, the calibration card allowed careful calculation of the magenta value associated with the pressure in the region of interest, as shown in Figure 12. The magenta value is then used with pressure film manufacturer-supplied tables to determine the associated pressure. The calculations and tables are provided in Appendix B.

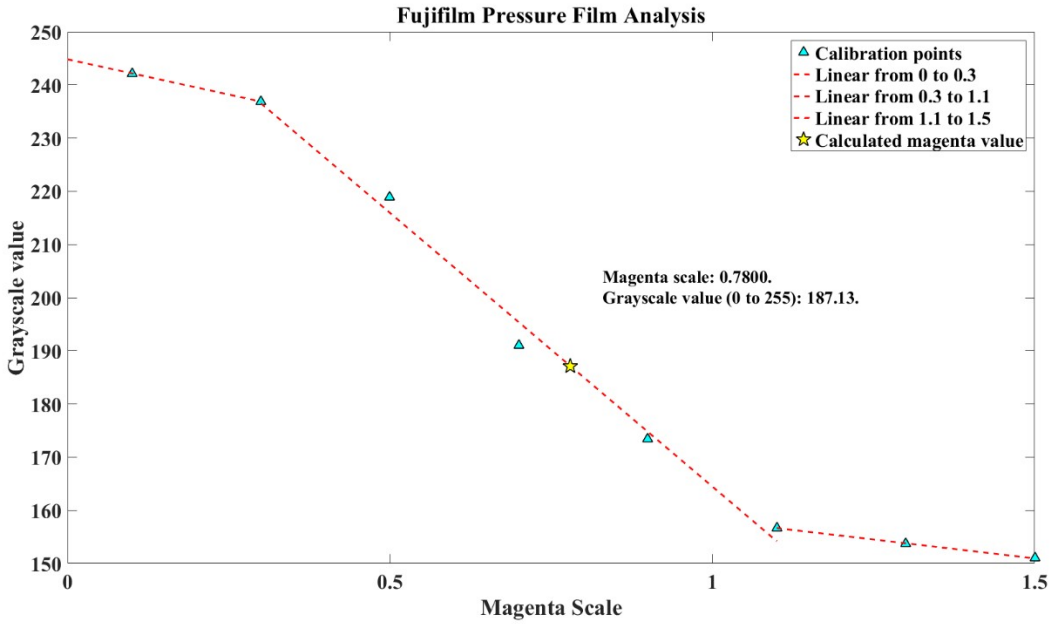

Figure 12. Calculated magenta value of left-side interlock region, equivalent to 4.6 ksi.

From a low-range pressure film analyzing a dynamic test at 36% load (12 kips, a lightly loaded railcar), shown in Figure 13, the interlocks are, at both ends, the only locations that remain in contact continuously. The color density in this region exceeded the maximum calibration scale, therefore the value of pressure in this region is not known, but the nature of the load distribution is seen. If the energy harvester were to be located within a region that did not remain loaded (in contact at the ends), the Terfenol-D would be subjected to impacts upon loading and unloading, potentially during travel as well. Therefore, the interlock is a suitable location for the implementation of a vibrational energy harvester.

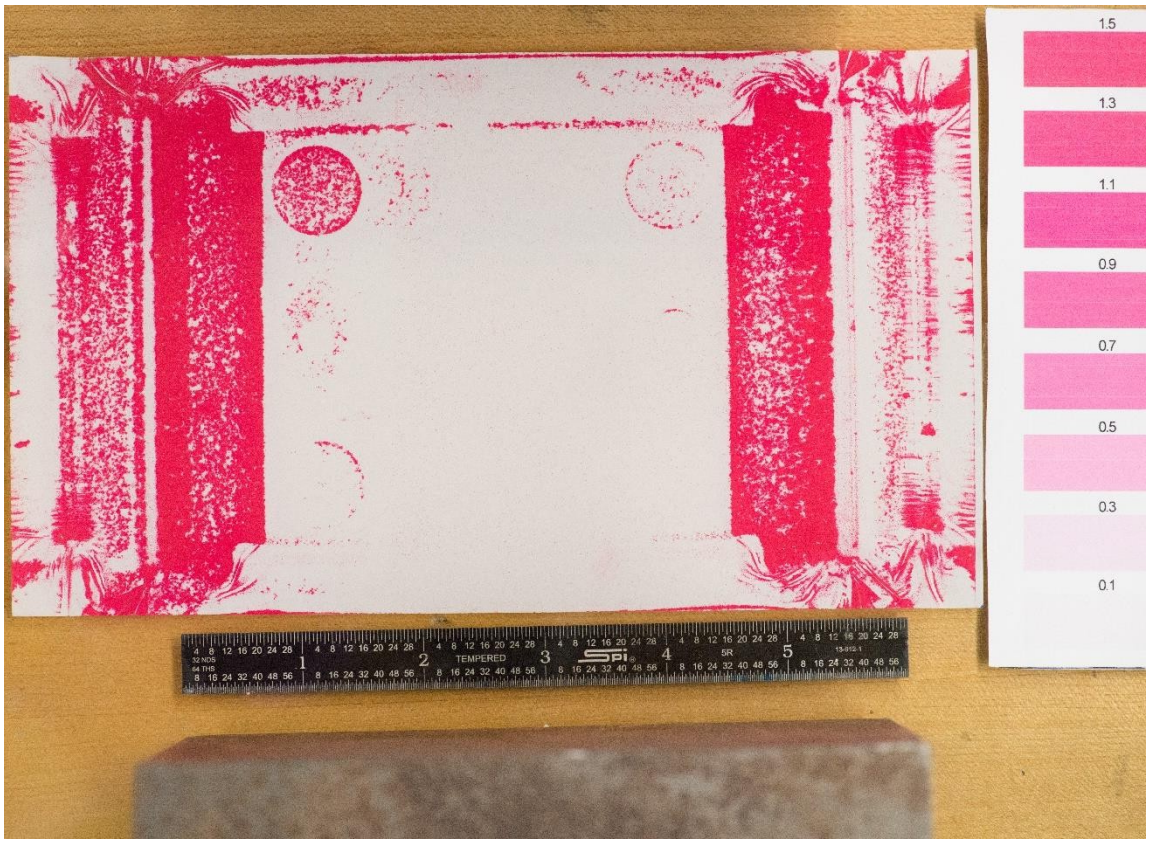

Figure 13. Low pressure film, 36% dynamic load applied.

3.4 Finite Element Analysis (FEA)

The pressure film test indicates that the bearing interlocks experience constant load and are the location of highest stress. Before machining the adapter, however, it is imperative to ensure the safety and structural integrity of implementing a proposed modification to the pad. Finite element analysis is performed to test potential modification scenarios. The size of the Terfenol-D rod intended for use in this experiment is 8 mm tall with a diameter of 10 mm. The material removed from the steel adapter to allow for the fixture will be cylindrical. From the analysis of the pressure film at 120% load, the maximum pressure seen by the adapter will be 4.64 ksi (32 MPa) at the interlocks. The system must sustainably provide power regardless of the direction of movement of the train, therefore, the proposed design will have four energy

harvesting fixtures, two on either end of the adapter interlocks. This would provide energy from at least two fixtures at a time.

The dimensions of a class F bearing adapter were used to create a CAD model. The model was modified to emulate the removal of material associated with the proposed location of the energy harvesting fixtures. Figures 14a and 14b show a typical (unmodified) bearing adapter and a modified bearing adapter, respectively. The constraints applied to the model for the simulation include the pinned constraint, as shown in Figure 15a, from the bottom surface of the bearing adapter to the geometric center of the axle. The force, shown in Figure 15b, is applied as a pressure across the interlocks and the exterior surfaces of the Terfenol-D fixtures to simulate a fully-loaded railcar.

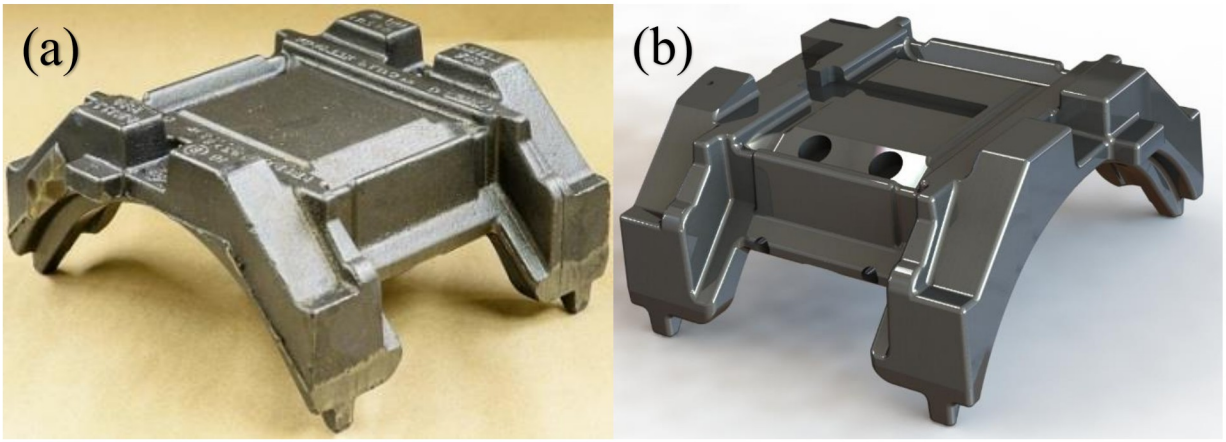

Figure 14. (a) Typical bearing adapter, and (b) proposed energy harvester locations.

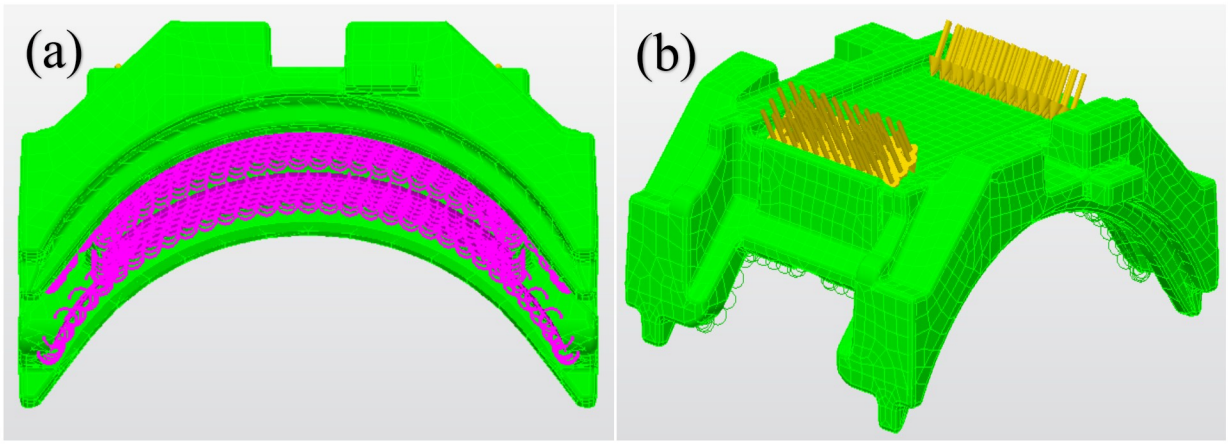

Figure 15. (a) Pinned conditions from underside of bearing adapter to geometric center of axle, and (b) force applied to the interlocks and through the center of the Terfenol-D.

The results of the pressure test are shown in Figure 16. The detailed calculations, along with software commands and material properties can be found in Appendix C. The point of highest stress is 10.6 ksi. The compressive yield strength is over 80 ksi for cast iron, and the fatigue strength is 30 ksi. This conservative simulation supports the supposition that the proposed modifications are safe for use in this manner.

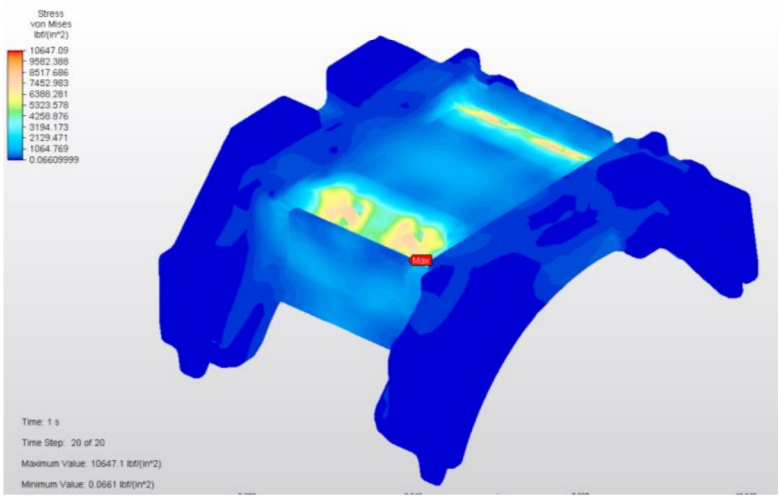

Figure 16. FEA model, Von Mises stress level.

CHAPTER IV

SIMULATION DEVELOPMENT

4.1 Introduction

In 2015, the UTCRS performed a field test at the Transportation Technology Center Inc. (TTCI) in Pueblo, CO. TTCI is equipped with multiple tracks and laboratories for research and testing purposes. The tests were performed on the Railroad Test Track (RTT) and the Precision Test Track (PTT). The tests collected onboard measurements of temperature and vibration data. It is presumed the standardized geometries of rail length, wheel size, and other components would contribute to the presence of certain common frequencies if subjected to similar conditions, of speed and railcar load. The data is analyzed with the intention of using the frequency and relative magnitude of vibrations present in practical use to build a reliable experimental model that simulates real-world vibrations found in the bearing adapter of a moving freight car.

4.2 TTCI Test Setup and Data Collection

The tests were performed with a railcar that was purposefully equipped with four healthy bearings and four bearings that had defects. The orientation and location of each bearing is shown in Figure 17.

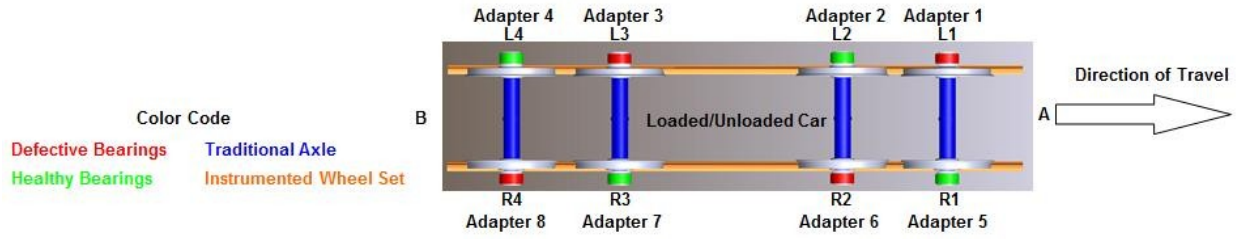

Figure 17. TTCI test railcar setup.

Each bearing adapter was instrumented with two accelerometers and one thermocouple, as shown in Figure 18, where SA refers to the accelerometer's attachment to the SmartAdapter location and R refers to the Radial location. The data of importance to this thesis is collected by the accelerometers, so thermocouple data is neglected. The sixteen accelerometers were sampled at 5.556 kHz, requiring two DAQ devices for each four bearings tested. Each test recorded data from either the front four bearings or the rear four bearings. The tachometer was also monitored to ensure measurements were taken when the locomotive maintained the appropriate steady-state speed. It is notable that no balance car was used for these experiments.

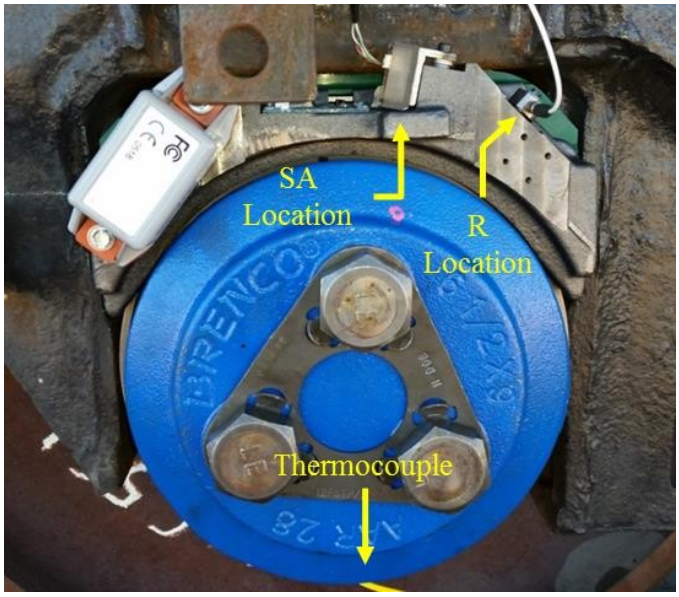

Figure 18. Bearing adapter instrumentation locations.

Measurements were taken at a variety of speeds with either an unloaded or fully-loaded freight car. Table 3 shows the speeds and loading conditions of each test performed.

Table 3. TTCI testing conditions.

Test	Day	Track	Orientation	Speed (mph)	Load
1	1	RTT	Front	30	Loaded
2	1	RTT	Front	50	Loaded
3	1	RTT	Front	55	Loaded
4	1	RTT	Rear	30	Loaded
5	1	RTT	Rear	40	Loaded
6	1	RTT	Rear	50	Loaded
7	1	RTT	Rear	55	Loaded
8	1	RTT	Rear	57	Loaded
9	1	RTT	Rear	60	Loaded
10	2	PTT	Front	30	Loaded
11	2	PTT	Front	40	Loaded
12	2	PTT	Front	50	Loaded
13	2	PTT	Front	55	Loaded
14	2	PTT	Rear	30	Loaded
15	2	PTT	Rear	40	Loaded
16	2	PTT	Rear	50	Loaded
17	2	PTT	Rear	55	Loaded
18	3	PTT	Front	30	Unloaded
19	3	PTT	Front	40	Unloaded
20	3	PTT	Front	50	Unloaded
21	3	PTT	Rear	40	Unloaded
22	3	PTT	Rear	50	Unloaded
23	3	RTT	Front	40	Unloaded
24	3	RTT	Front	50	Unloaded
25	3	RTT	Front	55	Unloaded
26	3	RTT	Front	60	Unloaded
27	3	RTT	Front	65	Unloaded
28	3	RTT	Rear	30	Unloaded
29	3	RTT	Rear	40	Unloaded
30	3	RTT	Rear	50	Unloaded
31	3	RTT	Rear	55	Unloaded
32	3	RTT	Rear	60	Unloaded
33	3	RTT	Rear	65	Unloaded

4.3 Vibration Analysis and Frequency Selection

Each dataset collected contains vibration information for two healthy and two defective bearings. The defective bearings are expected to introduce vibrational components that are not representative of the test parameters stated, and they are therefore neglected. The vibrational components representing rail, wheel, and other pertinent geometries to this thesis are present below 200 Hz, thus, higher frequencies are neglected. The lack of balance car, it was found, introduced a significant amount of noise into the results for the bearings located on the rear-end of the locomotive. The additional noise is exemplified when comparing the frequency spectrum, shown in Figures 19 and 20, for two specific tests: the Day 1, RTT Track, 50 mph, Loaded Scenario as measured from the front bearings and the rear bearings, respectively. The frequency spectrum below 200 Hz is seen for both healthy bearings measured during each test. The relative clarity with which peaks are differentiated from noise-level vibrations is more substantial from the data collected from the front bearings as opposed to the rear bearings.

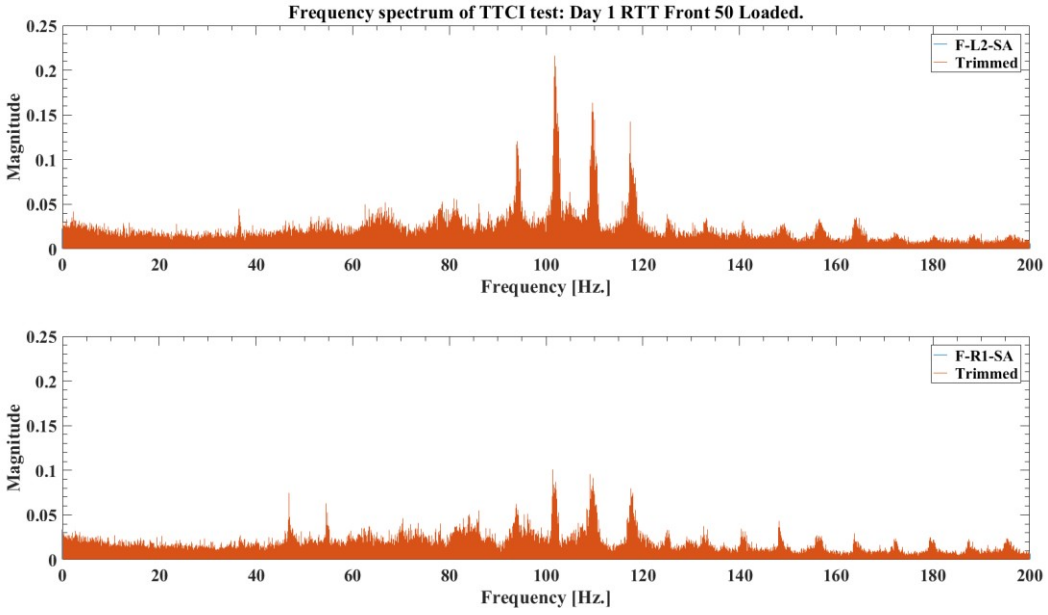

Figure 19. Frequency spectrum of two healthy bearings measured at 50 mph with a loaded railcar, measured from the front of the railcar.

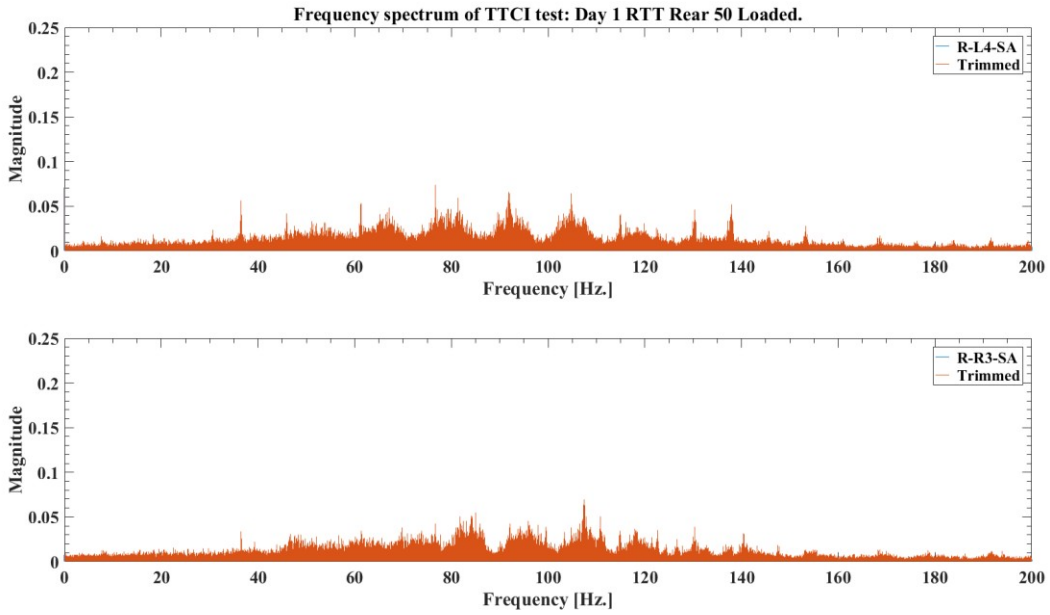

Figure 20. Frequency spectrum of two healthy bearings measured at 50 mph with a loaded railcar, measured from the rear of the railcar.

Each test was representative of a specific speed/load condition. Some of the test scenarios were duplicated. At the very least, each speed/load scenario contains data for two healthy bearings collected simultaneously.

Each dataset from the accelerometers was processed with the Fast Fourier Transform (FFT) function using the mathematical software package MATLAB®. The representative frequencies were filtered to reflect only the frequencies below 200 Hz for the healthy bearings. Due to the nature of FFT calculations, collecting data over different lengths of time would naturally produce different-sized frequency bins. Creating uniform bin sizes is imperative when comparing the relative incidence of common frequencies. The error in the frequency measurement was derived from the measurement error of the tachometer, which was then used to create appropriately sized bins to redistribute the FFT results uniformly across all datasets, then the datasets were normalized. The resolution of the tachometer's measurements was determined

by data inspection. This produced a value referred to as d_{speed}, measured in mph. The d_{speed} was correlated to the desired frequency resolution, d_{Hz}, by the 36-inch wheel diameter as:

$$d_{Hz} = d_{speed} * \frac{1\ hr}{3600\ s}\frac{63360\ in}{1\ mi}\frac{(2\pi)\ rad}{(36\pi)\ in} \quad (1)$$

The frequencies were binned with a width, d_{Hz}, which was found to be 0.006424 Hz. The appropriate number of bins to traverse the spectrum from 0 to 200 Hz was used. The frequency content from each dataset was re-binned using this bin procedure.

The top percent frequency magnitude refers to the incidence with which a frequency can be expected to be seen within a dataset. A Fourier transform analyzes the relative incidence within a dataset that frequencies are present, and as such, can be thought of as an average of that calculation over the entire length of the measurement. This means, simultaneously, that a larger dataset includes more information about the frequencies present because it analyzes more cycles, and noise would be reduced.

The magnitudes of the normalized frequencies were then used to compare the relative importance of each frequency based on the parameters of the testing environment of speed and load. The common frequencies present among the top 0.25%, 2%, 4%, 10% and 20% frequency magnitude of each speed/load scenario were calculated. These cutoffs were selected because, across each test situation, the goal was to separate the relative importance of each frequency in a method that would progress from more selective to less selective. As can be seen in Figure 21, the top 0.25% of the signal is representative of about ten peaks, the top 2% represents an additional 7 peaks, and so on. Additionally, the peaks present among the top 0.25% are still represented by the top 2%, but among a wider frequency band. The top 0.25% of a signal may not contain common frequencies among similar speed/load scenarios, but there may be some common frequencies among the top 2% or top 4%.

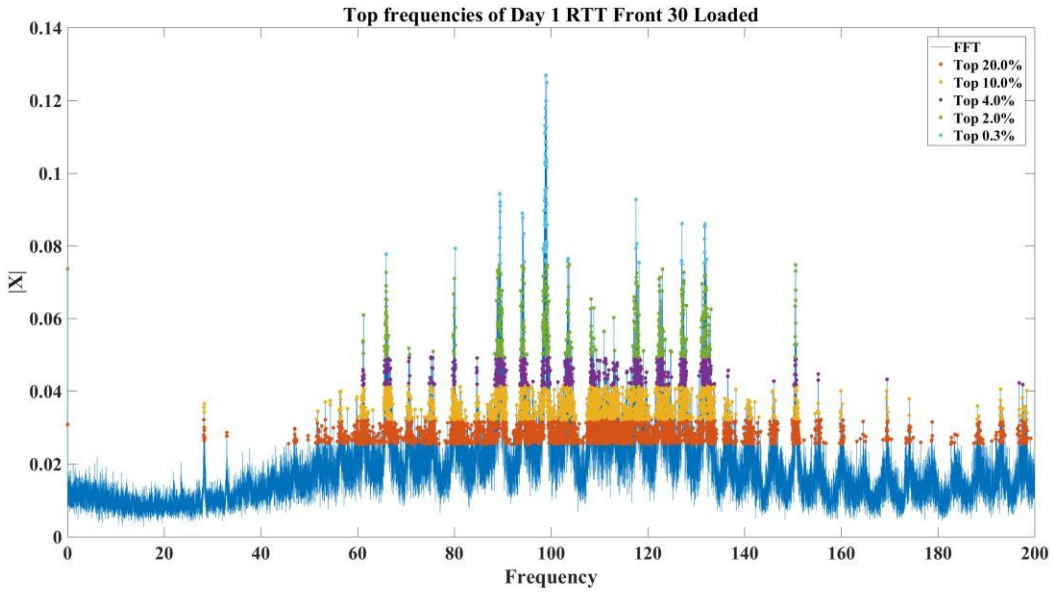

Figure 21. Top frequency percentage peaks determined.

For illustrative purposes and clarity, the process is outlined using the following few figures. Figure 22 presents an analysis of all 33 TTCI tests (66 healthy bearings), and the top 10% of each frequency present in all the signals, with each point coinciding with the frequency and the related magnitude of a specific bearing. At this point, the value of the magnitude is not as important as recognizing that a signal is present amongst every bearing tested under similar conditions, therefore, the magnitudes are replaced with an arbitrary point that represents the presence of a frequency component experienced by each bearing in Figure 23. After noting which of those bearings are related to a similar scenario, such as a front-measured, 55 mph, fully-loaded railcar, as seen in Figure 24, the relative percentage of bearings tested within that scenario containing similar frequency content is calculated for each representative frequency. An alternative view of the same calculation is given in Figure 25, where a highlighting line is drawn through the frequencies that have congruency amongst all relevant bearing measurements.

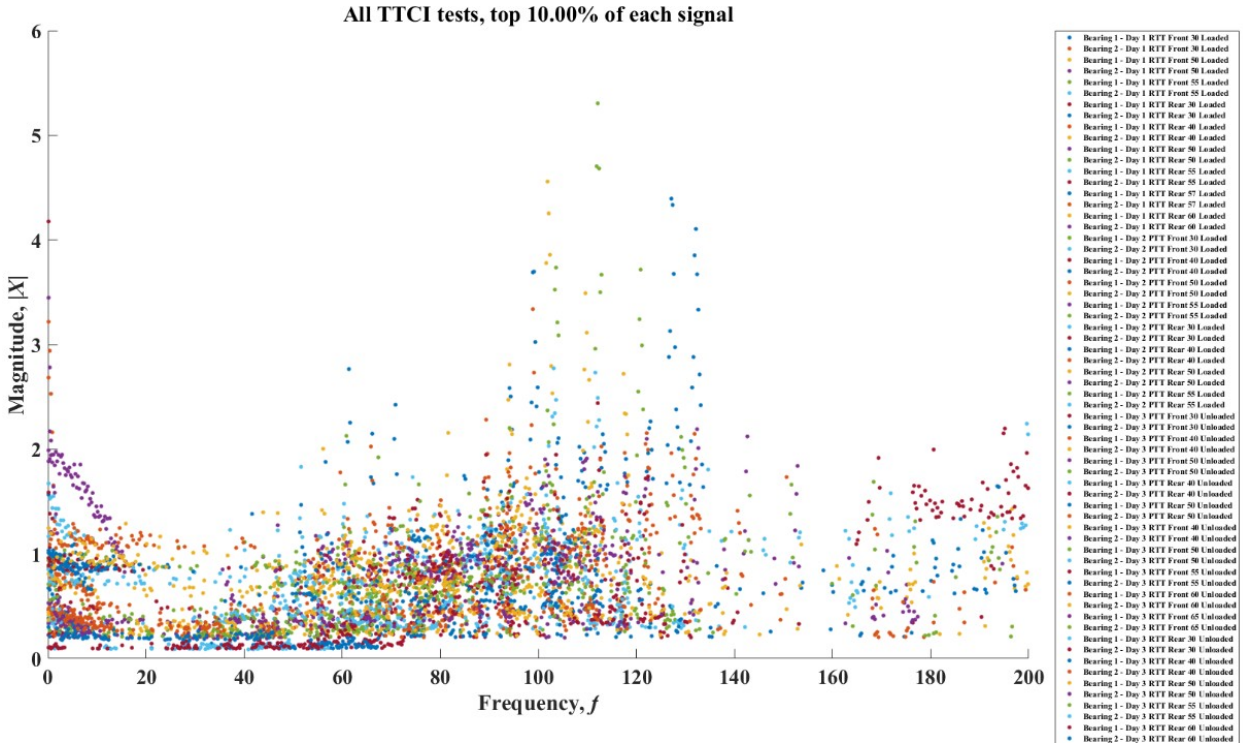

Figure 22. Top 10% of frequencies experienced by each bearing.

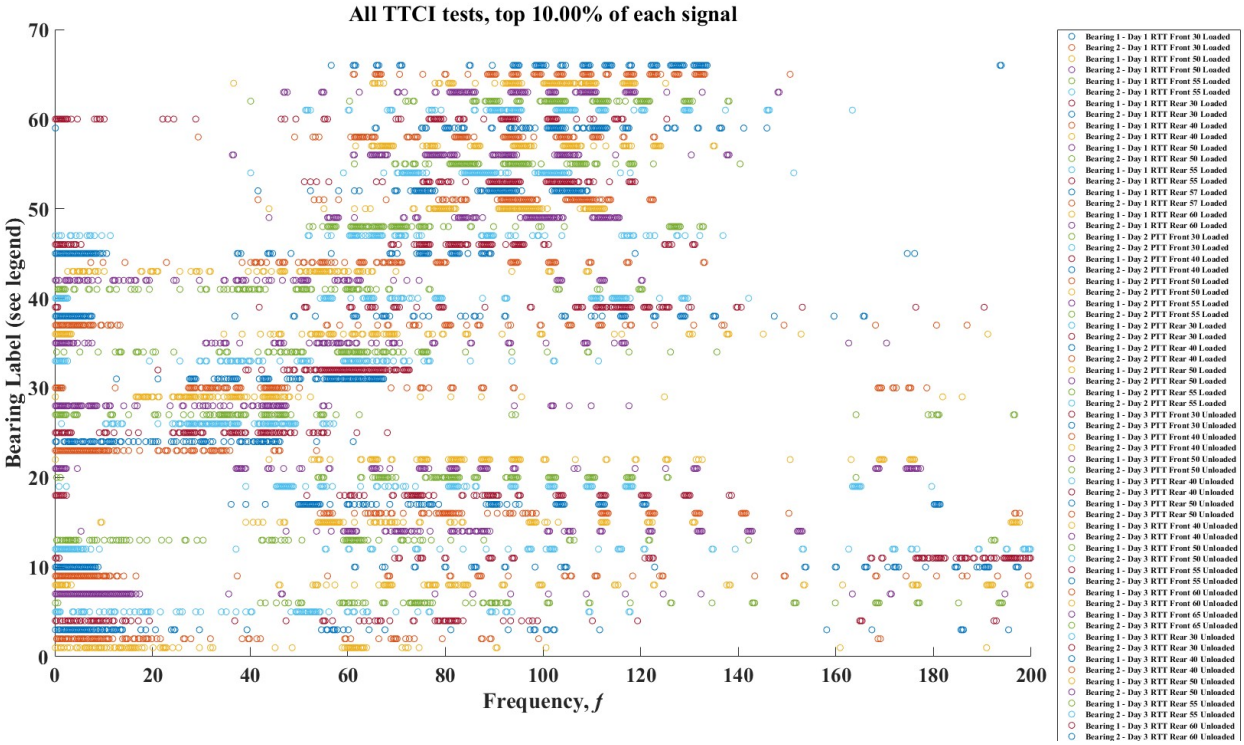

Figure 23. Top 10% of frequencies experienced by each bearing, reorganized.

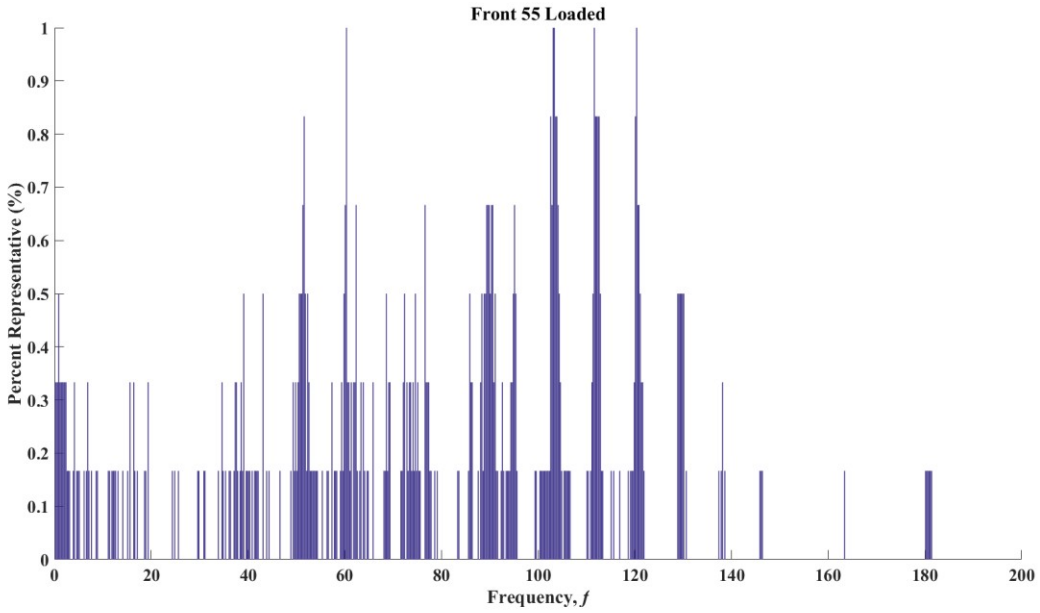

Figure 24. Commonality among front-measured, 55 mph, fully-loaded railcar bearings.

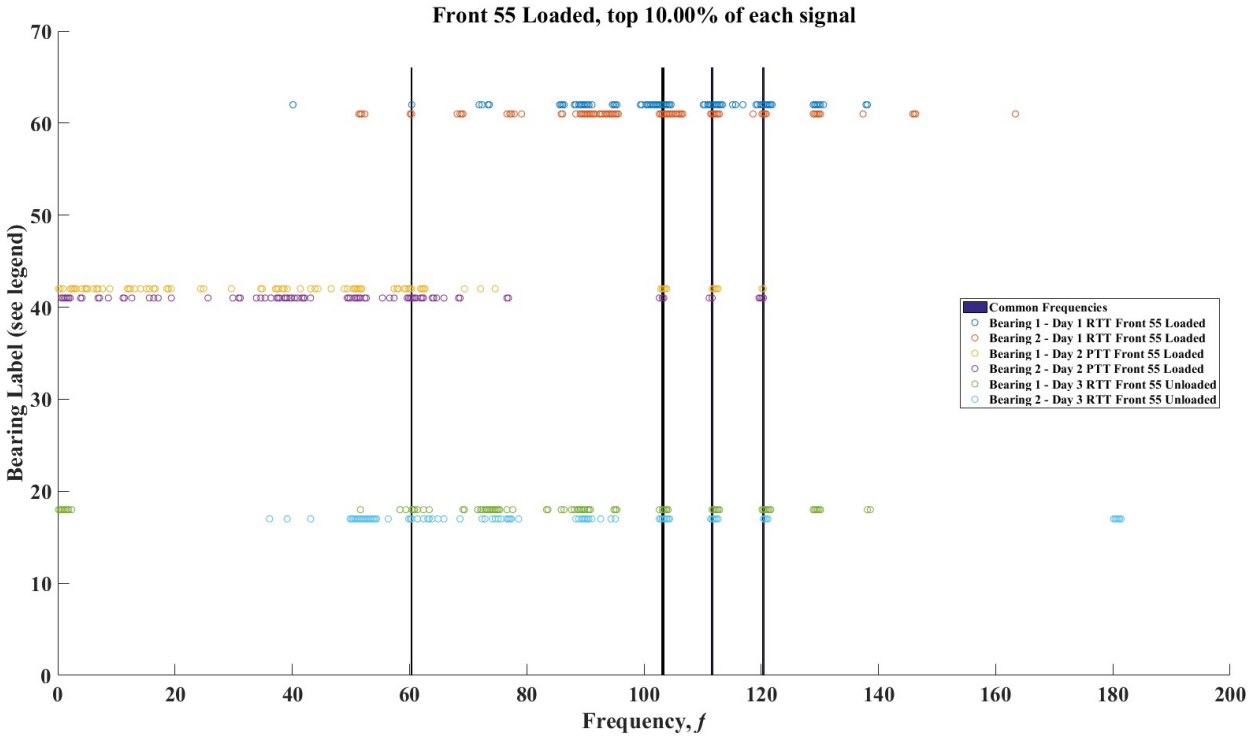

Figure 25. Reorganized front-measured, 55 mph, fully-loaded railcar bearings.

The common top 4% of frequency magnitudes were used to represent the typical frequencies of each speed/load scenario for simulation purposes because two to seven common representative frequencies were found for each scenario. Table 4 describes the frequencies expected to be present for each speed and load condition.

Table 4. Primary frequencies associated with speed/load conditions of freight railcar.

Test Parameters	Common Frequencies (Hz)						
Front 30 Loaded	61.375	66.125	99.125	127.375	127.625		
Front 40 Loaded	81.375	81.875	87.625	88.125			
Front 50 Loaded	46.875	93.625	94.125	101.625	101.875		
Front 55 Loaded	51.625	103.125	111.625	111.875	112.375		
Front 30 Unloaded	55.875	57.125	61.875	62.125	62.375		
Front 40 Unloaded	0.125	37.375	37.625	75.125	81.375	87.625	
Front 50 Unloaded	46.875	94.125					
Front 55 Unloaded	103.125	103.375	103.625	103.875	111.625	111.875	112.125
Front 60 Unloaded	112.375	112.625	112.875	131.125	196.625		
Front 65 Unloaded	60.875	61.625	71.125	121.625	142.125		

CHAPTER V

TESTING PROCEDURES AND RESULTS

5.1 Experimentation Setup

Although the initial trials were instrumental in providing information about methods, process and strategy in building a generic energy harvester, the aim of this thesis has been to test the feasibility of a vibrational energy harvester instrumented into a bearing adapter. A bearing adapter was machined, in agreement with the specifications of the FEA simulation performed earlier and described at the end of Chapter III. The modifications are pictured in Figure 26.

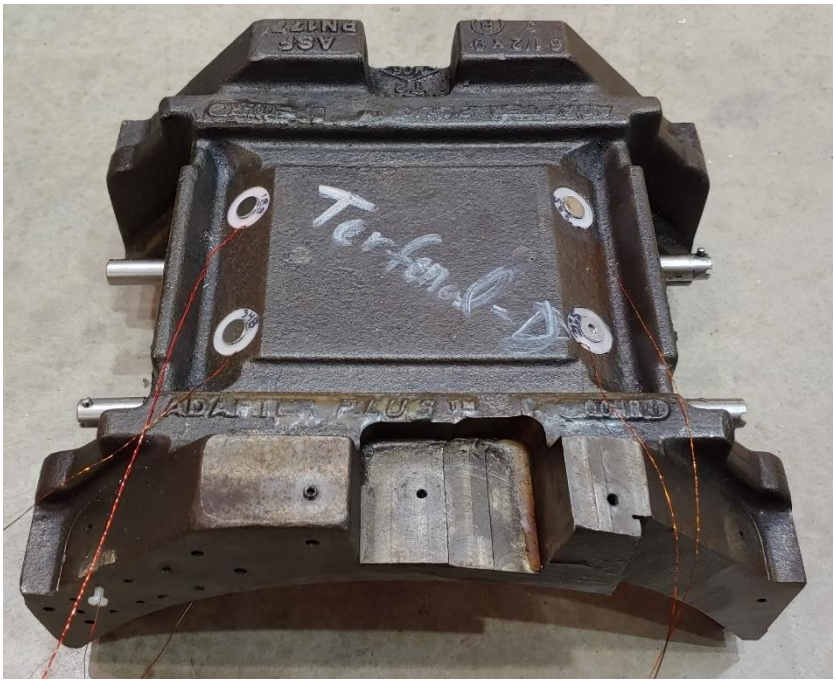

Figure 26. Bearing adapter machined to incorporate four energy harvesting fixtures.

The signals of interest in this experiment are those of the energy extracted by each of the Terfenol-D fixtures, the force supplied by the MTS, and a coincident time scale. Concerns about the fragility of the coil leads when a 20-kip load is applied prompted machining a protective channel within the bearing adapter as shown in Figure 27. Heat shrink was applied to the leads to improve protection, shown in Figure 28. Fixtures are numbered 1 through 4 for reference, progressing clockwise from the bottom left to the bottom right.

Figure 27. Machined channels providing an exit for the coil leads.

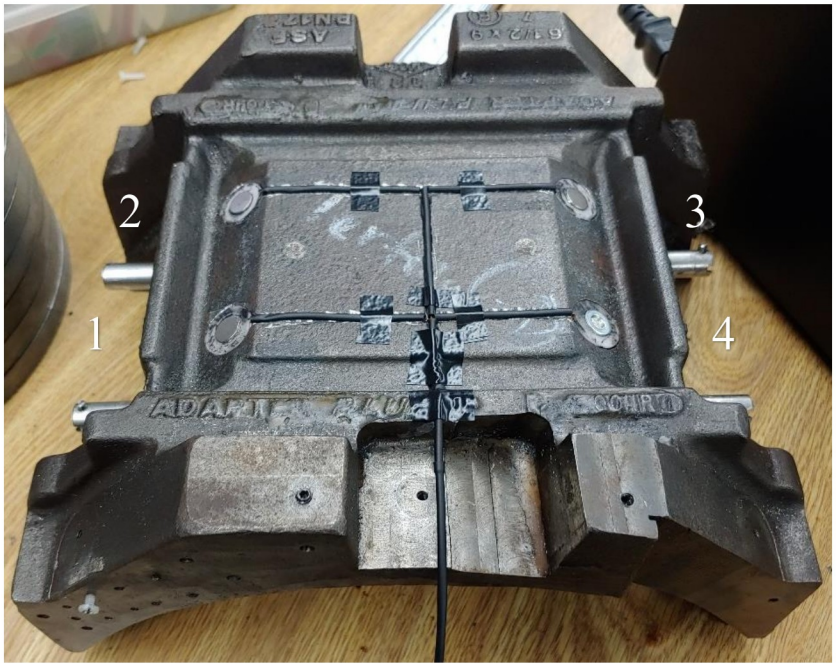

Figure 28. Energy harvesting fixtures implemented and coil leads protected.

Each fixture is built within the cylindrical portions removed along the interlocks. From bottom to top, the bearing adapter is in contact with the first magnet, then the thin Permalloy film, the Terfenol-D rod, a second Permalloy layer, and the final magnet which contacts the polymer pad of the bearing adapter. Surrounding the Terfenol-D rod is a Delrin spool with magnet wire spooled around it. The gauge of wire, number of turns, and measured coil resistance for each coil are listed in Table 5.

Table 5. Coil details for final setup.

Coil	AWG	Number of turns	Resistance (ohm)
1	30	383	15.27
2	30	348	13.14
3	30	364	14.38
4	30	371	13.72

Each fixture within the bearing adapter required material removal to a depth of 0.3625 inch (9.21 mm) with a bore diameter of 0.75 inch (19.05 mm). The Terfenol-D cores were

measured to have a length of 0.300 inch (7.62 mm) with a diameter of 0.393 inch (9.98). The Delrin spool was then machined to specifications provided in Figure 29. Each spool was hand-wound with 30 AWG wire.

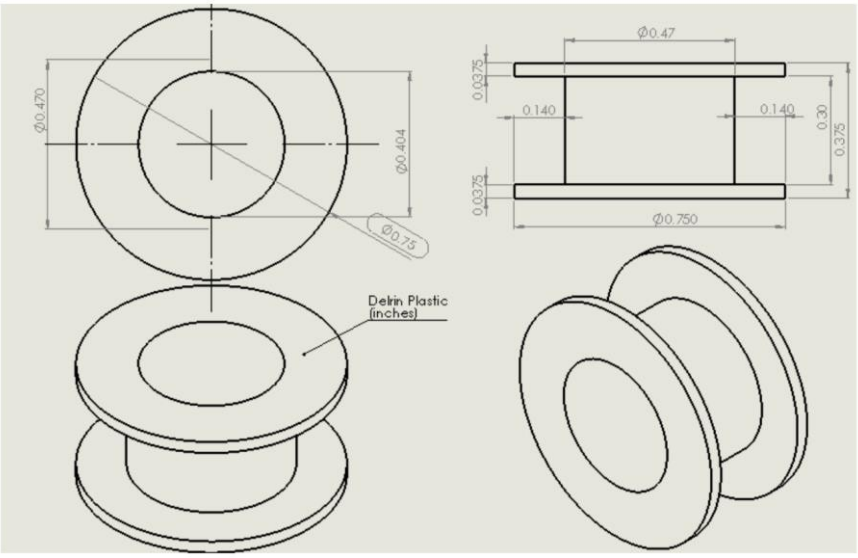

Figure 29. Delrin spool dimensions in inches.

The utilization of a new Terfenol-D rod required the recalculation of appropriately sized magnets to improve energy harvesting potential. An experimental cyclic load test was performed with the Terfenol-D rod and Delrin spool to be used in the bearing adapter. The fixture was compressed in a sinusoidal fashion between 50 and 950 lb at a load rate ranging from 10 lbs/sec to 120 kips/sec. The resulting peak-to-peak voltage, as shown in Figure 30, is maximized when using either the 1085 Gauss or 1217 Gauss magnets, but the 1217 Gauss magnets produced better results at most of the load rates. The magnets are 3/8-inch diameter by 1/32-inch thick. They are N52 neodymium discs with axial magnetization. They have a listed maximum operating temperature of 80-degrees Celsius.

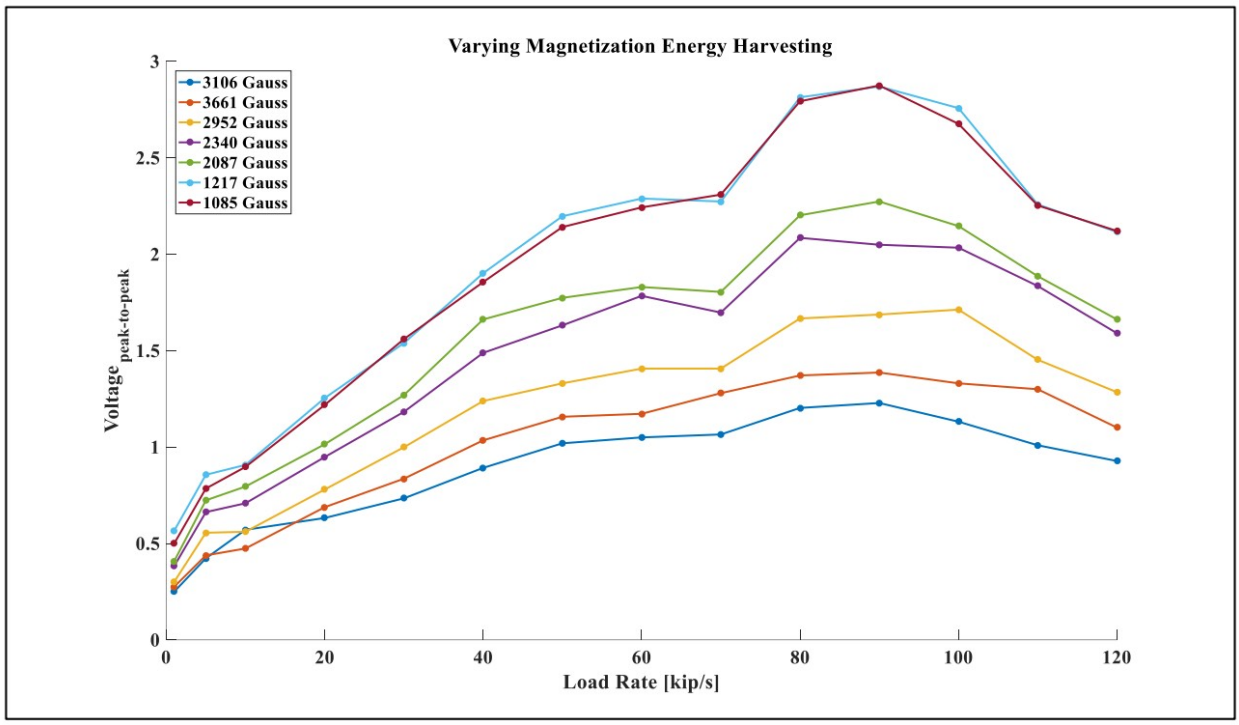

Figure 30. Varying magnetization energy harvesting.

The experimentation setup is depicted in Figure 31. The instrumented adapter is used to test all four Terfenol-D energy harvesting fixtures simultaneously. The bearing adapter is supported underneath by a modified bearing hemisphere and above by an I-beam with additional support flanges. As before, the leveling platen was used to ensure the test remained aligned properly. The DAQ was wired to measure the Terfenol-D signals for the three coils in locations 1, 2 and 3 along with the force applied by the MTS. The fourth coil was unable to be included because the DAQ restricted measurement to four signals at a time, and the output from the MTS was required to relate each signal to the appropriate frequency. Each coil is placed in parallel with a resistive load of 12 ohms for maximum power transfer, determined empirically from placing different loads until the voltage measured from the coil is halved.

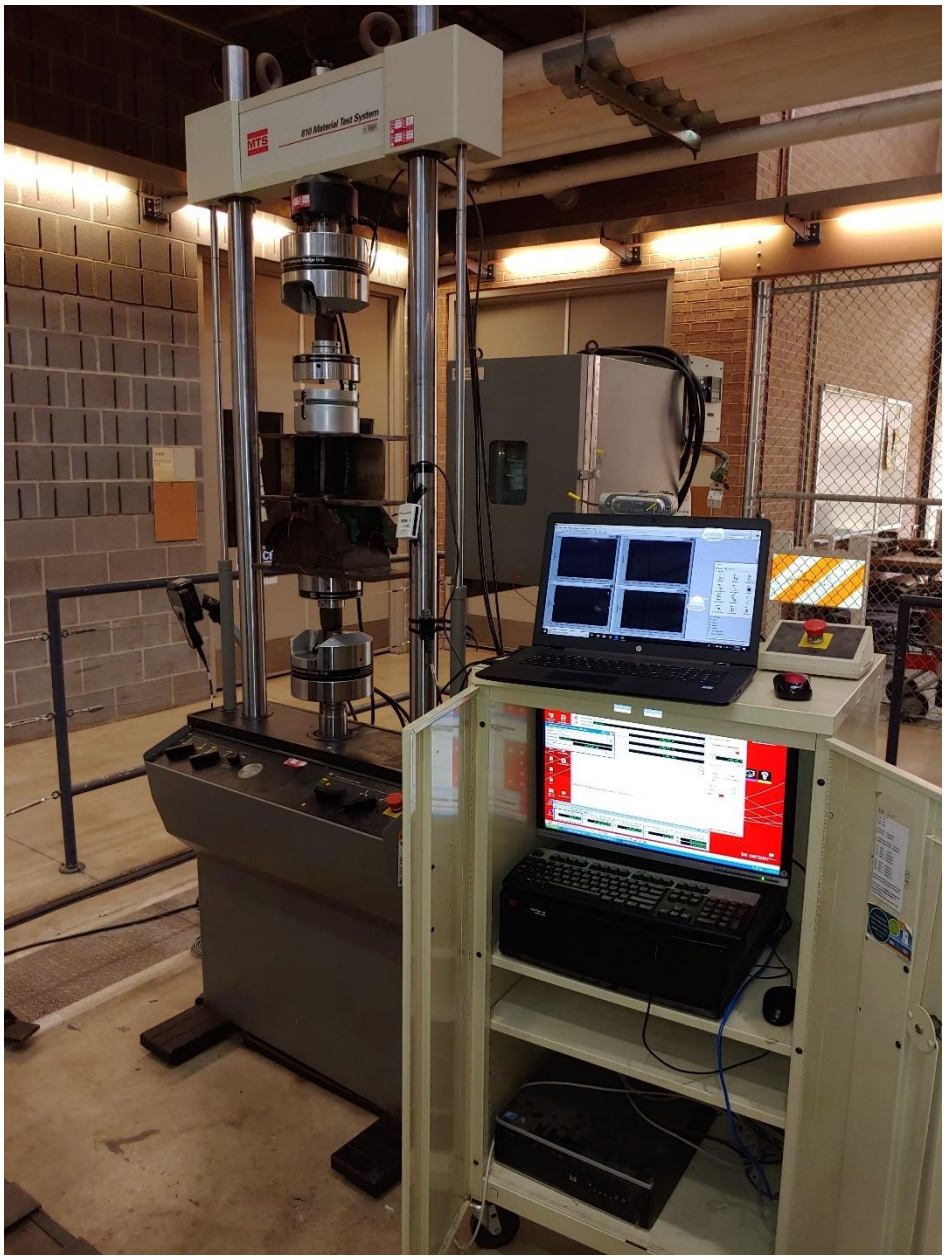

Figure 31. Experimentation setup.

5.2 Test Development and Trials

To perform an experiment based on the compressive force of a fully-loaded car vibrating as a function of time, the MTS system was programmed using the MultiPurpose TestWare software. A primary limitation of using the MTS to perform the experiments is that the maximum applied compressive load possible is 20 kips. Ideally, the test would be performed

with parameters mimicking a fully-loaded train at 34,400 lbs (153 kN) per bearing. Nevertheless, testing with this limitation would provide conservative results. The energy harvesting capability of the system should be increased with load and with frequency.

5.2.1 Force function

To expand the implementation of the simulation to an experimental test on the MTS, a function was developed that would define the compressive force applied as a function of time. In other words, the frequency and phase information were used to develop a function that represented the relative importance of the frequency content desired. Using the method outlined in Appendix B, the constant load and dynamic load values were used to express this function as a force changing with time. An FFT analysis of the developed input function showed congruence between the input function and the desired frequency content. However, upon analysis of the data, the energy harvested was negligible. On further inspection, the MTS was found to be incapable of producing the force magnitude demanded by the test. Figure 32 presents a comparison of the input force function defined and the actual force output applied by the MTS. Although the general shape of the function is accurately followed, the magnitude is not consistently reached. This experiment was conducted with the original Terfenol-D fixture, and the strategy was intended to expand to use with the instrumented adapter if successful. However, the MTS's failure to follow the force function as prescribed was seen as an insurmountable obstacle to the function's continued use.

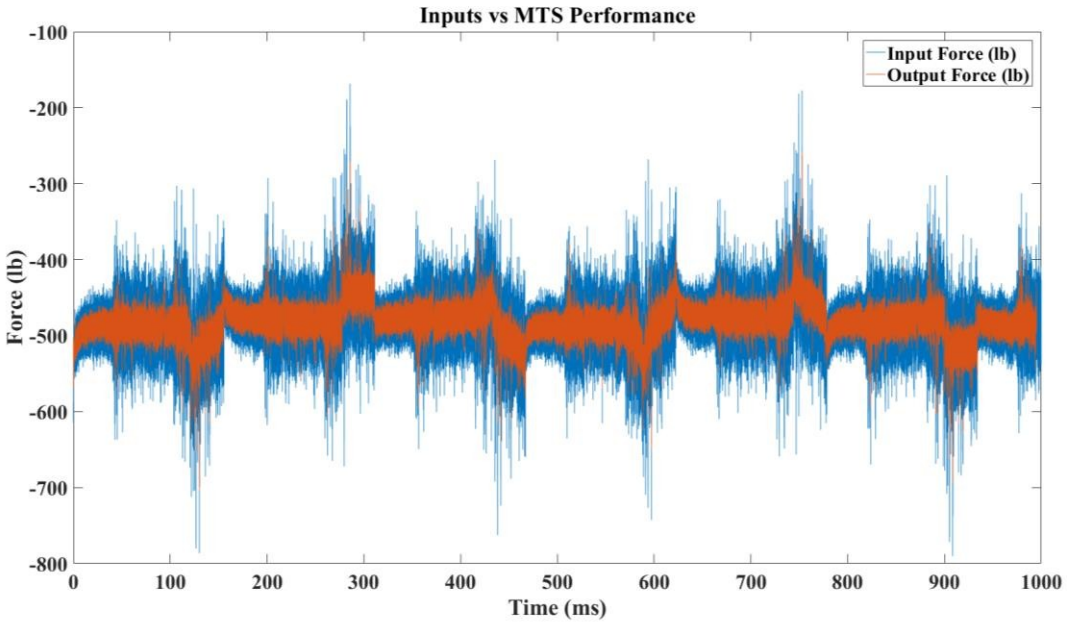

Figure 32. Comparison of input and output forces using force function method.

5.2.2 Built-in Sine Function Frequency

In the initial trial experiments, the MTS could reach significant loads and frequencies using the built-in sine function programmable commands. Although this strategy neglects the influence of wave interference typical in a complex natural environment, the ability to execute a command as defined is important as well. This method allows for the testing of specific frequencies, where the minimum and maximum forces are defined. For this experimental method, the compressive load is centered at 10 kips with an amplitude of 9,950 lbs. A pre-stress of 10 kips is held for fifteen minutes before beginning the experiment, then each frequency is tested for five seconds, in increasing order. The frequencies tested in this manner are listed in Table 6. The load profile as measured from the output of the MTS is plotted in Figure 33.

Table 6. Frequencies tested on the MTS.

Frequencies tested (Hz)						
0.13	3.14	8.56	19.83	33.05	60.88	101.63
0.66	3.49	9.34	20.00	34.00	61.38	101.88
0.75	3.72	10.12	21.00	35.25	61.63	103.13
0.85	3.83	10.30	22.00	36.35	61.88	103.38
0.94	3.90	10.89	23.00	37.38	62.13	103.63
1.03	4.18	11.00	23.13	37.63	62.38	103.88
1.13	4.53	11.67	24.00	39.66	66.13	111.63
1.22	4.61	12.00	25.00	42.96	71.13	111.88
1.32	4.67	12.45	26.00	43.75	75.13	112.13
1.50	4.88	13.00	26.44	46.27	75.38	112.38
1.69	5.23	13.32	27.00	46.88	81.38	112.63
1.75	5.45	14.00	28.00	49.57	81.88	112.88
1.88	5.58	15.00	29.00	51.38	87.63	121.63
2.07	5.97	16.00	29.74	51.63	88.13	127.38
2.09	6.22	16.56	30.00	52.88	93.63	127.63
2.26	7.00	17.00	31.00	55.88	94.13	131.13
2.44	7.78	18.00	32.00	56.56	99.13	142.13
2.79	8.30	19.00	33.00	57.13	101.38	196.93

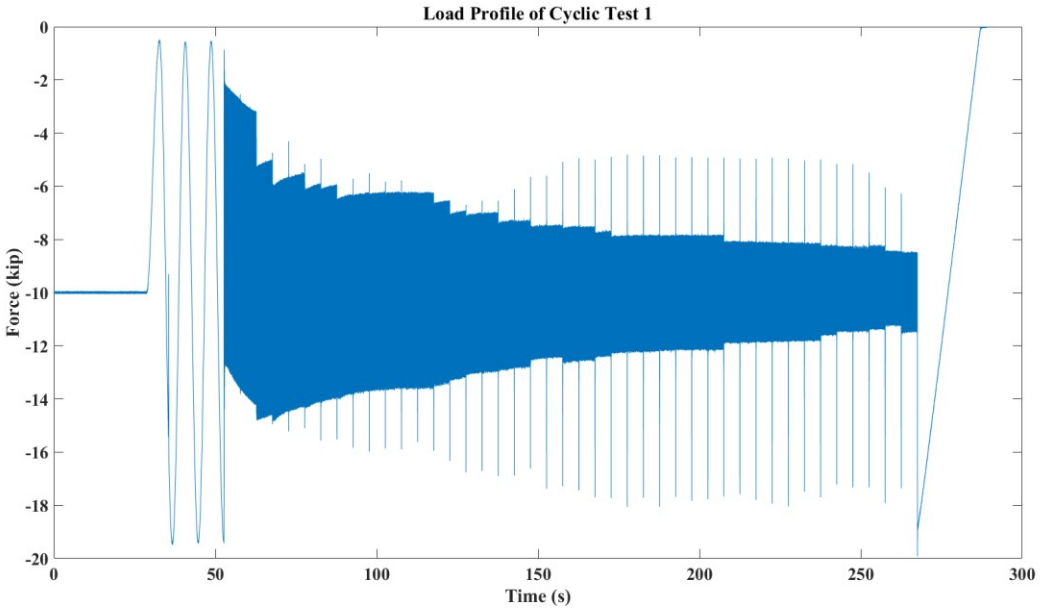

Figure 33. Load profile followed for first set of frequencies tested.

CHAPTER VI

CONCLUSIONS AND FUTURE WORK PROPOSED

6.1 Test Limitations

The maximum applied load possible with the MTS machine is 20 kips, which is about 60% of the load experienced by one bearing in a static, fully-loaded railcar. The load seen by a dynamic railcar may be 70% higher than its static load, making the 20-kip load roughly 35% of the maximum loads possible for a fully-loaded railcar. Nevertheless, this is a conservative approach and is acceptable if a minimum threshold of energy harvesting can be accomplished. The MTS, however, also has a load-rate limitation; an increase in frequency can be accomplished only with a simultaneous decrease in force amplitude, as shown in Figure 34. This is not desirable, as each test reflects a change in amplitude and frequency instead of frequency alone. Figure 34 represents the data from Figure 33 with the deletion of one second of transition time between tests, then color coordinated for clarity. Removing the transition peaks more clearly shows the reduced load amplitudes. An alternate representation, shown in Figure 35, plots the force amplitude against the frequency tested; all frequencies are intended to maintain a force amplitude of 9500 lb. Testing all frequencies at a lower amplitude is also avoided, as the load is already limited to 60% of the maximum, and tests performed at 17% load would reflect the load applied by empty freight cars. Although it is impossible to compare the results from frequency to frequency with constant load amplitude, the results will be more meaningful if a conservative

estimate of the best energy harvesting available is attempted. Therefore, the tests are continued despite these limitations.

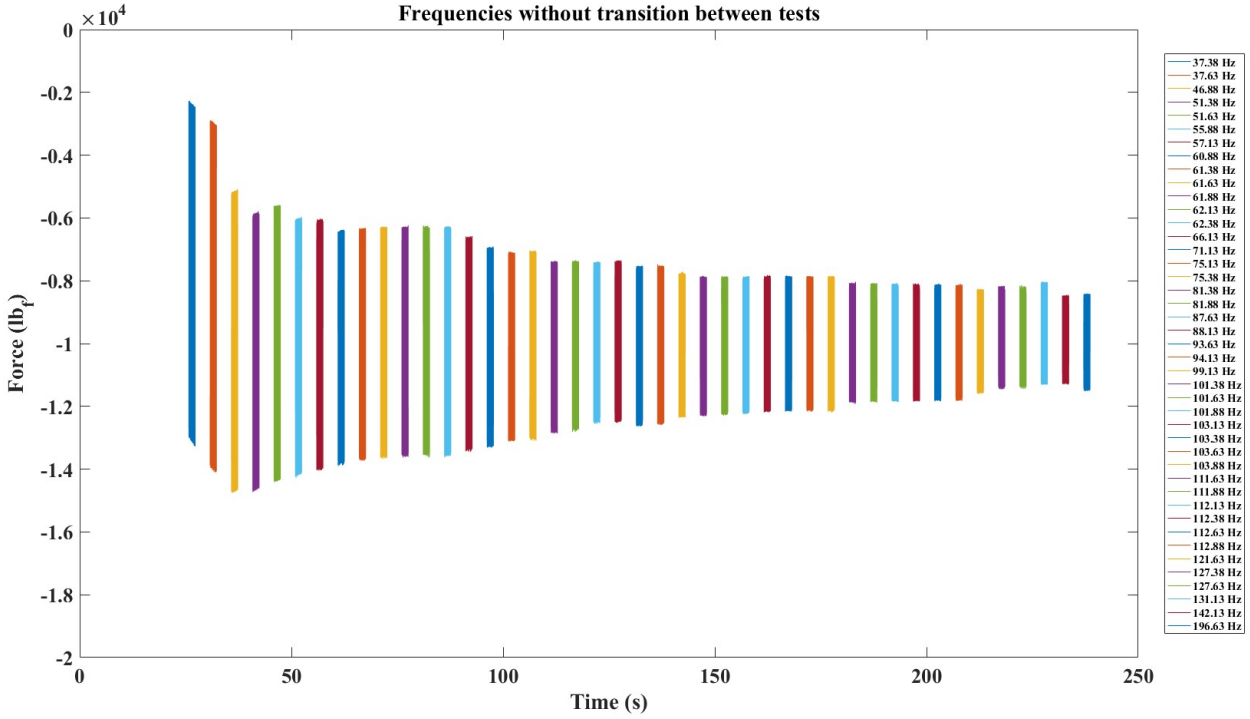

Figure 34. Unintended decrease in force amplitude.

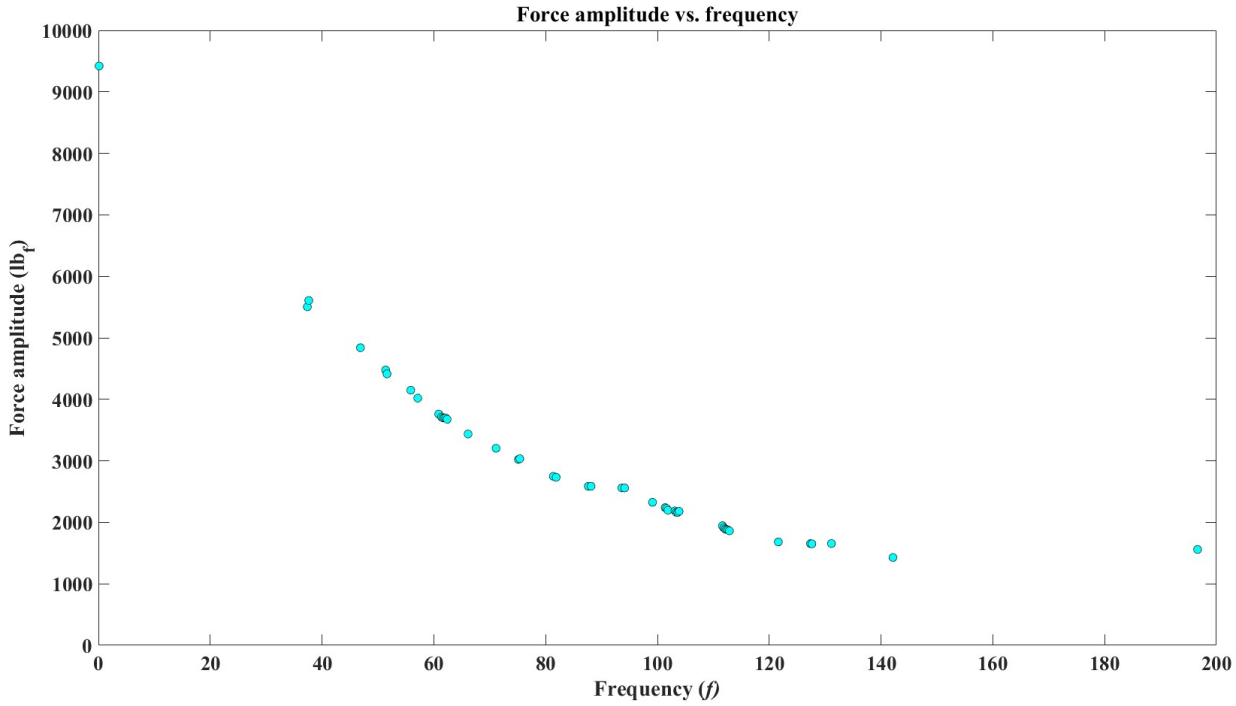

Figure 35. Force amplitude versus frequency.

6.2 Test Results

The load profiles that were followed for all three tests are shown in Figures 36, 37 and 38. The load profiles do not show the pre-stress portion of the experiment where, for 15 minutes, the experiment was held under a load of 10 kips. For all three tests, as the frequency increases, the MTS is unable to meet the desired force amplitude. The power output that is associated with each scenario is calculated as:

$$P = \frac{V^2}{R} \tag{2}$$

where V is the voltage across the leads of the coil and R is the resistive load applied. Figures 39, 40 and 41 show the instantaneous and multi-cycle average power output of three energy harvesting fixtures as the force profile is executed.

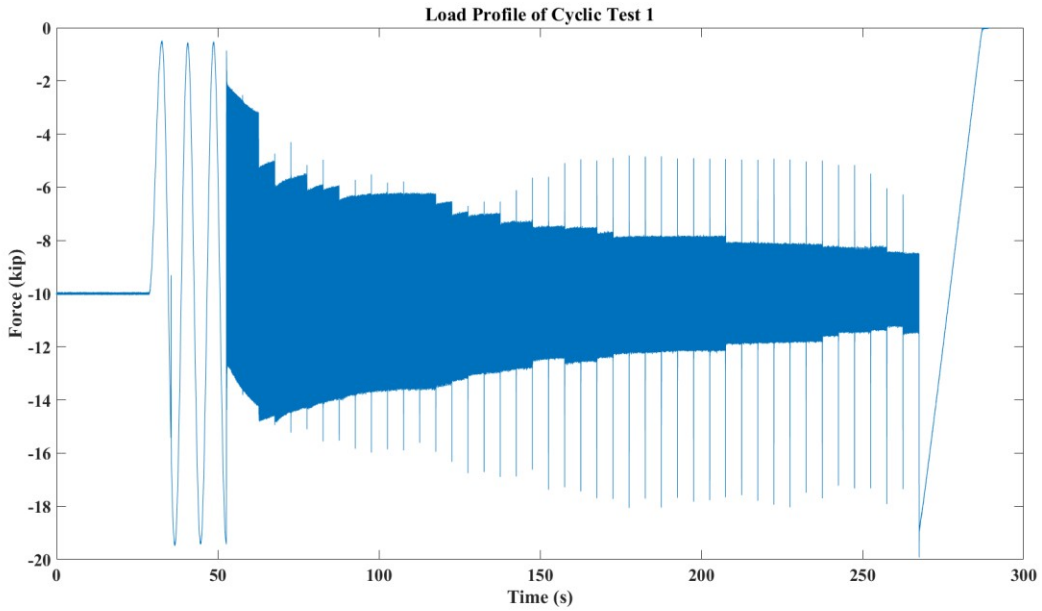

Figure 36. Load profile of cyclic test 1.

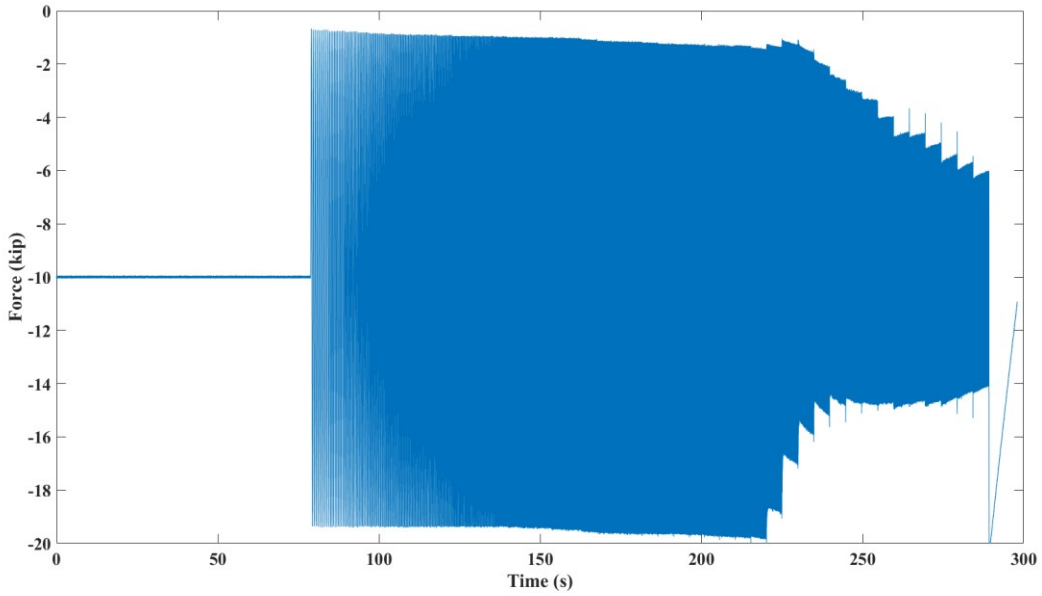

Figure 37. Load profile of cyclic test 2.

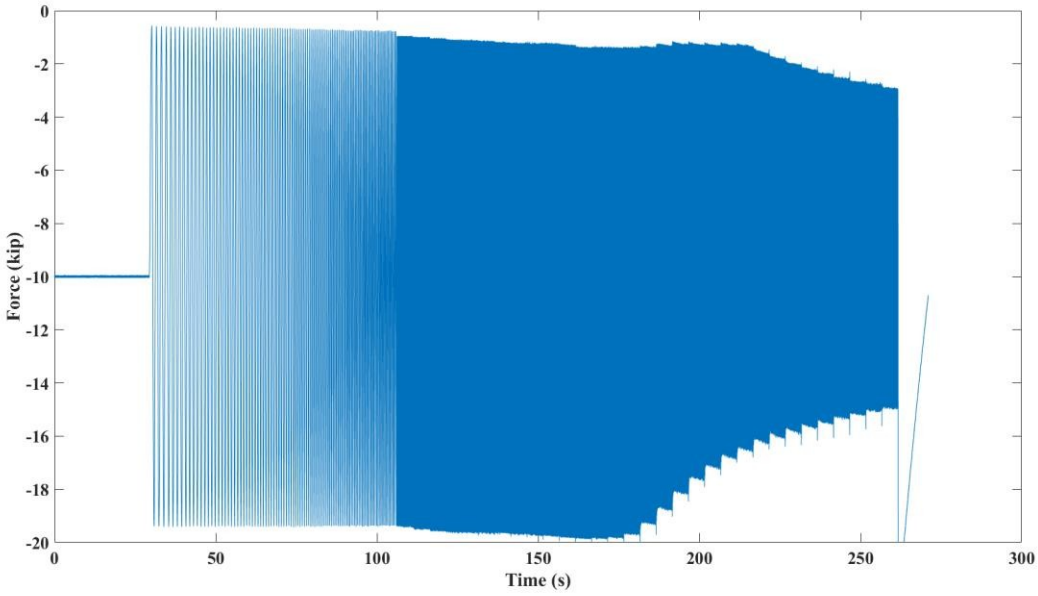

Figure 38. Load profile of cyclic test 3.

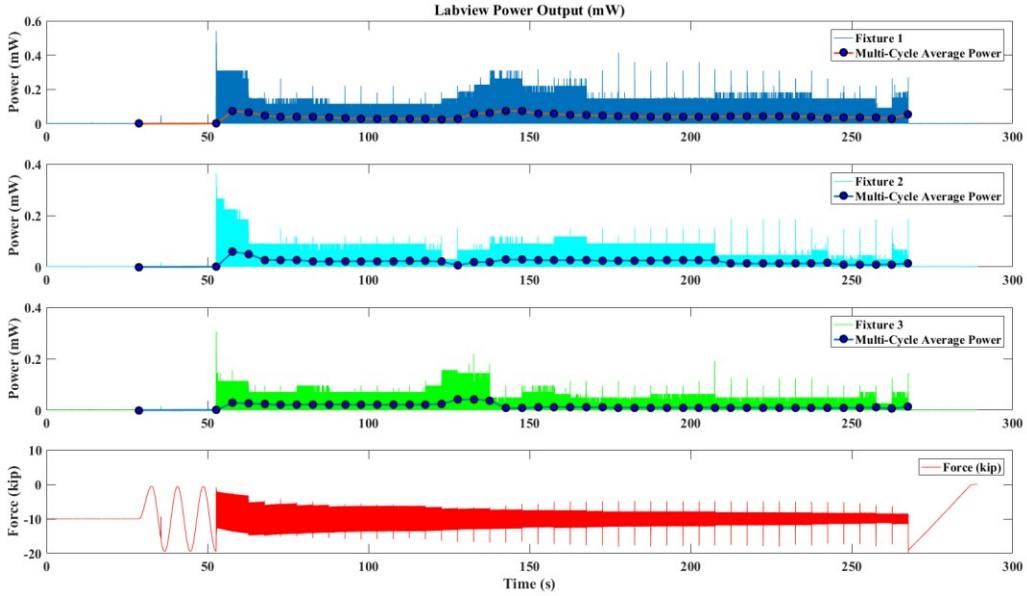

Figure 39. Power output from cyclic test 1.

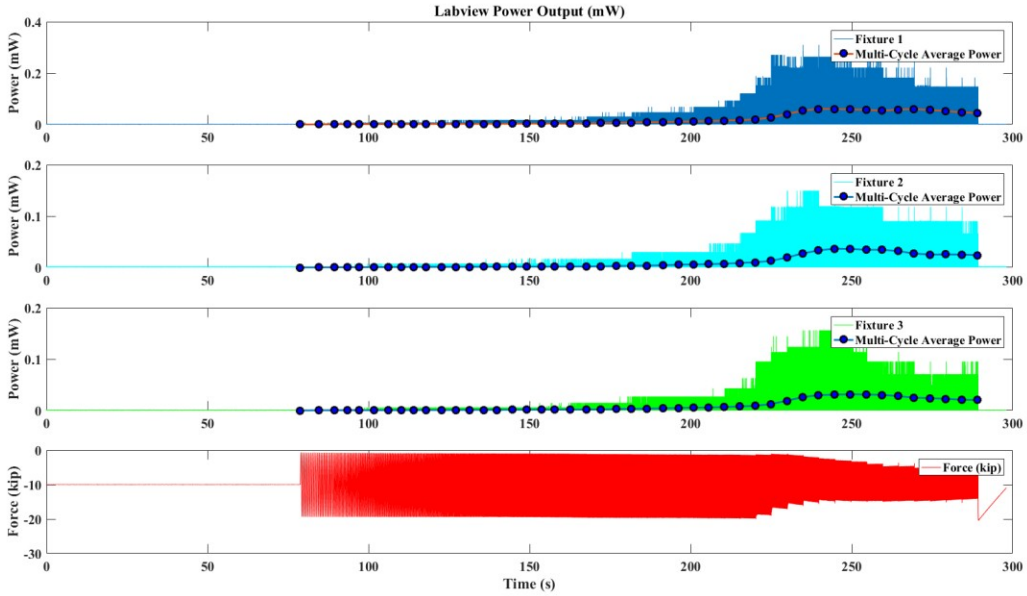

Figure 40. Power output from cyclic test 2.

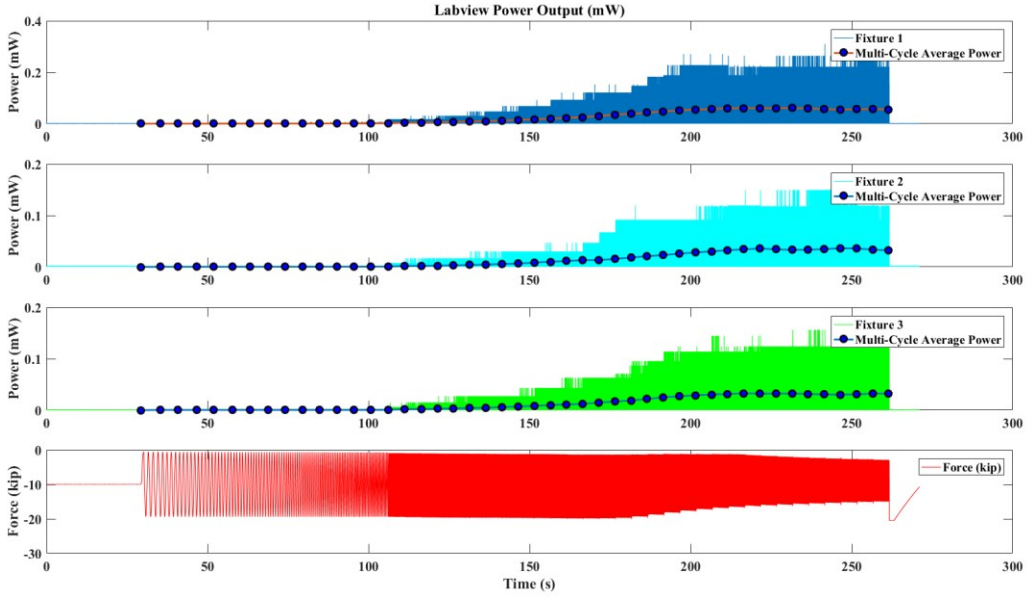

Figure 41. Power output from cyclic test 3.

The multi-cycle average power as a function of frequency is shown in Figure 42, in which the cyclic tests are graphed together as well. Each cyclic test proceeded from low frequency to high frequency. A table of the power calculations is given in Appendix D.

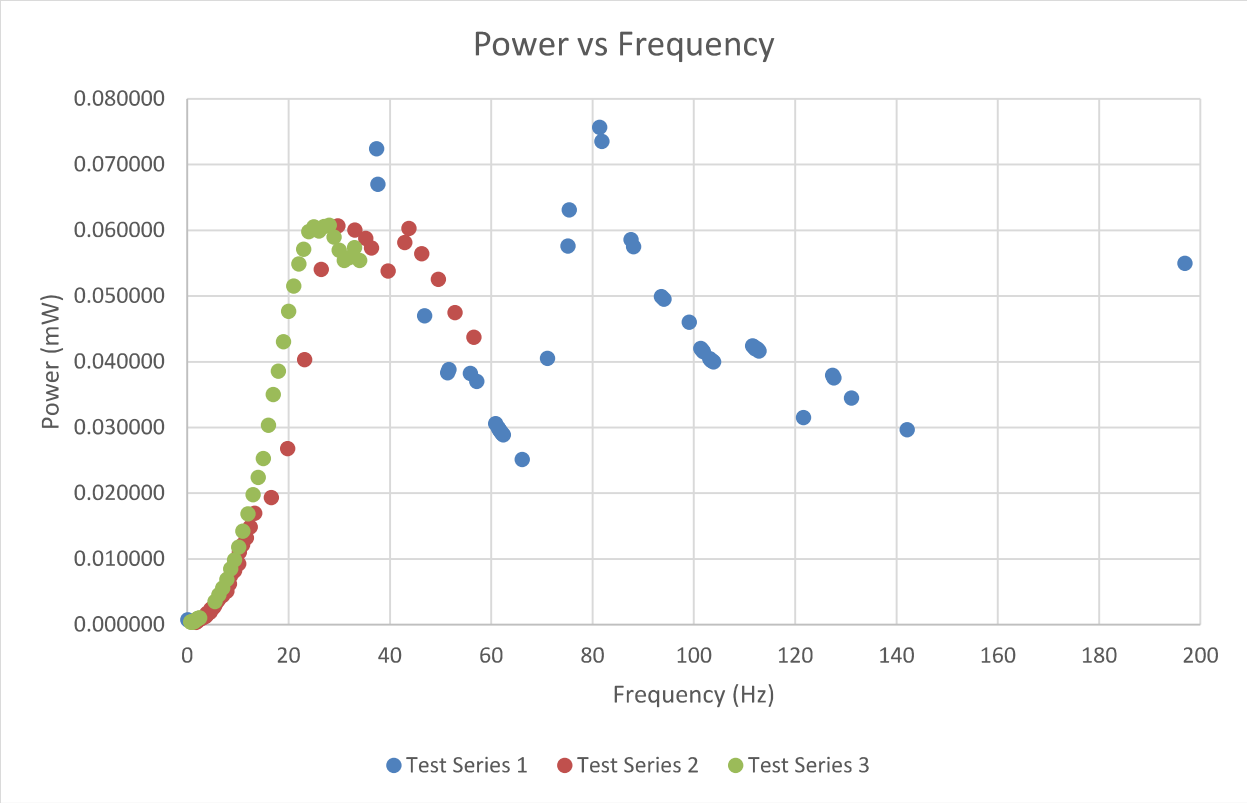

Figure 42. Power versus frequency for all three tests.

Additionally, frequencies associated with certain speed-load conditions are illustrated in Figure 43. With the exception of one very low frequency, each of the characteristic frequencies produce an average power of at least 25 μW. The frequencies associated with a loaded vehicle are not necessarily producing higher power than the unloaded case. This is governed by the magnitude related by the Fourier transform. A loaded car tends to experience less noise, and therefore, although the loaded and unloaded vehicles may have similar characteristic peaks, the consistency with which the loaded vehicle will be excited by a representative frequency is higher. Table 7 lists the power associated with each representative frequency.

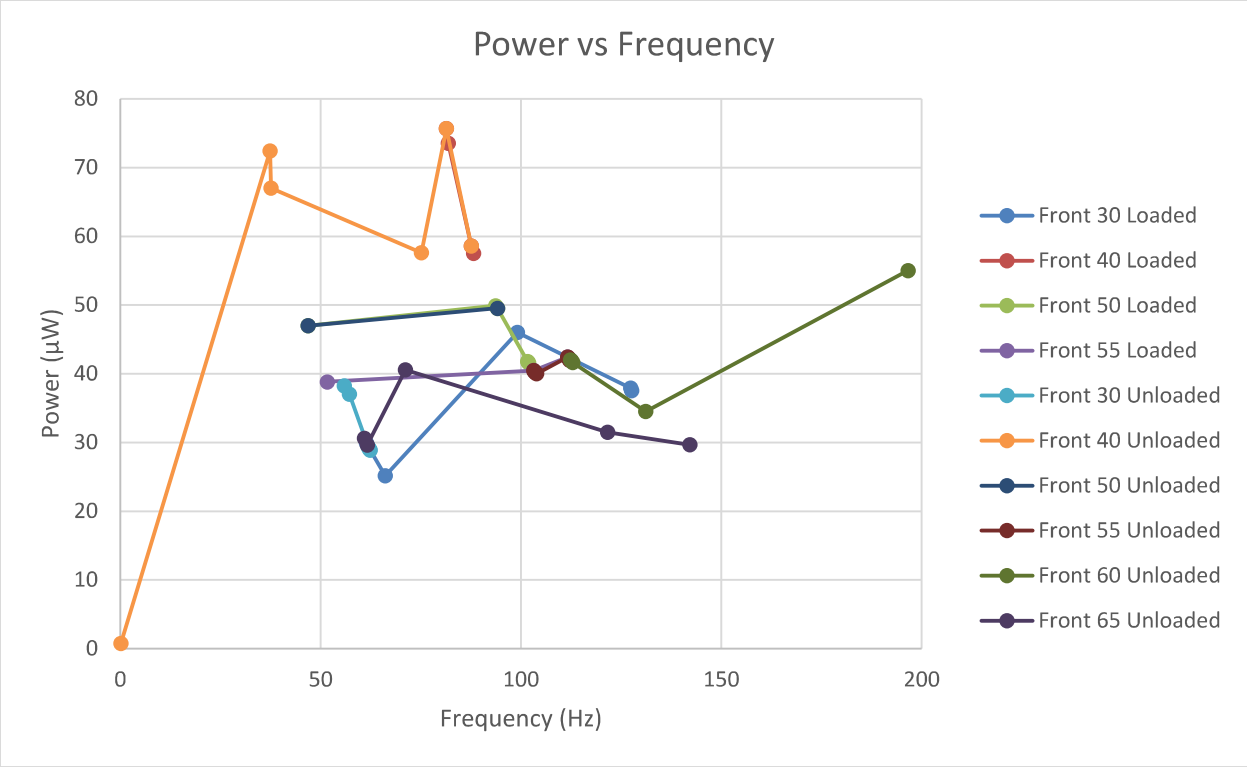

Figure 43. Power versus frequency for representative frequencies.

Table 7. Power extracted by representative frequencies.

Test Parameters	Common Frequencies (Hz) Power (μW)						
Front 30 Loaded	61.375 29.95	66.125 25.15	99.125 46	127.375 37.92	127.625 37.53		
Front 40 Loaded	81.375 75.65	81.875 73.53	87.625 58.59	88.125 57.51			
Front 50 Loaded	46.875 46.98	93.625 49.89	94.125 49.51	101.625 41.79	101.875 41.57		
Front 55 Loaded	51.625 38.81	103.125 40.45	111.625 42.41	111.875 42.29	112.375 42.02		
Front 30 Unloaded	55.875 38.24	57.125 37.01	61.875 29.35	62.125 29.07	62.375 28.87		
Front 40 Unloaded	0.125 0.752	37.375 72.41	37.625 67	75.125 57.62	81.375 75.65	87.625 58.59	
Front 50 Unloaded	46.875 46.98	94.125 49.51					
Front 55 Unloaded	103.125 40.45	103.375 40.25	103.625 40.15	103.875 39.99	111.625 42.41	111.875 42.29	112.125 41.98
Front 60 Unloaded	112.375 42.02	112.625 41.9	112.875 41.65	131.125 34.5	196.625 55		
Front 65 Unloaded	60.875 30.6	61.625 29.63	71.125 40.54	121.625 31.5	142.125 29.66		

6.3 Conclusions

The power produced by the test is a function of the frequency and the force amplitude, among other variables. The inability to control the variables posed a significant challenge. Nevertheless, the fixtures were able to produce some power. Cyclic tests two and three did not produce any notable power until the frequency of 10 Hz was surpassed. This is typical of harvesting energy from a magnetostrictive energy harvester. A further increase in frequency was accompanied by a smaller force amplitude. The power produced with increasing frequency was higher in some cases, and lower in others, but generally did not change much. This could be due to the resonant and harmonic frequencies of the system, or the energy harvesting potential could

be tied to the load rate of the Terfenol-D. Figure 42 suggested that the order in which the frequencies were tested may contribute to the energy harvested, indicating the pre-load or stress state of the material may be a more important factor than originally recognized. Alternatively, the internal components within the fixture may have changed, such as increased fracture of the coordinating magnets, rendering subsequent tests representative of different initial conditions.

The average energy harvested from each fixture was roughly 36.3 μW, while the maximum instantaneous power was 0.53 mW. An energy supply of 0.5 mW would be sufficient to run some forms of low-powered electronics. Although the results are not conclusive, they suggest that the proposed system can provide sufficient energy to power the onboard monitoring system, so long as some minor modifications are implemented.

6.4 Future Proposed Work

An instrumented bearing adapter used in a field service test, similar to the 2015 TTCI tests, would ideally prove the practicality of utilizing this type of energy harvesting system.

Some limitations and issues were encountered that could also be the topic of future study. The magnets used to guide the magnetic field through the fixture may not be serviceable in their intended use. Removing the setup after test completion showed the magnets had sustained some damage. Figure 44 depicts the removal of a fixture post-test, where cracks can be seen on the magnets. The Terfenol-D and the fragile coils did not appear to sustain any damage. The magnetism as a function of load was not investigated. The magnets, in service, be subjected to heat which could adversely affect the magnet's potency. It is possible the magnets' failed integrity reduced the energy that was harvested from the system.

Permalloy did prove to be a useful protective film, preventing damage to the Terfenol-D rods without sacrificing much power. The limitations of the Terfenol-D with this lubricant in place is promising.

The Terfenol-D pieces were able to harvest different levels of energy, although it was expected they should be roughly the same. This may be a manufacturing issue, or there may be other confounding variables that were not investigated.

Lastly, including a ferromagnetic cap in the fixture may ameliorate the low output power produced by the experiment, as it would help complete the electromagnetic circuit of the energy harvester.

Figure 44. Post-test damage to magnets.

REFERENCES

[1] "Freight Rail Overview." [Online]. https://www.fra.dot.gov/Page/P0362. [Accessed 3 March 2019].

[2] "Freight Rail and Intermodal." [Online]. https://www.aar.org/issue/freight-rail-intermodal/. [Accessed 3 March 2019].

[3] "Predicting Hot Box Detector Failures," *Predikto*. [Online]. Available: https://www.predikto.com/download/Predikto_CaseStudy_Railroad_HBD.pdf [Accessed 10 Oct 2018].

[4] Fry, G. "AAR Strategic Research Iitiatives Program to Improve Safety and Efficiency." Transportation Technology Center, Inc., 2017.

[5] "Trackside Acoustic Detection System. [Online]. https://aar.com/pdfs/TADS_OnePager.pdf [Accessed 3 March 2019].

[6] Aranda, James Alexandro, Radiative Heat Transfer Analysis of Railroad Bearings for Wayside Thermal Detector Optimization. Master of Science in Engineering (MSE), December, 2018, pp. 85.

[7] "Federal Railroad Administration Office of Safety Analysis." [Online]. Available:https://safetydata.fra.dot.gov/OfficeofSafety/default.aspx [Accessed 10 Feb 2017].

[8] Tabbachi, J.G., Newman, R.R., Leedham, R.C., Purta, D.A., Madered, G.G., Galli, R. "Hot Bearing Detection with the SMART-BOLT." *Proceedings of the 1990 ASME/IEEE Joint Railroad Conference*, p. 105-10. 1990. Print.

[9] D. Barke and W. K. Chiu, "Structural health monitoring in the railway industry: A review," *Struct. Health Monitor.*, vol. 4, no. 1, pp. 81–93, 2005.

[10] Montalvo, J., Tarawneh, C., and Fuentes, A. "Vibration-based Defect Detection for Freight Railcar Tapered-Roller Bearings." *2018 Joint Rail Conference*. pp. 1-9.

[11] Ruscelli, A.L., Cecchetti, G., Castoldi, P. "Energy Harvesting for On-Board Railway Systems," 2017 5th IEEE International Conference on Models and Technologies for Intelligent Transportation Systems (MT-ITS). 2017. pp. 397-407.

[12] Nurmanova, V., et al. "Feasibility Study on Wind Energy Harvesting System Implementation in Moving Trains." Electrical Engineering. (2018). Pp.

[13] Xie, J., et al. "Performance of Thin Piezoelectric Materials for Pyroelectric Energy Harvesting." *Journal of Intelligent Material Systems and Structures.* Vol. **21**. (2010). pp. 243-249.

[14] Elefsiniotis, A., et al. "Thermoelectric Energy Harvesting Using Phase Change Materials (PCMs) in High Temperature Environments in Aircraft." *Journal of Electronic Materials.* Vol. **43** (6). 2014. pp. 1809-1814

[15] Wang, J., et al. "Modeling on Energy Harvesting from a Railway System using Piezoelectric Transducers." *Smart Materials and Structures.* Vol. **24**. (2015). pp. 1-13.

[16] Woo, M.S., et al. "Study on the Strain Effect of a Piezoelectric Energy Harvesting Molecule." *Ferroelectrics*. Vol. **449**. pp. 33-41.

[17] Deng, Z. and Dapino, M. J. "Review of Magnetostrictive Vibration Energy Harvesters." *Smart Materials and Structures.* **26**. 2017. pp. 1-18.

[18] De Pasquale, G., et al. "Design, Simulation, and Testing of Energy Harvesters With Magnetic Suspensions for the Generation of Electricity From Freight Train Vibrations." *Journal of Computational and Nonlinear Dynamics.* Vol. **7**. 2012. pp. 1-9.

[19] Mori, K., et al. "Characteristics of Vibration Energy Harvesting Using Giant Magnetostrictive Cantilevers with Resonant Tuning." *Smart Materials and Structures*. Vol. **24**. 2015.

[20] Dai, X. "An Vibration Energy Harvester With Broadband and Frequency-Doubling Characteristjcs Based on Rotary Pendulums." *Sensors and Actuators A: Physical.* **241** (2016). 161-168

[21] Estrada, Raul, Applications of Magnetostrictive Materials in the Real-Time Monitoring of Vehicle Suspension Components. Master of Science (MS), December, 2014, pp. 100.

[22] "Terfenol-D". [Online]. http://tdvib.com/terfenol-d/. [Accessed 9 September 2018].

[23] Colussi, M., et al. "Effect of the Loading Rate on the Brittle Fracture of Terfenol-D Specimens in Magnetic Field: Strain Energy Density Approach." *Strength of Materials.* Vol. **48** (6). 2016. pp. 791-800.

APPENDIX A

```
%% TTCI Test Frequency Analysis
% (1) Perform FFT
% (2) Create Figures
% (3) Output to create Excel database
%

clear all; close all; clc;
%path = ['Z:\01 Experiments\2015\ADXL'];
path = ['C:\Users\jahco\Desktop\Work\TTCI Tests\2015\ADXL'];
path = uigetdir(path,'Please select the folder the files are located in');
check = regexp(path, '\');
folder = path(check(4)+1:end);
%folder_name = folder;
folder_name = path(check(8)+1:end);
check3 = regexp(folder, '_');
testday = folder(check3(1)-5:check3(1)-1);                                  %
testing day
track = folder(check3(1)+1:check3(2)-1);                                    %
track type
carend = folder(check3(2)+1:check3(3)-1);                                   %
end of the railcar
tracktype = questdlg('Which track type would you like to analyze?','Track
Type','Smooth','Perturbation','default');
carload = folder(check3(4)+1:end);
speed = folder(check3(4)-2:check3(4)-1);

%% Folder details
switch track
    case 'PTT'
        track_type = 1;
    case 'RTT'
        track_type = 0;
end
switch testday
    case 'Day 1'
        testday_type = 1;
    case {'Day 2','Day 3'}
        testday_type = 0;
end
switch carend
    case 'Front'
        carend_type = 1;
    case 'Rear'
        carend_type = 0;
end
switch tracktype
    case 'Perturbation'
        tracktype_type = 1;
    case 'Smooth'
        tracktype_type = 0;
end
switch carload
    case 'Unloaded'
        carload_type = 1;
```

```
    case 'Loaded'
        carload_type = 0;
end

if carload_type == 1
    load = 17;
else
    load = 100;
end

%% Hunting and Integration Range

progressbar('Parsing through all sample windows...');


%% Import accelerometer data
if track_type == 1
    d = dir([path '\' tracktype '\70gAccelerometerData*.lvm']);
    interim = d.name;
    file = fullfile([path '\' tracktype],interim);
else
    d = dir([path '\70gAccelerometerData*.lvm']);                          %
changes working directory to selected folder and extracts all lvm files
    interim = d.name;
    file = fullfile(path,interim);
end
raw = dlmread(file,'\t',23,0);                                             %
extracts data from file
[m tester] = size(raw);                                                    %
number of accelerometers

%% Parameter set up
SR = 1/0.00018;                                                            %
sampling rate for ADXL


%% ADXL sensitivity
if exist([path '\Sensitivity'],'dir')
    rpath = [path '\Sensitivity'];
    dreset = dir([rpath '\Reset_70gAccelerometerData*.lvm']);
    interim2 = dreset.name;
    creset = dir([rpath '\70gAccelerometerData*.lvm']);
    interim3 = creset.name;
    filereset = fullfile(rpath,interim2);
    filedc = fullfile(rpath,interim3);
    rawreset = dlmread(filereset,'\t',24,0);
    rawresetc = dlmread(filedc,'\t',23,0);
    datareset = rawreset(:,2:tester);
    datadc = rawresetc(:,2:tester);
    sens = (rms(datareset)-mean(datadc))./140;
else
    sens = [.0242 .0242 .0242 .0242 .0242 .0242 .0242 .0242];
end

%% Looping through sample windows
```

```
    for j = 1:(tester-1)
% loops for each accelerometer

        data(1:length(raw(:,j+1)),j) = 0.5*((raw(:,j+1) -
mean(raw(:,j+1))))/sens(j);       % processes data for fourier transform

        x(:,j) = data(1:length(raw(:,j+1)),j) -
mean(data(1:length(raw(:,j+1))));

        progressbar(1/j)
    end

progressbar(1)


figure()
time = (0:1/SR:(m-1)/SR); % sec
if carend_type == 1 && testday_type == 1
        names = {'F-L2-SA' 'F-R1-SA'};
        plot(time,x(:,2),time,x(:,5));
        acc_time_data1 = x(:,2);
        acc_time_data2 = x(:,5);
    elseif carend_type == 1 && testday_type == 0
        names = {'F-L2-SA' 'F-R1-SA'};
        plot(time,x(:,2),time,x(:,3));
        acc_time_data1 = x(:,2);
        acc_time_data2 = x(:,3);
    elseif carend_type == 0 && testday_type == 0
        names = {'R-L4-SA' 'R-R3-SA'};
        plot(time,x(:,2),time,x(:,3));
        acc_time_data1 = x(:,2);
        acc_time_data2 = x(:,3);
    elseif carend_type == 0 && testday_type == 1
        names = {'R-L4-SA' 'R-R3-SA'};
        plot(time,x(:,2),time,x(:,4));
        acc_time_data1 = x(:,2);
        acc_time_data2 = x(:,4);
end
title('ADXL: RMS vs. Time');
xlabel('Time [sec.]');
ylabel('RMS [g]');
set(gca,'FontSize',20,'FontName', 'Times','FontWeight','bold', ...          %
sets the axis font
            'XMinorTick','on','YMinorTick','on')
set(gcf, 'position', [100 100 1000 750])
set(findall(gcf,'Type','Text'),'Fontname','Times','Fontsize',22,...
            'FontWeight','bold')

nameindex = 1:2;
legend(names(nameindex));

%% FFT v2 to verify original fft's

dt = 1/SR; % seconds per sample
N = length(acc_time_data1); % Number of samples taken
```

```
NFFT = 2^nextpow2(N);

X = 1/N*fftshift(fft(acc_time_data1,NFFT)); % NFFT_ - point complex dft
X2 = 1/N*fftshift(fft(acc_time_data2,NFFT)); % NFFT_ - point complex dft

df = SR/NFFT; % frequency resolution
sampleIndex = -NFFT/2:NFFT/2-1; % ordered index for fft plot
f = sampleIndex*df; % x-axis index converted to ordered frequencies

X_A1 = 2*(X(numel(X)/2+1:numel(X)));
X_A2 = 2*(X2(numel(X2)/2+1:numel(X2)));
f_A = f(numel(f)/2+1:numel(f));

%% Frequency simplify -> Find primary frequencies (0 to 200 Hz)

freq_data1a = X_A1;
freq_data2a = X_A2;
f_a = f_A;
freq_data1b = [0 0];
freq_data2b = [0 0];
f_b = [0 0];

for i=1:NFFT/2
    if f_A(i)<200
        freq_data1b(numel(f_b)+1) = freq_data1a(i);
        freq_data2b(numel(f_b)+1) = freq_data2a(i);
        f_b(numel(f_b)+1) = f_a(i);
    end
end
freq_data1b = freq_data1b(3:end);
freq_data2b = freq_data2b(3:end);
f_b = f_b(3:numel(f_b));

% plot new pairs of frequencies
figure
plot(f_a,abs(freq_data1a),f_a,abs(freq_data2a));
xlabel('Frequency [Hz.]');
ylabel('Magnitude');
title(sprintf('%s %s %s %s
%s',folder_name(1:5),track,carend,speed,carload),'FontSize',24,'FontName',
'Times','FontWeight','bold');
legend(names(nameindex));
set(gca,'FontSize',20,'FontName', 'Times','FontWeight','bold', ...          %
sets the axis font
            'XMinorTick','on','YMinorTick','on')
set(gcf, 'position',  get(0, 'Screensize'))
set(findall(gcf,'Type','Text'),'Fontname','Times','Fontsize',22,...
            'FontWeight','bold')

%% Compare original and trimmed frequency data

figure
subplot(2,1,1)
h = stem(f,2*abs(X)); hold on;
set(h,'Marker','none')
```

```
h = stem(f_b,abs(freq_data1b));
set(h,'Marker','none')
title(sprintf('Frequency spectrum of TTCI test: %s %s %s %s
%s.',testday,track,carend,speed,carload))
xlabel('Frequency [Hz.]');
ylabel('Magnitude');
legend(names(nameindex(1)),'Trimmed');
set(gca,'FontSize',20,'FontName', 'Times','FontWeight','bold', ...          %
sets the axis font
            'XMinorTick','on','YMinorTick','on')
set(gca,'xlim',[0 2600]);
set(findall(gcf,'Type','Text'),'Fontname','Times','Fontsize',22,...
            'FontWeight','bold')

subplot(2,1,2)
h = stem(f,2*abs(X2)); hold on;
set(h,'Marker','none')
h = stem(f_b,abs(freq_data2b));
set(h,'Marker','none')
xlabel('Frequency [Hz.]');
ylabel('Magnitude');
legend(names(nameindex(2)),'Trimmed');
set(gca,'FontSize',20,'FontName', 'Times','FontWeight','bold', ...          %
sets the axis font
            'XMinorTick','on','YMinorTick','on')
set(gca,'xlim',[0 2600]);
set(gcf, 'position',  get(0, 'Screensize'));
set(findall(gcf,'Type','Text'),'Fontname','Times','Fontsize',22,...
            'FontWeight','bold')
set(gcf, 'position',  get(0, 'Screensize'));
print(folder_name,'-dpng','-r0');
subplot(2,1,1); set(gca,'xlim',[0 200]);
subplot(2,1,2); set(gca,'xlim',[0 200]);
print(sprintf('%s zoom',folder_name),'-dpng','-r0');

%% Output data to excel file

folder_strings_a = {'Day 1_RTT_Front_30_Loaded';
    'Day 1_RTT_Front_50_Loaded';
    'Day 1_RTT_Front_55_Loaded';
    'Day 1_RTT_Rear_30_Loaded';
    'Day 1_RTT_Rear_40_Loaded';
    'Day 1_RTT_Rear_50_Loaded';
    'Day 1_RTT_Rear_55_Loaded';
    'Day 1_RTT_Rear_57_Loaded';
    'Day 1_RTT_Rear_60_Loaded';
    'Day 2_PTT_Front_30_Loaded';
    'Day 2_PTT_Front_40_Loaded';
    'Day 2_PTT_Front_50_Loaded';
    'Day 2_PTT_Front_55_Loaded';
    'Day 2_PTT_Rear_30_Loaded';
    'Day 2_PTT_Rear_40_Loaded';
    'Day 2_PTT_Rear_50_Loaded';
    'Day 2_PTT_Rear_55_Loaded';
    'Day 3_PTT_Front_30_Unloaded';
    'Day 3_PTT_Front_40_Unloaded';
```

```
    'Day 3_PTT_Front_50_Unloaded';
    'Day 3_PTT_Rear_40_Unloaded';
    'Day 3_PTT_Rear_50_Unloaded';
    'Day 3_RTT_Front_40_Unloaded';
    'Day 3_RTT_Front_50_Unloaded';
    'Day 3_RTT_Front_55_Unloaded';
    'Day 3_RTT_Front_60_Unloaded';
    'Day 3_RTT_Front_65_Unloaded';
    'Day 3_RTT_Rear_30_Unloaded';
    'Day 3_RTT_Rear_40_Unloaded';
    'Day 3_RTT_Rear_50_Unloaded';
    'Day 3_RTT_Rear_55_Unloaded';
    'Day 3_RTT_Rear_60_Unloaded';
    'Day 3_RTT_Rear_65_Unloaded'};
folder_strings = string(folder_strings_a);


folder_tab = 1;
for i = 1:33
    if contains(folder_strings(i),folder_name)~=1
        folder_tab = folder_tab+1;
    else
        break
    end
end

output_header1 = [folder_name;
    names(1);
    names(2)];

output_header2 = [{'Frequency (Hz)','Real','Imag','Frequency
(Hz)','Real','Imag'}];

output_data1 = [f_b' real(freq_data1b)' imag(freq_data1b)' f_b'
real(freq_data2b)' imag(freq_data2b)'];
output_data_end = length(f_b)+6;

xlswrite('TTCI_Frequency_outputs_v2.xlsx',output_header1,folder_tab,'A1');
xlswrite('TTCI_Frequency_outputs_v2.xlsx',names(1),folder_tab,'A5');
xlswrite('TTCI_Frequency_outputs_v2.xlsx',names(2),folder_tab,'D5');
xlswrite('TTCI_Frequency_outputs_v2.xlsx',output_header2,folder_tab,'A6:F6');
xlswrite('TTCI_Frequency_outputs_v2.xlsx',output_data1,folder_tab,sprintf('A7
:F%.0f',output_data_end));

close(3);
close(2);
close(1);
```

```
%% MTS Simulation Tests
% (1) Read data from Labview
%     - four voltages from Terfenol D with coils (no load), LabVIEW DAQ
% (2) Calibrate to expected power of each
%     - With given parameters, expected power
% (3) Read data from MTS
```

```
%     - time and force, MTS DAQ
% (4) Figures and Table output
%     - Fig: Force profile met expected
%     - Fig: Power vs frequency
%     - Fig: Load vs Frequency
%     - Table: Power vs frequency
%     - Table: Load vs Frequency
clear all; close all; clc; format short g; format compact;

%% (1) Read data from Labview
%     - four voltages from Terfenol D with coils (no load), LabVIEW DAQ
labview = importdata('test_3.lvm','\t',23); % 23 header lines
time = labview.data(:,1); % s
V_1 = labview.data(:,2); % V
V_2 = labview.data(:,3); % V
V_3 = labview.data(:,4); % V
V_4 = labview.data(:,5); % V
MTS_time = time;
MTS_force = V_3*-2; % kip

%% (2) Calibrate to expected power of each
% given parameters
% calculated expected power
turns1 = 348; % number of turns on coil
turns2 = 188; % number of turns on coil
turns3 = 335; % number of turns on coil
turns4 = 325; % number of turns on coil
gauss = 1085; % magnet gauss
r_coil_1 = 14; % ohm
r_coil_2 = 3.39; % ohm
r_coil_3 = 14; % ohm
r_coil_4 = 14; % ohm

% no load was used
% assume (gross simplification) max power is v^2/r, where:
% assume max power where r_load = r_coil
% assume load, if applied, v_measured would have been halved
% therefore, theoretical power would be:
% P = [(v_measured/2)^2]/(r_coil) = (1/4)*(v_measured/r_coil)

power_1_inst = 1000*(V_1.^2)/r_coil_1; % mW
power_2_inst = 1000*(V_2.^2)/r_coil_2; % mW
power_3_inst = 1000*(V_3.^2)/r_coil_3; % mW
power_4_inst = 1000*(V_4.^2)/r_coil_4; % mW


b=59305
c=523292
Power_1_avg = mean(power_1_inst(b:c)); % mW
Power_2_avg = mean(power_2_inst(b:c)); % mW
                  % % % Power_3_avg = mean(power_3_inst(b:c)); % mW
Power_4_avg = mean(power_4_inst(b:c)); % mW
Overall_power = mean([Power_1_avg Power_2_avg Power_4_avg]); % mW

%% (3) Read data from MTS and LabVIEW
```

```
%     - time and force, MTS DAQ
%     - determine frequencies at each test

%MTS_data = importdata('test_1.dat','\t',5);
%MTS_force = MTS_data.data(:,1); % lbf
%MTS_time_1 = MTS_data.data(:,2); % sec
%MTS_time = MTS_time_1-MTS_time_1(1); % sec

% MTS frequency separation
%f_input =
[0.125;37.375;37.625;46.875;51.375;51.625;55.875;57.125;60.875;61.375;61.625;
61.875;62.125;62.375;66.125;71.125;75.125;75.375;81.375;81.875;87.625;88.125;
93.625;94.125;99.125;101.375;101.625;101.875;103.125;103.375;103.625;103.875;
111.625;111.875;112.125;112.375;112.625;112.875;121.625;127.375;127.625;131.1
25;142.125;196.625];
%n_f = numel(f_input)-1;
%start = find(MTS_time==24.006830000000036); % start of first test NOT 0.125
%d_f = floor(5/(MTS_time(2))-1); % number of samples of each frequency
%d_f_keep = floor(d_f*.3); % keep central 1.5 seconds of testing
%f_analysis = zeros(d_f_keep,3,n_f);

%for i = 1:n_f
%    for j = 1:d_f_keep;
%         f_analysis(j,1,i) = f_input(i+1);
%         f_analysis(j,2,i) = MTS_time(start+(i-1)*d_f+(j-1)+floor(d_f*.35));
%         f_analysis(j,3,i) = MTS_force(start+(i-1)*d_f+(j-
1)+floor(d_f*.35));
%     end
% end
%
% mts_output = zeros(n_f+1,5);
% mts_output(1,1) = f_input(1);
% mts_output(1,2) = -max(MTS_force(floor(start/4):floor(3*start/4))); % load
min
% mts_output(1,3) = -min(MTS_force(floor(start/4):floor(3*start/4))); % load
max
% mts_output(1,4) = (mts_output(1,3)-mts_output(1,2))/2; % force amplitude
% mts_output(1,5) = mts_output(1,3)/344; % percent load of 34,400 lb
% for i = 1:n_f
%     mts_output(i+1,1) = f_input(i+1);
%     mts_output(i+1,2) = -max(f_analysis(:,3,i)); % load min
%     mts_output(i+1,3) = -min(f_analysis(:,3,i)); % load max
%     mts_output(i+1,4) = (mts_output(i+1,3)-mts_output(i+1,2))/2; % force
amplitude
%     mts_output(i+1,5) = mts_output(i+1,3)/344; % percent load of 34,400
% end
%
% % Labview Frequency separation
%
% start = find(MTS_time==24.006830000000036); % start of first test NOT 0.125
% d_f = floor(5/(MTS_time(2))-1); % number of samples of each frequency
% d_f_keep = floor(d_f*.3); % keep central 1.5 seconds of testing
% f_analysis = zeros(d_f_keep,3,n_f);
%
% for i = 1:n_f
%     for j = 1:d_f_keep;
```

```
%         f_analysis(j,1,i) = f_input(i+1);
%         f_analysis(j,2,i) = MTS_time(start+(i-1)*d_f+(j-1)+floor(d_f*.35));
%         f_analysis(j,3,i) = MTS_force(start+(i-1)*d_f+(j-
1)+floor(d_f*.35));
%     end
% end
%
% mts_output = zeros(n_f+1,5);
% mts_output(1,1) = f_input(1);
% mts_output(1,2) = -max(MTS_force(floor(start/4):floor(3*start/4))); % load
min
% mts_output(1,3) = -min(MTS_force(floor(start/4):floor(3*start/4))); % load
max
% mts_output(1,4) = (mts_output(1,3)-mts_output(1,2))/2; % force amplitude
% mts_output(1,5) = mts_output(1,3)/344; % percent load of 34,400 lb
% for i = 1:n_f
%     mts_output(i+1,1) = f_input(i+1);
%     mts_output(i+1,2) = -max(f_analysis(:,3,i)); % load min
%     mts_output(i+1,3) = -min(f_analysis(:,3,i)); % load max
%     mts_output(i+1,4) = (mts_output(i+1,3)-mts_output(i+1,2))/2; % force
amplitude
%     mts_output(i+1,5) = mts_output(i+1,3)/344; % percent load of 34,400
% end

%% (4) Figures and Table output
%     - Fig 1: Force profile met expected
%     - Fig 2: Force profile, trimmed met expected
%     - Fig 3: Voltage vs frequency
%     - Fig 4: Power vs frequency
%     - Fig 5: Load vs Frequency
%     - Fig 6: Test Amp vs Frequency
%     - Table: Power vs frequency
%     - Table: Load vs Frequency
%     - Table: Test Amp vs Frequency

figure(1)
plot(MTS_time,MTS_force)
xlabel('Time (s)'); ylabel('Force (kip)');
set(gca,'Ylim',[-20 0]);
set(gca,'fontname','times','fontweight','b','fontsize',20)

% figure(2)
% pre_legend = cell(1,n_f);
% for i = 1:n_f
%     plot(f_analysis(:,2,i),f_analysis(:,3,i)); hold on;
%     pre_legend{i+1} = sprintf('%3.2f Hz',f_input(i+1));
% end
% pre_legend{1} = sprintf('%3.2f Hz',f_input(1));
% h_legend = legend(pre_legend(2:end));
% xlabel('Time (s)'); ylabel('Force (lb_f)');
% set(gca,'Ylim',[-20000 0]);
% set(gca,'fontname','times','fontweight','b','fontsize',20)
% set(h_legend,'location','eastoutside','fontsize',11.5)

figure(3)
subplot(4,1,1)
```

```
plot(time,V_1)
title('Labview Voltage Output');
legend(sprintf('Turns = %3.0f, R = %3.2f Ohm',turns1,r_coil_1))
set(gca,'fontname','times','fontweight','b','fontsize',16)
subplot(4,1,2)
plot(time,V_2)
legend(sprintf('Turns = %3.0f, R = %3.2f Ohm',turns2,r_coil_2))
set(gca,'fontname','times','fontweight','b','fontsize',16)
subplot(4,1,3)
plot(time,V_3)
legend(sprintf('Turns = %3.0f, R = %3.2f Ohm',turns3,r_coil_3))
set(gca,'fontname','times','fontweight','b','fontsize',16)
subplot(4,1,4)
plot(time,V_4)
legend(sprintf('Turns = %3.0f, R = %3.2f Ohm',turns4,r_coil_4))
set(gca,'fontname','times','fontweight','b','fontsize',16)


figure(4)
subplot(4,1,1)
plot(time,power_1_inst)
title('Labview Power Output (mW)');
ylabel('Power (mW)');
legend(sprintf('Fixture 1'))
set(gca,'fontname','times','fontweight','b','fontsize',16)
subplot(4,1,2)
plot(time,power_2_inst,'c')
ylabel('Power (mW)');
legend(sprintf('Fixture 2'))
set(gca,'fontname','times','fontweight','b','fontsize',16)
subplot(4,1,3)
plot(time,power_4_inst,'g')
ylabel('Power (mW)');
legend(sprintf('Fixture 3'))
set(gca,'fontname','times','fontweight','b','fontsize',16)
subplot(4,1,4)
plot(time,MTS_force,'r')
ylabel('Force (lb_f)');
xlabel('Time (s)');
legend(sprintf('Force (lb)'))
set(gca,'fontname','times','fontweight','b','fontsize',16)

% figure(5)
%
plot(mts_output(:,1),mts_output(:,5),'yo','MarkerSize',8,'MarkerEdgeColor','k
','MarkerFaceColor','y')
% xlabel('Frequency (\it{f})');ylabel('Percent load (%)');
% set(gca,'Ylim',[0 60]);
% set(gca,'fontname','times','fontweight','b','fontsize',20)
%
%
% figure(6)
%
plot(mts_output(:,1),mts_output(:,4),'co','MarkerSize',8,'MarkerEdgeColor','k
','MarkerFaceColor','c')
% xlabel('Frequency (\it{f})');ylabel('Force amplitude (lb_f)');
```

```
% set(gca,'Ylim',[0 10000]);
% set(gca,'fontname','times','fontweight','b','fontsize',20)




% figure(55)
% subplot(2,1,1)
% plot(MTS_time,MTS_force)
% set(gca,'Ylim',[-20000 0]);
% subplot(2,1,2)
% plot(time,power_1_inst); hold on;
% plot(time,power_2_inst);
% plot(time,power_3_inst);
% plot(time,power_4_inst);
```

```
%% Comparing many types of frequency/speed types
% compare frequencies from database
% create figures for visualization


clear all; close all; clc; format short g; format compact
tic



% pick both
folder_tab = 4; % coincide with case_picked (1:10) [1,2,3,4,6,
percent_used = 4; % 1:5 is [0.25;2;4;10;20];

% [4,3] [6,3]
% [1,2] [3,2]
% [2,1]

% cases 11-14 updated to include loaded and unloaded conditions together
% rerun specifying folder_tab 11-14
% all percent scenarios
% fix excel sheet outputs and loops first


%% Prep Access data in Excel tabs

folder_strings_a = {'Day 1_RTT_Front_30_Loaded';
        'Day 1_RTT_Front_50_Loaded';
        'Day 1_RTT_Front_55_Loaded';
        'Day 1_RTT_Rear_30_Loaded';
        'Day 1_RTT_Rear_40_Loaded';
        'Day 1_RTT_Rear_50_Loaded';
        'Day 1_RTT_Rear_55_Loaded';
        'Day 1_RTT_Rear_57_Loaded';
        'Day 1_RTT_Rear_60_Loaded';
        'Day 2_PTT_Front_30_Loaded';
        'Day 2_PTT_Front_40_Loaded';
        'Day 2_PTT_Front_50_Loaded';
```

```
        'Day 2_PTT_Front_55_Loaded';
        'Day 2_PTT_Rear_30_Loaded';
        'Day 2_PTT_Rear_40_Loaded';
        'Day 2_PTT_Rear_50_Loaded';
        'Day 2_PTT_Rear_55_Loaded';
        'Day 3_PTT_Front_30_Unloaded';
        'Day 3_PTT_Front_40_Unloaded';
        'Day 3_PTT_Front_50_Unloaded';
        'Day 3_PTT_Rear_40_Unloaded';
        'Day 3_PTT_Rear_50_Unloaded';
        'Day 3_RTT_Front_40_Unloaded';
        'Day 3_RTT_Front_50_Unloaded';
        'Day 3_RTT_Front_55_Unloaded';
        'Day 3_RTT_Front_60_Unloaded';
        'Day 3_RTT_Front_65_Unloaded';
        'Day 3_RTT_Rear_30_Unloaded';
        'Day 3_RTT_Rear_40_Unloaded';
        'Day 3_RTT_Rear_50_Unloaded';
        'Day 3_RTT_Rear_55_Unloaded';
        'Day 3_RTT_Rear_60_Unloaded';
        'Day 3_RTT_Rear_65_Unloaded'};

cases = cell(14,1);
        cases{1} = 'Front 30 Loaded';
        cases{2} = 'Front 40 Loaded';
        cases{3} = 'Front 50 Loaded';
        cases{4} = 'Front 55 Loaded';
        cases{5} = 'Front 30 Unloaded';
        cases{6} = 'Front 40 Unloaded';
        cases{7} = 'Front 50 Unloaded';
        cases{8} = 'Front 55 Unloaded';
        cases{9} = 'Front 60 Unloaded';
        cases{10} = 'Front 65 Unloaded';
        cases{11} = 'Front 30'; %'Front 30 Loaded';
        cases{12} = 'Front 40'; %'Front 40 Loaded';
        cases{13} = 'Front 50'; %'Front 50 Loaded';
        cases{14} = 'Front 55'; %'Front 55 Loaded';

percent_used_tabs = ['A:D';'E:H';'I:L';'M:P';'Q:T'];
case_picked = cases{folder_tab};
check_b = regexp(case_picked, ' ');
percent_output_tab = ['B','C','D','E','F'];
percents = [0.25;2;4;10;20];
percentage = percents(percent_used);
speed_used = case_picked(check_b(1)+1:check_b(1)+2);
speed_used = str2double(speed_used);
%loading_condition = case_picked(check_b(2)+1:end);
data_percent = sprintf('%s',percent_used_tabs(percent_used,:));
folder_strings = folder_strings_a;
folder_namea = char(folder_strings);
for i = 1:33
    [name_r,name_c] = find(folder_namea(i,1:27)=='_'); folder_namea(i,name_c)
= ' ';
    folder_name(i,1:27) = folder_namea(i,1:27);
end
access_tabs = ones(33,1);
```

```
percent_used_tabs = ['A:D';'E:H';'I:L';'M:P';'Q:T'];

folder_strings_name = cell(33,1);
for i = 1:33
    folder_strings_name{i} = folder_name(i,:);
end

%% Prep Binning to find frequencies used

d_Hz = 0.25; % Hz - derived from error in speed measurement: 0.006424
simple 0.25
remainder = rem(200,d_Hz);
n_bins = floor(200/d_Hz)+1;
edges_in = linspace(-remainder/2,200+remainder/2,n_bins);

%f_bins = zeros(size(fft_bins1));
for i = 1:800
    f_bins(i) = mean(edges_in(i:i+1));
end

%% Prep to find appropriate analysis groups and pair together.

check_a = regexp(folder_strings_a, '_');

for i = 1:33
    check(i,1:4) = check_a{i};
end

testday = cell(33,1);
track = cell(33,1);
carend = cell(33,1);
speed_a = cell(33,1);
carload = cell(33,1);

for i = 1:33
    folder_strings_b = folder_strings_a{i};
    testday{i} = folder_strings_b(1:check(i,1)-1);
    track{i} = folder_strings_b(check(i,1)+1:check(i,2)-1);
    carend{i} = folder_strings_b(check(i,2)+1:check(i,3)-1);
    speed_a{i} = folder_strings_b(check(i,3)+1:check(i,4)-1);
    carload{i} = folder_strings_b(check(i,4)+1:end);
end

%% Folder details

for i = 1:33

switch track{i}
    case 'PTT'
        track_type(i,1) = 1;
    case 'RTT'
        track_type(i,1) = 0;
end
switch testday{i}
```

```
    case 'Day 1'
        testday_type(i,1) = 1;
    case {'Day 2','Day 3'}
        testday_type(i,1) = 0;
end
switch carend{i}
    case 'Front'
        carend_type(i,1) = 1;
    case 'Rear'
        carend_type(i,1) = 0;
end
switch carload{i}
    case 'Unloaded'
        carload_type(i,1) = 1;
    case 'Loaded'
        carload_type(i,1) = 0;
end
if carload_type(i,1) == 1
    load(i,1) = 17;
else
    load(i,1) = 100;
end
speed(i,1) = str2double(speed_a{i,1});

end
% switch loading_condition
%     case 'Unloaded'
%         loading_type(1) = 1;
%     case 'Loaded'
%         loading_type(1) = 0;
% end

%% Read in all data

data1(:,1:4,1) =
xlsread('TTCI_Frequency_outputs_v4_simple.xlsx',1,data_percent);
data1(:,1:4,2) =
xlsread('TTCI_Frequency_outputs_v4_simple.xlsx',2,data_percent); %
percent_used = [0.25;2;4;10;20];
data1(:,1:4,3) =
xlsread('TTCI_Frequency_outputs_v4_simple.xlsx',3,data_percent); %
percent_used_tabs = ['A:D';'E:H';'I:L';'M:P';'Q:T'];
data1(:,1:4,4) =
xlsread('TTCI_Frequency_outputs_v4_simple.xlsx',4,data_percent);
data1(:,1:4,5) =
xlsread('TTCI_Frequency_outputs_v4_simple.xlsx',5,data_percent);
data1(:,1:4,6) =
xlsread('TTCI_Frequency_outputs_v4_simple.xlsx',6,data_percent);
data1(:,1:4,7) =
xlsread('TTCI_Frequency_outputs_v4_simple.xlsx',7,data_percent);
data1(:,1:4,8) =
xlsread('TTCI_Frequency_outputs_v4_simple.xlsx',8,data_percent);
data1(:,1:4,9) =
xlsread('TTCI_Frequency_outputs_v4_simple.xlsx',9,data_percent);
data1(:,1:4,10) =
xlsread('TTCI_Frequency_outputs_v4_simple.xlsx',10,data_percent);
```

```
data1(:,1:4,11) =
xlsread('TTCI_Frequency_outputs_v4_simple.xlsx',11,data_percent);
data1(:,1:4,12) =
xlsread('TTCI_Frequency_outputs_v4_simple.xlsx',12,data_percent);
data1(:,1:4,13) =
xlsread('TTCI_Frequency_outputs_v4_simple.xlsx',13,data_percent);
data1(:,1:4,14) =
xlsread('TTCI_Frequency_outputs_v4_simple.xlsx',14,data_percent);
data1(:,1:4,15) =
xlsread('TTCI_Frequency_outputs_v4_simple.xlsx',15,data_percent);
data1(:,1:4,16) =
xlsread('TTCI_Frequency_outputs_v4_simple.xlsx',16,data_percent);
data1(:,1:4,17) =
xlsread('TTCI_Frequency_outputs_v4_simple.xlsx',17,data_percent);
data1(:,1:4,18) =
xlsread('TTCI_Frequency_outputs_v4_simple.xlsx',18,data_percent);
data1(:,1:4,19) =
xlsread('TTCI_Frequency_outputs_v4_simple.xlsx',19,data_percent);
data1(:,1:4,20) =
xlsread('TTCI_Frequency_outputs_v4_simple.xlsx',20,data_percent);
data1(:,1:4,21) =
xlsread('TTCI_Frequency_outputs_v4_simple.xlsx',21,data_percent);
data1(:,1:4,22) =
xlsread('TTCI_Frequency_outputs_v4_simple.xlsx',22,data_percent);
data1(:,1:4,23) =
xlsread('TTCI_Frequency_outputs_v4_simple.xlsx',23,data_percent);
data1(:,1:4,24) =
xlsread('TTCI_Frequency_outputs_v4_simple.xlsx',24,data_percent);
data1(:,1:4,25) =
xlsread('TTCI_Frequency_outputs_v4_simple.xlsx',25,data_percent);
data1(:,1:4,26) =
xlsread('TTCI_Frequency_outputs_v4_simple.xlsx',26,data_percent);
data1(:,1:4,27) =
xlsread('TTCI_Frequency_outputs_v4_simple.xlsx',27,data_percent);
data1(:,1:4,28) =
xlsread('TTCI_Frequency_outputs_v4_simple.xlsx',28,data_percent);
data1(:,1:4,29) =
xlsread('TTCI_Frequency_outputs_v4_simple.xlsx',29,data_percent);
data1(:,1:4,30) =
xlsread('TTCI_Frequency_outputs_v4_simple.xlsx',30,data_percent);
data1(:,1:4,31) =
xlsread('TTCI_Frequency_outputs_v4_simple.xlsx',31,data_percent);
data1(:,1:4,32) =
xlsread('TTCI_Frequency_outputs_v4_simple.xlsx',32,data_percent);
data1(:,1:4,33) =
xlsread('TTCI_Frequency_outputs_v4_simple.xlsx',33,data_percent);

%% Test plot all overlapped Data

figure(1)
hold on;
for i = 1:33
    plot(data1(:,1,i),data1(:,2,i),'.','MarkerSize',12)
    plot(data1(:,3,i),data1(:,4,i),'.','MarkerSize',12)
    Pre_legend{2*i-1} = sprintf('Bearing 1 - %s',folder_strings_name{i});
    Pre_legend{2*i} = sprintf('Bearing 2 - %s',folder_strings_name{i});
```

```
end

xlabel('Frequency, \it{f}'); ylabel('Magnitude, \it{|X|}');
title(sprintf('All TTCI tests, top %0.2f%% of each signal',percentage)); %
fix percents
set(gca,'FontName','Times','FontSize',20,'FontWeight','b');
set(gca,'Xlim',[0 200]);
h_legend = legend(Pre_legend);
set(h_legend,'FontSize',7.5,'FontWeight','b','location','eastoutside');
set(gcf, 'position', [0 0 1800 900])
%print('-f1','simple_20\simple_20','-dpng'); % fix percents
%savefig('simple_20\simple_20.fig'); % fix percents

%% Setup Data to plot as a grid chart

% scatter plot
size_1 = size(data1);
size_2 = size_1; size_2(3) = 2*size_2(3);
data2 = zeros(size_2);

figure(3)
hold on;

for i = 1:33
    data2(:,1,i) = data1(:,1,i);
    data2(:,3,i) = data1(:,3,i);
    data2(:,2,i) = 67-(2*i-1);
    data2(:,4,i) = 67-(2*i);

    scatter(data2(:,1,i),data2(:,2,i));
    scatter(data2(:,3,i),data2(:,4,i));
end
xlabel('Frequency, \it{f}'); ylabel('Magnitude, \it{|X|}');
title(sprintf('All TTCI tests, top %0.2f%% of each signal',percentage)); %
fix percents
set(gca,'FontName','Times','FontSize',20,'FontWeight','b');
set(gca,'Xlim',[0 200]);
h_legend = legend(Pre_legend);
set(h_legend,'FontSize',7.5,'FontWeight','b','location','eastoutside');
set(gcf, 'position', [0 0 1800 900])

%% Select Data scenario to be analyzed

figure(4)
hold on;
j = 0;
total_f_count = zeros(size(f_bins));
m = 0;

% change condition name and three conditions in 'if statement'
for i = 1:33
    if carend_type(i)==1 && speed(i)==speed_used %&&
carload_type(i)==loading_type
        % 1 = front && 30, 40, 50, 55, 57, 60, 65 && 0 = loaded
        scatter(data2(:,1,i),data2(:,2,i))
```

```
        scatter(data2(:,3,i),data2(:,4,i))
        j = j+1;
        m = m+2; %
        Pre_legend_front{2*j-1} = sprintf('Bearing 1 -
%s',folder_strings_name{i});
        Pre_legend_front{2*j} = sprintf('Bearing 2 -
%s',folder_strings_name{i});

        for k = 1:size_1(1)
            f_space1 = find(f_bins==data2(k,1,i));
            f_space2 = find(f_bins==data2(k,3,i));
            total_f_count(f_space1) = total_f_count(f_space1)+1;
            total_f_count(f_space2) = total_f_count(f_space2)+1;
        end
    end
end

xlabel('Frequency, \it{f}'); ylabel('Magnitude, \it{|X|}');
title(sprintf('%s, top %0.2f%% of each signal',case_picked,percentage)); %
fix percents
set(gca,'FontName','Times','FontSize',20,'FontWeight','b');
set(gca,'Xlim',[0 200]);
h_legend = legend(Pre_legend_front);
set(h_legend,'FontSize',7.5,'FontWeight','b','location','eastoutside');
set(gcf, 'position', [0 0 1800 900])
h4 = gca;

total_f_count = total_f_count/m;
figure(5)
hold on;
bar(f_bins,total_f_count)
xlabel('Frequency, \it{f}'); ylabel('Percent Representative (%)');
title(sprintf('%s',case_picked));
set(gca,'FontName','Times','FontSize',20,'FontWeight','b');
set(gca,'Xlim',[0 200]);
set(gcf, 'position', [0 0 1800 900])


present100 = find(total_f_count==1);
present_100 = f_bins(present100);

f6 = figure(6);
copyobj(h4,f6);
hold on;
h1 = bar(present_100,66*ones(size(present_100)));
uistack(h1,'bottom')


%% Output Data to excel

output_header1 = cell(1,1);
output_header1{1} = case_picked(:)';
output_header2 = cell(1,5);
output_header3 = {'PercentUsed';'f'};
output_header2{1} = percents(1);
```

```
output_header2{2} = percents(2);
output_header2{3} = percents(3);
output_header2{4} = percents(4);
output_header2{5} = percents(5);

output_data1 = present_100';
output_end = numel(present_100)+4;
percent_output = percent_output_tab(percent_used);

%xlswrite('TTCI_Frequency_outputs_v5_simple.xlsx',output_header1,folder_tab,'
A1');
%xlswrite('TTCI_Frequency_outputs_v5_simple.xlsx',output_header2,folder_tab,'
B4:F4');
%xlswrite('TTCI_Frequency_outputs_v5_simple.xlsx',output_header3,folder_tab,'
A4:A5');
%xlswrite('TTCI_Frequency_outputs_v5_simple.xlsx',output_data1,folder_tab,spr
intf('%s5:%s%.0f',percent_output,percent_output,output_end));


%% if Data 1 fails, document and then run with next most.

 next_highest = 0.5; % fill out next_highest value if 100% not available
 present75 = find(total_f_count>=next_highest);
 present_75 = f_bins(present75);
 output_data2 = present_75';
 output_end = numel(present_75)+4;
 percent_output = percent_output_tab(percent_used);

%xlswrite('TTCI_Frequency_outputs_v5_simple.xlsx',next_highest,folder_tab,spr
intf('%s3',percent_output));

%xlswrite('TTCI_Frequency_outputs_v5_simple.xlsx',output_data2,folder_tab,spr
intf('%s5:%s%.0f',percent_output,percent_output,output_end));
```

APPENDIX B

FUJIFILM

PRESCALE instruction sheet

FUJI PRESCALE PRESSURE MEASURING FILM

MS - *Medium Pressure Range* (mono sheet type)

Type of Prescale Film available ranges

Fuji Film manufacture up to eight types of *Prescale Films*, available to cover a very wide range of pressure (five ranges are as two sheet type xxxxW; three ranges are as mono sheet type xxS).

Left side shown a list of existing ranges with related film sizes.

Film type	Pressure range[MPa] 0.05 0.2 0.5 0.6 2.5 10 50 150 300	Product size W[mm]×L[m]
Extreme Low Pressure (LLLLW)		310×3
Ultra Super Low Pressure (LLLW)		270×5
Super Low Pressure (LLW)		270×6
Low Pressure (LW)		270×12
Medium Pressure (MW)		270×12
Medium Pressure (MS)		270×12
High Pressure (HS)		270×12
Super High Pressure (HHS)		270×12

Structure of Prescale film - how it works (Prescale MS is a mono sheet type)

As explained, and depending from its measuring range, *Prescale Film* is available by two possible formats, one based on two sheets (A + C), and another as a mono sheet.

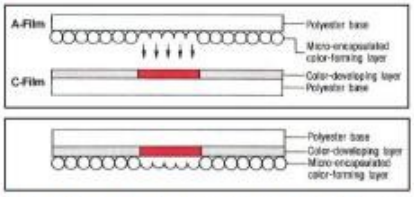

Two sheets film - *Prescale* is composed of an A film (made of a PET base) which is coated with a micro encapsulated colour forming material, and a C film (made of a PET base), which is coated with a colour developing material. When used, the two films should be placed with the coated (rough and opaque) surfaces facing each other.

Mono sheet film - A first colour forming layer is coated on polyester film base. A further micro encapsulated colour forming material is layered on the top of film.

How it works - When pressure is applied on the film, microcapsules are broken with distribution and "density" of magenta colour depending by true pressure distribution and magnitude. When microcapsules are broken, their material is released and it react with the colour developing material and this process will cause magenta colour forming. Through PSC technology (*Particle Size Control*), microcapsules are designed to react to various degrees of pressures, releasing their colour forming material at a density that correspond to specific levels of applied pressure.

Properties of Prescale Film

- typical accuracy: ±10% or less (measured with densitometers @ 23°C / 73.4 °F, 65% RH)
- recommended temperature range: from 20°C up to 35 °C (from 68°F up to 95°F)
- recommended humidity range: from 35% RH up to 80% RH

Method of use of Prescale Film (mono sheet type shown by side picture)

Cut *Prescale Film* into required shape and size.
Coated (rough and opaque) side of film shall be kept saved from water or oil.
Where necessary, use the additional PET protection sheet supplied, to protect the coated (rough and opaque) side of film. Insert shaped *Prescale Film* into area to be measured and then apply pressure or force phenomenon.
Remove impressed film and observe pressure distribution and magnitude.

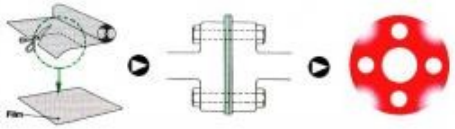

Typical conditions for applying under measurement pressure to Prescale Film

By mean of *Prescale Film* both extended and momentary measurement and analysis of pressure phenomenon are possible.

Extended (continuous) pressure measurements - With extended pressure method, applied pressure is increased gradually up to the given level, and it will be maintained continuously at that level. In order to get the best and accurate results (and where it is possible and applicable), preferably pressure should be applied gradually up to its highest value by a 2 minutes time basis, and it should be maintained at the highest level for other 2 minutes.

Momentary pressure measurements - If necessary *Prescale Film* could be also used for impact pressure measurements, with application time depending from application itself. When possible (and where applicable) preferably pressure should be applied gradually up to its highest magnitude by a 5 seconds time basis, and it should be maintained at the highest level for other 5 seconds.

Determining the pressure level and distribution over a mono sheet type film

As explained, with pressure applied, *Prescale Film* turn into a several level of magenta colour (red), whose intensity (density), is directly proportional to the amount of pressure being applied. Where high pressure was applied, dark magenta will be shown. Conversely where low pressure was applied, a light magenta colour will be on the film areas. The correct interpretation of described results will be performed by three basic steps:

Step 1 - Compare exposed *Prescale* film to magenta's sample table shown on the back side of present data sheet. Each magenta sample correspond to a specific density figure so take a note of it; if exposed film colour is between samples, interpolate it. To read place the impressed film over few sheets of white paper or the like, and observe the film from the polyester base side (the smooth surface), in a well lit area.

Step 2 - With reference to followings temperature and humidity smaller chart, determine the ambient condition of your experience and try to recognize the type of area (A, B, etc.) that better match your true experiment conditions; be accurate as possible since for each working area a specific density curve (A, B, etc.) will be related on next step.

Step 3 - by type of performed pressure exposition (*Extended* or *Momentary*), and using the proper curve recognized as the closest to experiment ambient condition (see step 2), it should be possible to locate point corresponding to where recorded density intersects the curve previously determined. From this point of intersection and following the line down to X axis where is possible to obtain the actual pressure value in *MPa*.

Graph of temperature and humidity (*)

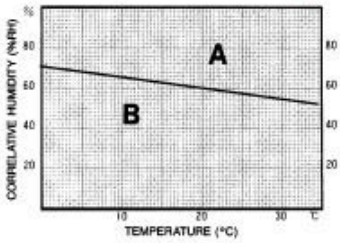

Magenta's samples table

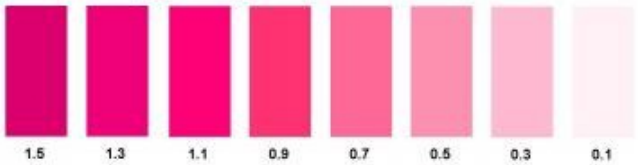

Even if *Prescale* can offer a "visual" direct imaging of pressure distribution and magnitude, better results are achievable by mean of shown standard charts and magenta's colour table. In choosing the proper curve (*), check for ambient temperature and humidity conditions and make sure which area is the closest to your experiment (see side chart). For example, if the room temperature is 25°C and the humidity factor is 60% RH, acquire the pressure using the A curve in standard charts.

MS (10÷50 MPa) - *Extended* pressure chart

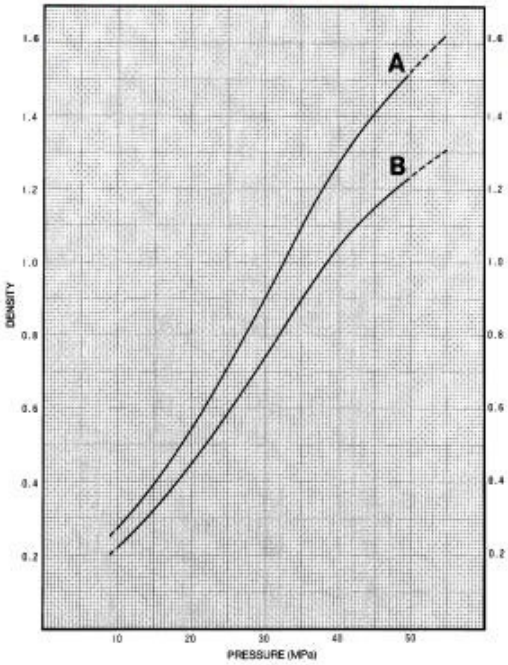

MS (10÷50 MPa) - *Momentary* pressure chart

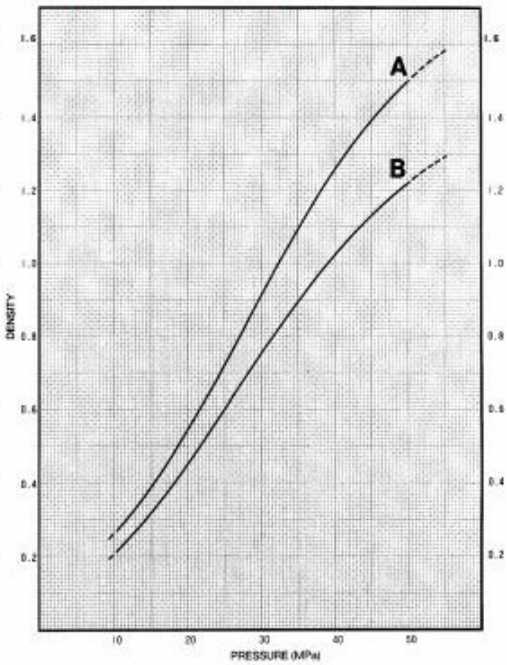

As the pressure ranges indicated by the broken lines in the above graphs may exceed the permissible error range, they should be used for reference only.

Precautions on use and storage

A film (on two sheets film format) react with high sensitivity even to minute pressure. Do not hold tight or rub it before use. Wipe the surfaces to be measured before use. Water, oil or dust, if present on coated surfaces of films, will hinder proper colour development. Avoid friction between A and C films. The films should be bound together at the edge before to start the test (if shearing force is expected) and not shifted later. Use *Prescale Film* at temperatures within 20 °C to 35 °C (68 ÷95 °F), and an humidity range of 35% RH up to 80% RH. Measurements performed outside this region could be not accurate. *Prescale Film* is not reusable. It should be also utilized within the given shelf life. Be particularly careful in handling single sheet *Prescale Film* types (**xxS**) as they are self colour developing and could easily develop on their own. Avoid film exposure to sunlight or in location close to fire or excessive heating. During storage avoid film contact with carbon paper, Diazo copying paper, solvents, water, oil or other chemicals, vinyl plastic or adhesive tapes, rubber products or with papers written by marking pens. Unused films should be placed in the original polyethylene bags and stored in the original box. Keep used C film in a paper bag. After development, avoid storing of the impressed C film (or the mono sheet type film) with the colour developer material sides making contact with each other.

Please be aware that Fuji Prescale film could be also "measured" by more capable and repeatable means like colour densitometers and specific software facilities based on a calibrated A4 format scanner (quantitative pressure values). Please contact our sales department for any further detail. Spare can also offer you several further diagnosis tools and instrumentation. Please submit us your application details as we will check the more cost effective and the best "requirements tailored" solution.

SPARE
Spare s.a.s.
Strumentazione sistemi e sensori
Via Carlo Spagnolo, 4 - 27057 Varzi - Pavia - Italia
tel.: ++39 - 0383 - 54.51.51 - fax: ++39 - 0383 - 54.50.51
www.spareonweb.com/prescale.htm - sales@spare.it

Pressure film – Region of interest – interlock pressure – magenta value 0.7889

= 32 MPa = 4641 psi (Fujifilm brochure table)

Pressure film – region of interest – total pressure for 120% load – magenta value 0.6180

= 26.25 MPa = 3807.24 psi (Fujifilm brochure table)

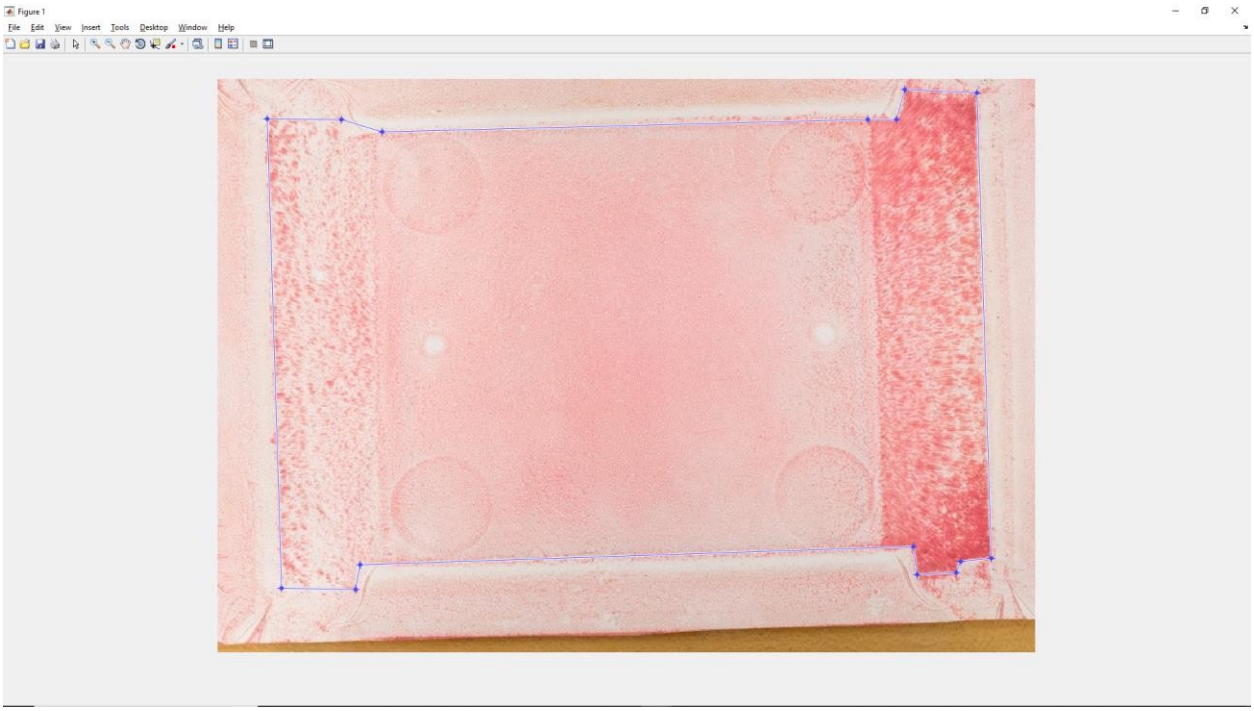

Interlock 2 pressure – 0.4837 magenta = 21.75 MPa = 3154 psi

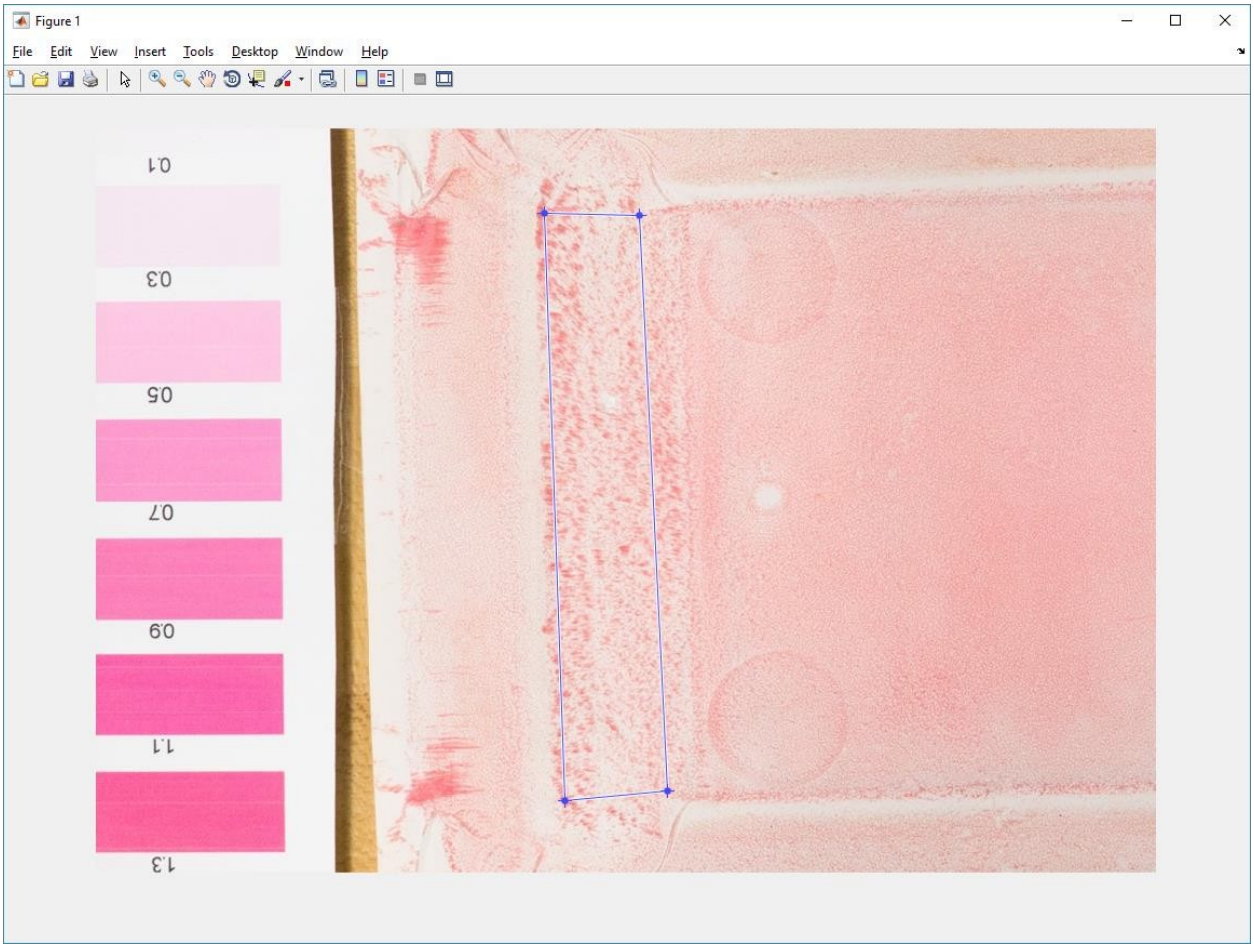

Additional calculations:

Image 2, total pressure at 120% load (41.28 kips) for area 18.37 in^2 is expected to be 2.247 ksi, but is measured as 3.807 ksi. This is due to pressure capsules bursting at maximum loading, equivalent to load plus dynamic variance maximum. In this case, 2.247 ksi (load) plus 1.560 ksi (dynamic) caused 3.807 ksi total max pressure measurement.

Relatively, the dynamic constituent of the maximum pressure is 69 percent of the applied load (1.560 ksi /2.247 ksi).

Additionally, load accounts for 59% of the pressure (2.247 ksi/3.807 ksi) and the dynamic portion accounts for 41% (1.560 ksi/3.807 ksi).

The interlock sees 206% of the pressure that would be seen if the load were distributed evenly (4.641 ksi/2.247 ksi).

If the area of the Terfenol-D piece is known and applied into the interlocks, it can be expected to see

[(% load/area)*(206%)*(59%)] steady load + [(% load/area)*(206%)*(41%)] dynamic loading conditions.

For a fully-loaded vehicle, and a Terfenol-D rod with a radius of 0.26 inch, it can be expected to see roughly 483 lb load with 336 lb peak dynamic amplitude.

[(34400lb/18.37in)*2.06*.59*(pi*0.26^2) = 483 lb

APPENDIX C

Finite Element Analysis

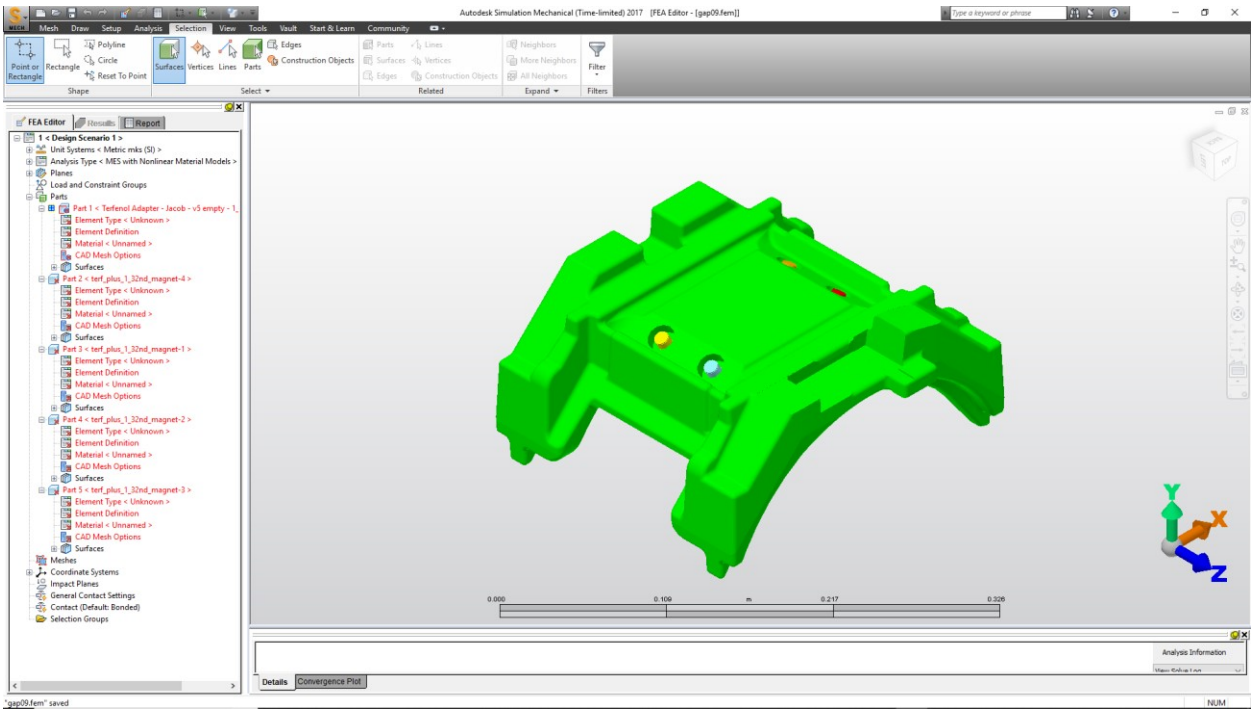

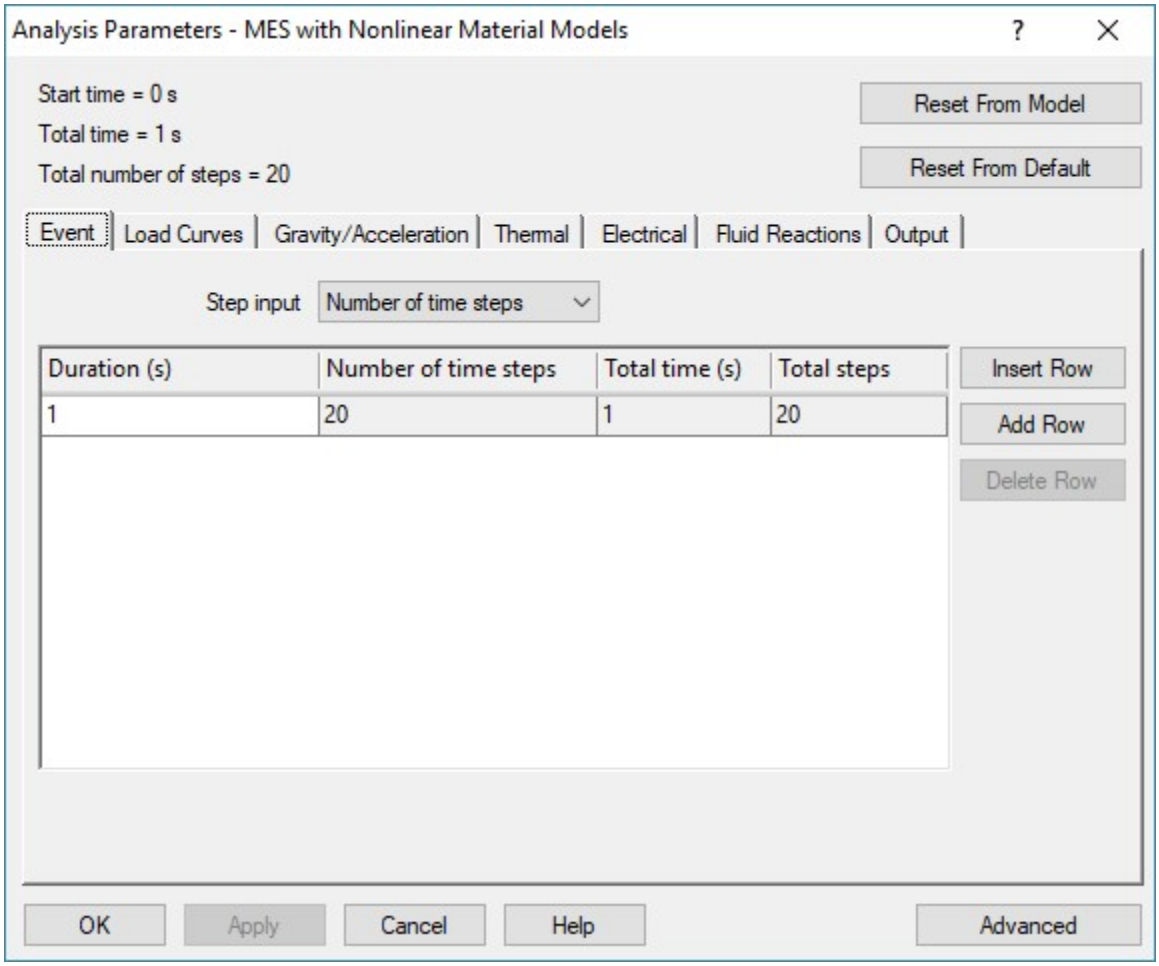
Analysis Parameters - MES with Nonlinear Material Models
Start time = 0 s
Total time = 1 s
Total number of steps = 20
Reset From Model
Reset From Default
Event
Load Curves
Gravity/Acceleration
Thermal
Electrical
Fluid Reactions
Output
Step input
Number of time steps
Duration (s)
Number of time steps
Total time (s)
Total steps
1
20
1
20
Insert Row
Add Row
Delete Row
OK
Apply
Cancel
Help
Advanced

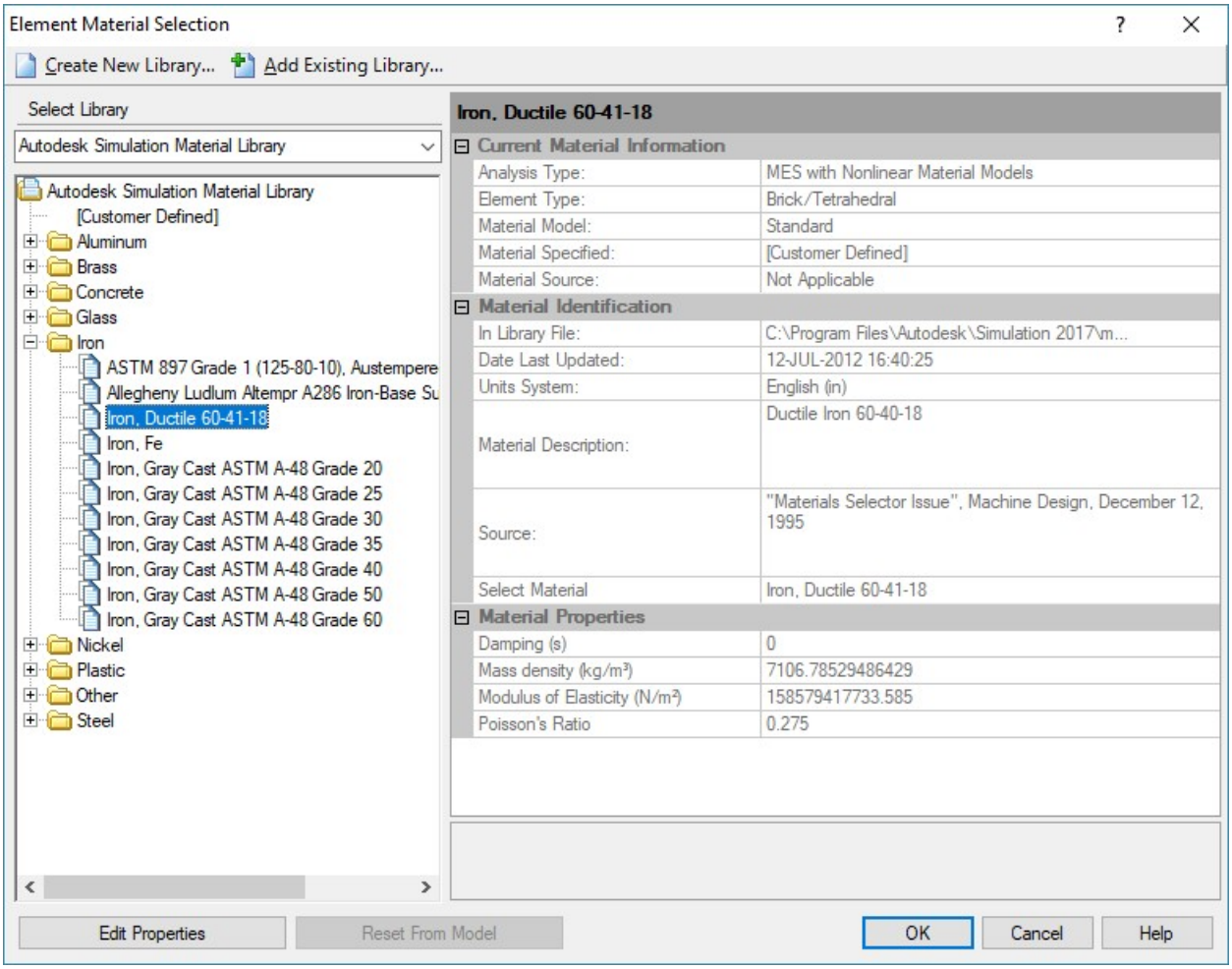

Terfenol-D defined property

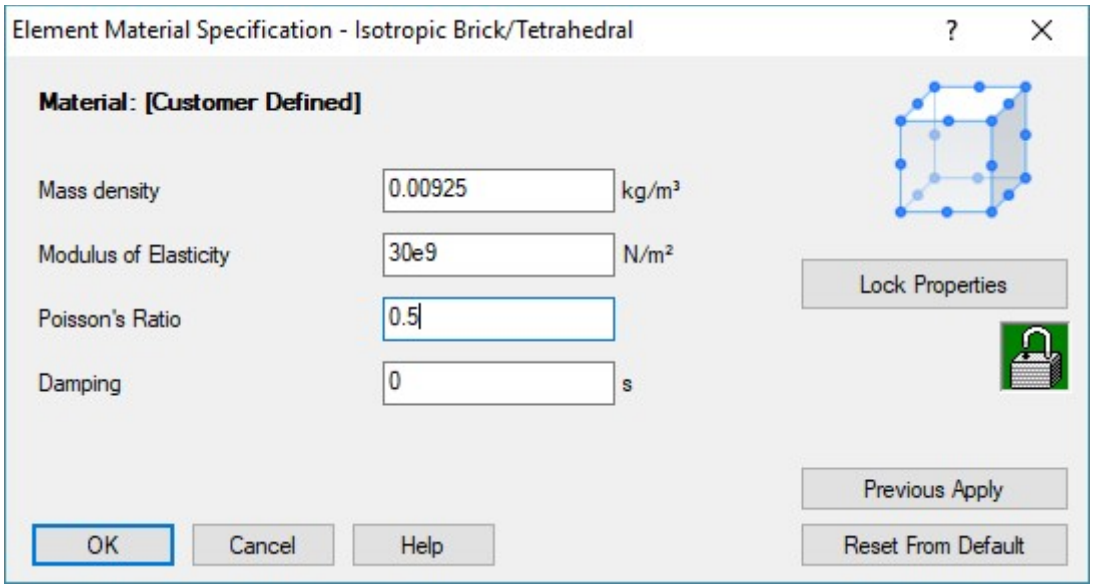
Element Material Specification - Isotropic Brick/Tetrahedral
Material: [Customer Defined]
Mass density
0.00925
kg/m³
Modulus of Elasticity
30e9
N/m²
Poisson's Ratio
0.5
Damping
0
s
Lock Properties
Previous Apply
Reset From Default
OK
Cancel
Help

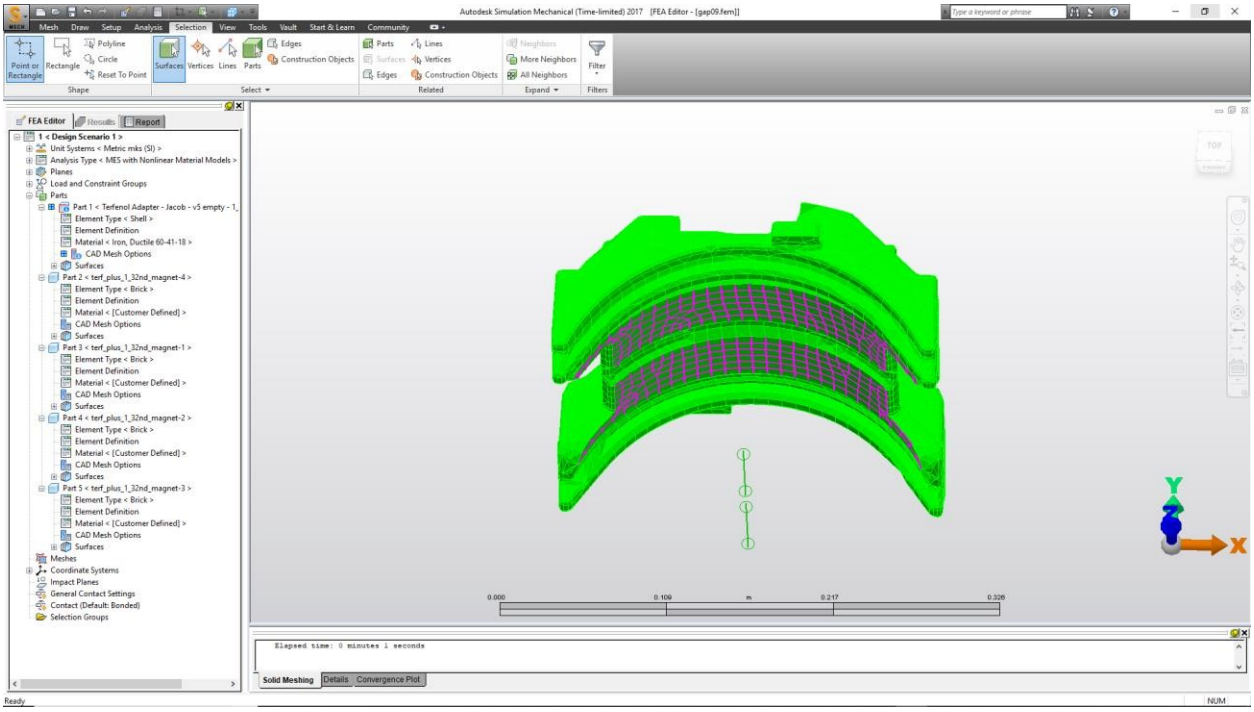

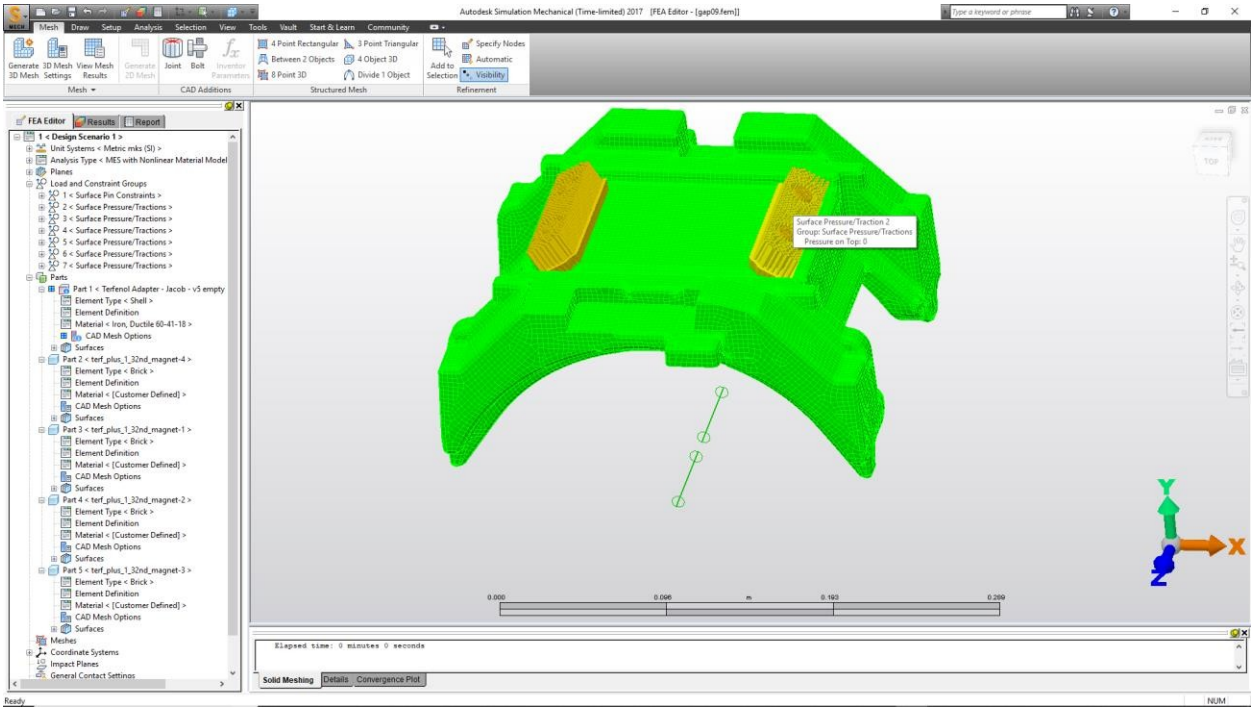
Autodesk Simulation Mechanical (Time-limited) 2017 [FEA Editor - [gap09.fem]]
Mesh
Draw
Setup
Analysis
Selection
View
Tools
Vault
Start & Learn
Community
Generate 3D Mesh
3D Mesh Settings
View Mesh Results
Generate 2D Mesh
Joint
Bolt
Inventor Parameters
4 Point Rectangular
3 Point Triangular
Between 2 Objects
4 Object 3D
8 Point 3D
Divide 1 Object
Add to Selection
Specify Nodes
Automatic
Visibility
Mesh
CAD Additions
Structured Mesh
Refinement
FEA Editor
Results
Report
1 < Design Scenario 1 >
Unit Systems < Metric mks (SI) >
Analysis Type < MES with Nonlinear Material Model
Planes
Load and Constraint Groups
1 < Surface Pin Constraints >
2 < Surface Pressure/Tractions >
3 < Surface Pressure/Tractions >
4 < Surface Pressure/Tractions >
5 < Surface Pressure/Tractions >
6 < Surface Pressure/Tractions >
7 < Surface Pressure/Tractions >
Parts
Part 1 < Terfenol Adapter - Jacob - v5 empty
Element Type < Shell >
Element Definition
Material < Iron, Ductile 60-41-18 >
CAD Mesh Options
Surfaces
Part 2 < terf_plus_1_32nd_magnet-4 >
Element Type < Brick >
Element Definition
Material < [Customer Defined] >
CAD Mesh Options
Surfaces
Part 3 < terf_plus_1_32nd_magnet-1 >
Element Type < Brick >
Element Definition
Material < [Customer Defined] >
CAD Mesh Options
Surfaces
Part 4 < terf_plus_1_32nd_magnet-2 >
Element Type < Brick >
Element Definition
Material < [Customer Defined] >
CAD Mesh Options
Surfaces
Part 5 < terf_plus_1_32nd_magnet-3 >
Element Type < Brick >
Element Definition
Material < [Customer Defined] >
CAD Mesh Options
Surfaces
Meshes
Coordinate Systems
Impact Planes
General Contact Settings
Surface Pressure/Traction 2
Group: Surface Pressure/Tractions
Pressure on Top: 0
0.000
0.096
m
0.193
0.289
Elapsed time: 0 minutes 0 seconds
Solid Meshing
Details
Convergence Plot
Ready
NUM

APPENDIX D

Power/Frequency Tables

Test Series 1				Test Series 2				Test Series 3			
Stage	f (Hz)	Cycles	Power (mW)	Stage	f (Hz)	Cycles	Power (mW)	Stage	f (Hz)	Cycles	Power (mW)
0	0.13	3	0.000752	0	1.75	10	0.000339	0	0.66	4	0.000407
1	37.38	187	0.072412	1	2.09	10	0.000559	1	0.75	4	0.000404
2	37.63	188	0.066999	2	2.44	10	0.000861	2	0.85	5	0.000433
3	46.88	234	0.046978	3	2.79	10	0.000958	3	0.94	5	0.000429
4	51.38	256	0.038332	4	3.14	15	0.001104	4	1.03	6	0.000447
5	51.63	258	0.038812	5	3.49	15	0.001214	5	1.13	6	0.000451
6	55.88	279	0.038240	6	3.72	15	0.001347	6	1.22	7	0.000462
7	57.13	285	0.037011	7	3.83	15	0.001559	7	1.32	7	0.000466
8	60.88	304	0.030601	8	3.90	15	0.001713	8	1.50	8	0.000556
9	61.38	306	0.029946	9	4.18	20	0.001742	9	1.69	9	0.000683
10	61.63	308	0.029626	10	4.53	20	0.001919	10	1.88	10	0.000799
11	61.88	309	0.029353	11	4.61	20	0.002166	11	2.07	11	0.000916
12	62.13	310	0.029069	12	4.67	20	0.002328	12	2.26	12	0.000992
13	62.38	311	0.028870	13	4.88	20	0.002461	13	2.44	13	0.001057
14	66.13	330	0.025146	14	5.23	25	0.002629	14	5.45	28	0.003531
15	71.13	355	0.040540	15	5.45	25	0.003000	15	6.22	32	0.004542
16	75.13	375	0.057619	16	5.58	25	0.003426	16	7.00	35	0.005564
17	75.38	376	0.063121	17	5.97	25	0.003634	17	7.78	39	0.006858
18	81.38	406	0.075652	18	6.22	30	0.003932	18	8.56	43	0.008505
19	81.88	409	0.073531	19	7.00	35	0.004462	19	9.34	47	0.009854
20	87.63	438	0.058589	20	7.78	35	0.005090	20	10.12	51	0.011816

			0.05750				0.00618		11.0		0.01422
21	88.13	440	9	21	8.30	40	1	21	0	55	1
			0.04989				0.00743		12.0		0.01685
22	93.63	468	4	22	8.56	40	8	22	0	60	0
			0.04950				0.00819		13.0		0.01979
23	94.13	470	9	23	9.34	45	8	23	0	65	2
			0.04600		10.1		0.00926		14.0		0.02243
24	99.13	495	4	24	2	50	5	24	0	70	0
	101.3		0.04202		10.3		0.01101		15.0		0.02529
25	8	506	9	25	0	50	7	25	0	75	1
	101.6		0.04179		10.8		0.01212		16.0		0.03035
26	3	508	0	26	9	50	7	26	0	80	8
	101.8		0.04156		11.6		0.01320		17.0		0.03501
27	8	509	6	27	7	55	6	27	0	85	8
	103.1		0.04045		12.4		0.01485		18.0		0.03857
28	3	515	3	28	5	60	3	28	0	90	7
	103.3		0.04025		13.3		0.01694		19.0		0.04305
29	8	516	0	29	2	65	6	29	0	95	0
	103.6		0.04015		16.5		0.01936		20.0		0.04767
30	3	518	4	30	6	80	3	30	0	100	0
	103.8		0.03998		19.8		0.02676		21.0		0.05153
31	8	509	9	31	3	95	9	31	0	105	1
	111.6		0.04240		23.1		0.04033		22.0		0.05488
32	3	558	9	32	3	115	4	32	0	110	4
	111.8		0.04228		26.4		0.05407		23.0		0.05711
33	8	559	6	33	4	130	6	33	0	115	3
	112.1		0.04198		29.7		0.06065		24.0		0.05978
34	3	560	4	34	4	145	4	34	0	120	7
	112.3		0.04202		33.0		0.06006		25.0		0.06052
35	8	561	1	35	5	165	2	35	0	125	5
	112.6		0.04189		35.2		0.05876		26.0		0.05987
36	3	563	9	36	5	175	6	36	0	130	5
	112.8		0.04164		36.3		0.05731		27.0		0.06057
37	8	564	5	37	5	180	1	37	0	135	5
	121.6		0.03150		39.6		0.05379		28.0		0.06078
38	3	608	0	38	6	195	5	38	0	140	3
	127.3		0.03792		42.9		0.05815		29.0		0.05899
39	8	636	0	39	6	210	0	39	0	145	1
	127.6		0.03753		43.7		0.06026		30.0		0.05695
40	3	638	1	40	5	215	9	40	0	150	9
	131.1		0.03449		46.2		0.05642		31.0		0.05541
41	3	655	5	41	7	230	0	41	0	155	9
	142.1		0.02965		49.5		0.05256		32.0		0.05585
42	3	710	7	42	7	245	1	42	0	160	2
	196.9		0.05500		52.8		0.04750		33.0		0.05735
43	3	983	0	43	8	260	6	43	0	165	6
					56.5		0.04371		34.0		0.05544
				44	6	280	4	44	0	170	0

BIOGRAPHICAL SKETCH

Jacob Nathaniel Bensen is married to an amazing, brilliant woman with whom they have three beautiful children. Jacob earned his Bachelor of Science in Mechanical Engineering with a GPA of 3.8 on May 2017 followed by his Master of Science in Engineering with a GPA of 3.32 on August 2019 from the University of Texas Rio Grande Valley. Jacob was not always an engineer; he worked at HEB for fifteen years, primarily as a pharmacy technician to support his family and his wife while she attended school. He has a passion for helping people, learning, teaching and making each day better than the last. He can be reached by e-mail at Jacob.N.Bensen@gmail.com. Jacob currently lives in Mission, TX.